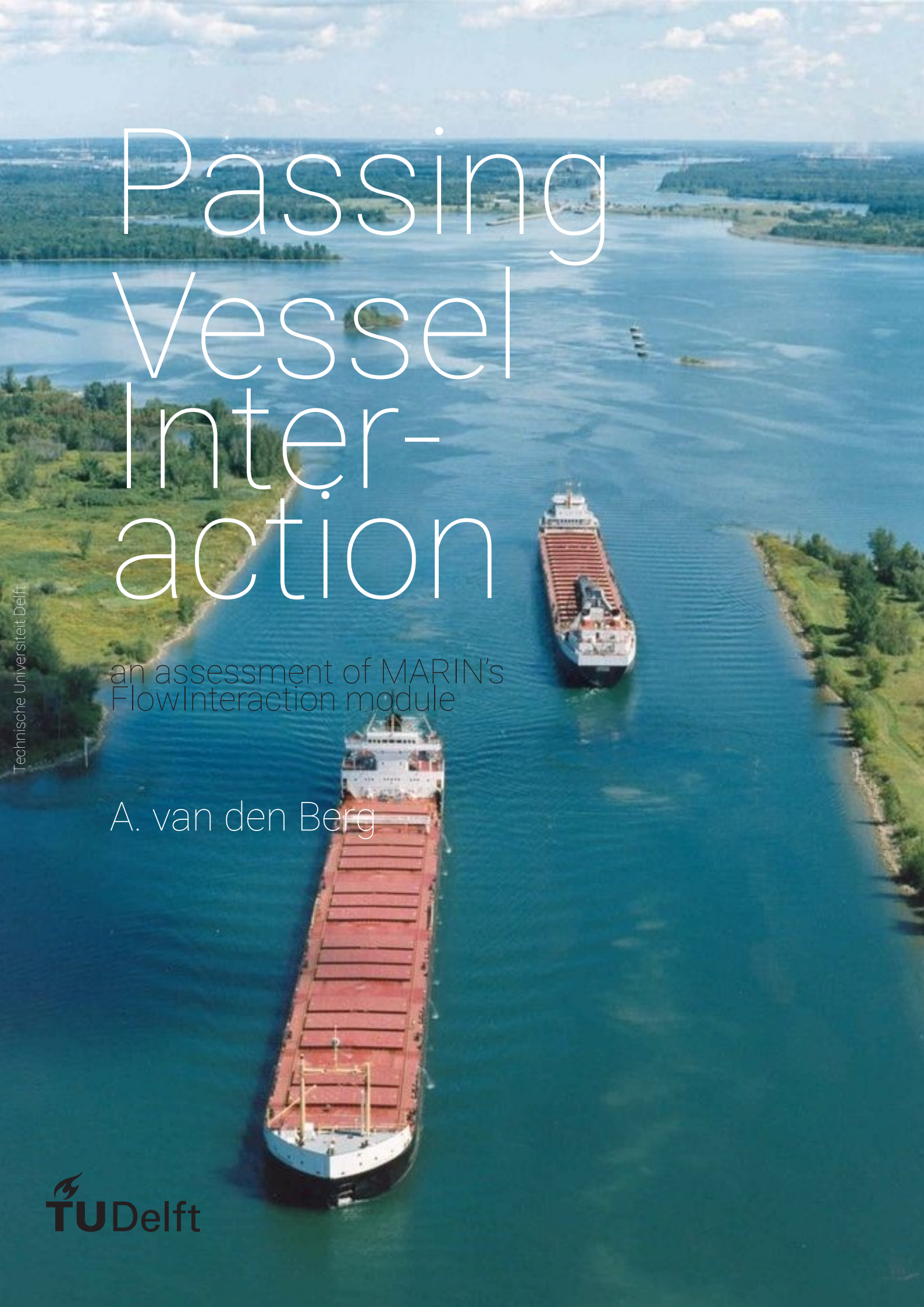

Passing Vessel Inter-action

an assessment of MARIN's FlowInteraction module

A. van den Berg

Technische Universiteit Delft

TU Delft

Passing Vessel Interaction

an assessment of MARIN's FlowInteraction module

by

A. van den Berg

to obtain the degree of Master of Science in Offshore and Dredging Engineering
at the Delft University of Technology,
to be defended publicly on Tuesday March 7, 2017 at 11:00 AM.

Student number:	4023390	
Project duration:	May 9, 2016 – March 7, 2017	
Thesis committee:	Prof. dr. A. V. Metrikine,	TU Delft, supervisor
	Dr. E. Lourens,	TU Delft
	Dr. F. Pisanó,	TU Delft
	Ir. K. van der Mijle,	MoorInsight Group B.V.
	Ir. E. Frickel,	MARIN

An electronic version of this thesis is available at `http://repository.tudelft.nl/`.

TU Delft

Sponsors

The work in this thesis was supported by MoorInsight Group B.V. and MARIN. Their cooperation is hereby gratefully acknowledged.

Abstract

In order to accurately predict passing vessel interaction forces, different simulation tools have been developed over the years. Many of these are based on a double body flow approach. MARIN (a hydrodynamic research institute located in the Netherlands) developed a simulation tool called the FlowInteraction (FI) module, which is part of the modular hydrodynamic simulation tool aNySIM. This module is based on double body flow theory – new is that it takes body motions into account in the force interaction. This is done by solving the equations of motion at every time step. The FI module has been verified and validated during this research.

An assessment was made of whether the physics in the FI module has been implemented correctly. To do this, verification and validation case studies have been done. The verification case studies have been evaluated based on expectations from the implemented physics and mathematics. Unexplainable results suggesting an incorrect implementation have been analyzed and used to draw conclusions. As validation material, a set of results from model tests done during the ROPES joint industry project has been used.

When the added mass force is neglected (as it is in the FI module) during a single body heave oscillation, cushion forces are dominant. This leads to a positive net mean force, which does not correspond with reality. Therefore, in order to simulate realistic behaviour, the added mass force should be included. Some numerical and discretization errors, due to the additional functionality of taking the body motions into account, are recognized. Based on these findings, recommendations on how to solve these problems are made.

It has been concluded that a double body flow model, as implemented in the FI module, only provides good force estimations when the added mass force is implemented. The usability is currently restricted to the simulation of captive ships; radiation forces can then be neglected without consequence. The FI module enables a fast hydrodynamic time domain simulation taking the influence of body motions on the interaction forces into account.

Preface

Hereby I am proud to present my thesis on hydrodynamic research, called: "Passing vessel interaction: an assessment of MARIN's FlowInteraction module". The research described in this thesis will be the final exercise before finishing my M. Sc. programme in Offshore and Dredging Engineering. I crossed many challenges on my the path towards the finalization of the nine months of work described in this thesis. I learned a lot from executing such a large research project on my own. The hardest part for me was that it felt somewhat solitary, but looking back I realize I always had people around me that helped me, if not by knowledge on hydrodynamics than by moral support. Looking back, I think it was a very valuable experience.

Before starting my Master Offshore and Dredging Engineering, I was a Bachelor student Mechanical Engineering. During my student life I did a lot of committees for Gezelschap Leeghwater (study association of Mechanical engineering TU Delft) and worked at the university. I feel greatly connected with the TU Delft, and it is with sorrow that I am leaving it. I really enjoyed the student life and I am grateful for having experienced it. I feel I learned a lot in the past 7,5 years and feel this all contributed greatly to this work. From learning to be independent, having a critical view on things to the knowledge on mechanics needed to finish such a research.

There are people I want to thank in person. First I want to thank everyone at MoorInsight Group B.V., for your financial support and also for helping me with my thesis. I really enjoyed the Friday afternoon drinks and the drinks on other occasions. I want to extend a special thanks to my supervisor Koen from MoorInsight Group BV. I really appreciate all the valuable input and the freedom in execution of this project. Your support has been extensive: from finding this research topic till the reviewing of the thesis at the end of the project.

Without the help of MARIN, who provided resources and knowledge, I could not have completed this research. A special thanks to Eelco, my supervisor from MARIN. Your input in the project was very helpful. You helped me with keeping the focus on the deliverable, next to that I valued your input on how to build up my presentations. Next to Eelco, I want to thank Gerben. He programmed the FI module. I really enjoyed the discussions and conversations we had about hydrodynamics, but also the general conversations. Thank you for your time and for reviewing my thesis.

From the university, I want to thank my daily supervisor Eliz-Mari Lourens. You have helped me a lot by reviewing my work and giving me clear, critical and constructive feedback. This contributed greatly to the quality of my report. I owe a special thanks to Prof. Metrikine as well. You really challenged me with hard questions, forcing me to go very deep into the theoretical material. During progress meetings there was always room for a joke, I really appreciated this.

Next to the people directly involved, I want to thank my parents for giving me the opportunity to study and enjoy this great time in my life. You supported me not only during this last part of study, but during my whole time as student with endless patience. You both are great and I am lucky to have you. Next to my parents, my sisters were a great support as well. Thank you for all the interest shown in the project and listening to my endless stories. A last thank you should go out to my friends and house mates who made my student time this memorable and great.

A. van den Berg
Delft, February 2017

Contents

List of Tables xi

List of Figures xiii

1 Introduction 1
- 1.1 Background . . . 1
- 1.2 Approach . . . 2
- 1.3 Thesis outline . . . 3

2 Passing vessel interaction 5
- 2.1 General axis convention . . . 5
- 2.2 Moored vessel behaviour . . . 5
- 2.3 Vessel interaction . . . 6
- 2.4 Double Body Flow . . . 6
- 2.5 Radiation forces . . . 7
- 2.6 Froude number . . . 7

3 Numerical modelling 9
- 3.1 Functionality FlowInteraction . . . 9
  - 3.1.1 Equation of motion . . . 9
- 3.2 Potential Theory . . . 10
- 3.3 Determining the potential field . . . 11
  - 3.3.1 Coordinate systems . . . 11
  - 3.3.2 Boundary Condition . . . 12
  - 3.3.3 Influence analysis . . . 12
  - 3.3.4 Solving the potential field . . . 15
- 3.4 Forces and Moments . . . 16
- 3.5 Clipping of panels . . . 17
- 3.6 Practical notes on implementation and functionality . . . 17

4 Verification 19
- 4.1 Verification set-up . . . 19
- 4.2 Expected FI forces . . . 19
- 4.3 Verification of expected FI forces . . . 21
  - 4.3.1 General implementation . . . 21
  - 4.3.2 Properties of module . . . 21
  - 4.3.3 Peculiar simulated behaviour . . . 22

5 Validation 27
- 5.1 Validation setup . . . 27
- 5.2 Expectation . . . 27
- 5.3 Evaluation . . . 28
  - 5.3.1 Magnitude forces . . . 28
  - 5.3.2 Force development . . . 30
- 5.4 Conclusion . . . 33

6 Conclusion 35
- 6.1 Main conclusions . . . 35
  - 6.1.1 Inertia forces . . . 35
  - 6.1.2 Discretization error . . . 35
  - 6.1.3 Time step minimization . . . 35
  - 6.1.4 Force interaction passing ships . . . 36

6.2 Recommendation on further development . . . 36
7 Discussion **37**
7.1 Radiation forces . . . 37
7.2 Influence of body motions in a DBF model on the interaction forces . . . 37
A ROPES model test data **39**
A.1 Test set-up . . . 39
A.2 Scale models . . . 39
A.3 Data from model test . . . 41
A.3.1 Drift angle . . . 41
B Verification cases **43**
B.1 Laplace Equation . . . 43
B.2 Mirror condition . . . 45
B.3 Horizontal translation . . . 46
B.3.1 General analysis . . . 46
B.3.2 Conclusion . . . 48
B.4 Kinematic excited heave oscillation . . . 51
B.4.1 General analysis . . . 51
B.4.2 Conclusion . . . 52
B.5 Kinematic excitation heave: influence of added mass . . . 55
B.5.1 General analysis . . . 55
B.5.2 Conclusion . . . 56
B.6 Free heave oscillation . . . 56
B.6.1 General analyses . . . 56
B.6.2 Conclusion . . . 58
B.7 Free heave oscillation - squat="false" . . . 62
B.7.1 General analysis . . . 62
B.7.2 Conclusion . . . 62
B.8 Free roll oscillation . . . 63
B.8.1 General analyses . . . 63
B.8.2 Conclusion . . . 64
B.9 Free roll oscillation - squat handle set to "false" . . . 66
B.9.1 General analyses . . . 66
B.10 FI handles and implemented properties . . . 67
B.10.1 Bank effect . . . 67
B.10.2 Banksuction handle . . . 68
B.10.3 Manoeuvring induced yaw . . . 69
B.10.4 Influence current-vessel . . . 70
B.10.5 soifactor . . . 71
B.10.6 perturbCurrent and vmin . . . 72
C User guide and limitations **75**
C.1 Practical recommendations . . . 75
C.2 Handles module . . . 76
C.2.1 Algorithm direct handle . . . 76
C.3 Properties of FI . . . 77
C.4 Possible problems for dis-functionality . . . 78
Bibliography **79**

List of Tables

4.1 Geometric properties verification body 19

A.1 Canal properties 39
A.2 Set-up parameters vessels 39
A.3 Towing tank model Passing ship 40
A.4 Towing tank model Moored ship 41
A.5 Drift angle observations August 2013 - Caland Canal [15] 42
A.6 Drift angle observations August 2012 - Oude Maas river near Puttershoek [14] 42

B.1 Geometric properties of body used for verification 43
B.2 Set simulation properties (FI handles) 43
B.3 Min. and max. flux through free surface 46
B.4 Mean shift in forced motion 52
B.5 Set simulation properties (FI handles) 68
B.6 Set simulation properties (FI handles) 69
B.7 Set simulation properties (FI handles) 70
B.8 Set simulation properties (FI handles) 71
B.9 Set simulation properties (FI handles) 73

List of Figures

2.1 Ship axes convention . . . 5
2.2 Linear fluid-body interaction forces potential theory . . . 7

3.1 Functionality FI module . . . 10
3.2 Panel with local coordinate system . . . 11
3.3 Mirroring technique . . . 14

4.1 Peculiar behaviour encountered in simulated verification case studies . . . 23
4.2 The ODE solver - evaluation of error . . . 24
4.3 FI forces versus FI forces with added mass . . . 25
4.4 Influence of added mass in vertical plane . . . 25

5.1 Magnitude of simulated forces vs model test forces . . . 29
5.2 Simulated forces with shallow water coefficient vs model test data . . . 30
5.3 Validation: comparing results at different Froude numbers . . . 31
5.4 Drift angle influence: comparing results . . . 32
5.5 Direct handle; additional local minima and maxima in force interaction . . . 33

A.1 Passing vessel model . . . 40
A.2 Moored vessel model . . . 40
A.3 Overview of set-up . . . 41

B.1 Control volume continuity . . . 44
B.2 Verification of Laplace equation . . . 45
B.3 Streamlines pitch-surge interaction . . . 48
B.4 Streamlines heave-surge interaction . . . 48
B.5 Accelerated barge, free motions simulated . . . 49
B.6 Accelerated barge, fixed DoF simulated . . . 50
B.7 Accelerated barge, free motions with dt=0.01s simulated . . . 51
B.8 Kinematic excited heave oscillation simulation - large amplitude . . . 53
B.9 Kinematic excited heave oscillation - small amplitude . . . 54
B.10 Kinematic excited heave oscillation - no self-inflicted FI forces . . . 55
B.11 Evaluation influence added mass . . . 56
B.12 Panel interfaces moving through the free surface . . . 58
B.13 Verification free heave oscillation . . . 61
B.14 Verification squat handle . . . 63
B.15 Verification roll oscillation . . . 65
B.16 Verification roll oscillation - time step variation . . . 66
B.17 Verification roll oscillation - no squat . . . 67
B.18 Evaluation of the bank effect. . . . 68
B.19 Verification of banksuction handle . . . 69
B.20 Forces on manoeuvring ship . . . 70
B.21 Verification neglect of free stream . . . 71
B.22 Verification soifactor handle . . . 72
B.23 Verification perturbCurrent and vmin handle . . . 73

C.1 Fast time eleven polygon approximation . . . 77

Nomenclature

Acronyms

APP	After perpendicular - end at stern of where L_{pp} is measured
DBF	Dubbel Body Flow
Drift angle	Yaw angle of the passing ship [deg]
EOM	Equations of Motion
FI	FlowInteraction (name of the module)
FPP	Fore perpendicular - end at bow of where L_{pp} is measured
FSE	Free Surface Effects
FT	Fast Time - a simulation where the direct handle is set to true
JIP	Joint Industry Project
LTI	Linear Time Invariant
ODE	Ordinary Differential Equations
Port side	Facing toward the bow of a vessel: the left side
ROPES	Research On Passing Effects on Ships
Starboard	Facing toward the bow of a vessel: the right side
TEU	Twenty feet Equivalent Unit

Greek Symbols

λ	wave length [m]
∇	gradient, the partial derivative of the function in (x,y,z)-direction
ω	rotational velocity of a body [rad/s]
ω_0	natural frequency [rad/s]
Φ	velocity potential [m^2/s]
ρ	density [kg/m^3]
σ	source strength [m/s]

Roman Symbols

$\bar{n}$	normal vector (x,y,z) on a plane pointed outwards [-]
$\bar{r}$	vector (x,y,z) with distance between two points [m]
$\mathbf{A}$	influence matrix [-]
$\vec{a}$	influence row vector [m]

$\vec{V}$	vector containing fluid velocities encounter by the collocation point [m/s]
A	amplitude of oscillation [m]
B	breadth ship [m]
F_{FI}	forces provided by the FI module [N]
g	gravitational constant [m/s^2]
h	water depth [m]
L_{pp}	length between perpendiculars (between bow and stern) of a ship [m]
N	amount of unknowns (panels) [-]
p	pressure [Pa]
r	distance between two points [m]
T	draft ship [m]
t	time [s]
T_0	period of oscillation [s]
u_0	relative velocity between vessel and water [m/s]
u_∞	undisturbed water velocity [m/s]
dt	time stepsize simulation [s]
Fn	Froude number [-]
S	surface area of the hull [m^2]
u	velocity in x-direction [m/s]
v	velocity in y-direction [m/s]
w	velocity in z-direction [m/s]

1 Introduction

Software package aNySIM is a modular hydrodynamic simulation tool, with each module adding functionality to the total program. The functionality of aNySIM is restricted to using input, different excitation forces and system parameters, in a hydrodynamic equation of motion. The different excitation forces can be for example: a wave spectrum, current and wind forces. On the other hand mooring lines or fender forces can be implemented to act as springs and dampers (linear or non-linear). Additional functionality is introduced by the FlowInteraction (FI) module. This module enables the ability for aNySIM to calculate an expression for the fluid domain. Every time step the dynamic fluid-body interaction forces are calculated and added to the equation of motion. This thesis can be considered an explanation and guidebook for the use and restrictions of the new FlowInteraction module. The core purpose of the new functionality is to add the ability to *simulate low speed passing vessel events and to find the interaction forces while including the body motions.*

In this thesis, the physical correctness of the FlowInteraction module is assessed. The reader who needs a deep understanding of the process and mathematics applied in the model can find this in Chapter 3, where the fundamentals can be studied. For the more general user, an user guide is provided in Appendix C.

The research questions of this thesis are:

- *Can a double body flow model be used to simulate motions through the vertical plane?*
- *What are the limitations of the applied physics?*
- *How does this effect the usability?*

The deliverable is a report in which the constraints on the use of the FI module is explained, with a recommendation regarding the use and further improvements of the module. Users who are in need of or desire a deep understanding of the physics should be able to find their answer in this thesis. An elaborate description of physics, mathematics and fundamental assumptions is part of the deliverable.

The deliverable of this research is:

- *A document containing the assessment of the physical correctness of the FlowInteraction module;*
- *Recommendations on further development;*
- *Recommendations on the usability of the module.*

1.1. Background

In the past decades global shipping has been growing substantially. The ship dimensions have increased significantly and for many ship types the size of the fleet grew as well. Around 20 years ago the largest container vessels were the Panamax size: typically 300x32 meters with a cargo capacity of around 3 500 TEU. The last decade fleets developed with large series of Post-Panamax-vessels, first with a cargo capacity of typically 6 500 TEU followed by 9 000 TEU and then the NewPanamax size of 14 000 TEU[13]. This trend implicates

that existing ports and waterways have to accommodate more and larger ships, at the same time more quay length and berths are required for loading and unloading these vessels. New terminals are often built in the existing infrastructure, along these busy waterways. Vessels navigating through the waterways cause pressure changes in the water. In shallow and narrow waterways these pressures, leading to interaction forces, can be substantial. For vessels moored in such a waterway or adjacent harbour, these forces can result in resonant horizontal vessel motions and large loads in the mooring lines.

In order to predict these interaction forces multiple simulation tools have been developed over the years. Methods as introduced by Korsmeyer et all [6] and further approaches by Pinkster [10], [11] use a potential theory double body flow approach. In these approaches the influence of the vessels free motions is not taken into account. The ROPES software, a product of the ROPES joint industry project, is based on the same approach with extended functionality through additional empirical coefficients. For this software an elaborate series of model tests was executed to validate and complement the simulation tool [13]. This research showed that for low Froude numbers (≤ 0.3) a double body flow model can predict passing ship interaction very well. At higher Froude numbers wave radiation, which cannot be simulated with a double body flow model, becomes significant.

The functionality of the in house software of Marin, called aNySIM, is now extended to determining fluid-body interaction. The FI module determines every time step the interaction forces between all concerned structures, taking the free motions of these structures into account. A useful application is found in software for simulators. A second application is the numerical modelling of a complete passing event in one simulation, including: fenders, mooring systems and other components. To make the functionality widely accessible, a wide range of test cases is simulated and verified.

1.2. Approach

The FI module was implemented and delivered without documentation. Based on a theoretical study, a mathematical disquisition of the implemented physics is provided. From this theory, limitations of the software are derived, verified and validated. During the verification cases some unexpected behaviour was encountered, the roots of which originates from different sources. Since FI is part of an elaborate modular program, some functionality is included through other modules in the aNySIM programming. A clear distinction on which results the FI module provides and which had to be excluded from the results because they are introduced by operational modules, was needed to come to sensible conclusions. This complicated the prediction of results and led to a complex puzzle of possible explanations for the simulated behaviour.

The verification cases substantiate the theory that the exclusion of added mass leads to non-physical responses in certain situations. Other inaccuracies were detected due to implementations to allow for free motion in a double body flow model. When simulated bodies describe motions through the free surface, non-physical behaviour is found. Some of this behaviour is explained by the clipping of panels at the free surface. Other behaviour is explained by disabled automatic time step adaptation of the numerical ordinary differential equation (ODE) solver, which leads to errors in the solution of the equation of motion. The exact roots of this non-physical behaviour and how to avoid it is an important part of the recommendations for users and improvement of the FI module.

The FI module is validated with measurement data from model tests done during the ROPES Joint Industry Project (JIP). The model tests were conducted with a keel clearance of the passing vessel of 1 meter. Channel geometry influence (for example: a bank, quay or bottom) needs to be included through panelled geometries, making the module not optimal for shallow water simulations. The limited work memory of the 32bit program, implicates that the module allows for a simulation of maximal 2000 panels. The memory is used to compose the influence matrix. This all resulted in the validation being done based on a comparison of deep water simulations with shallow water model test measurements. The magnitude of the forces varies because of this. Based on this validation and verification a conclusion was drawn on the functionality of the software.

1.3. Thesis outline

The knowledge documented in this thesis will provide insight in the theoretical fundamentals of the FI module. In this thesis the reader is guided from the basics of the relevant hydrodynamics towards a conclusion on the limitations of the FI module. In Chapter 2 a start is made with a theoretical introduction to conventions and hydrodynamic theory. After this, Chapter 3 details the numerical modelling in the FI module. From this theoretical framework expectations are set and, in Chapter 4, verified. The simulated cases to verify these expectations are documented in appendix B. The validation of the developed software is done based on cases documented in Appendix **??**. In chapter 5 these cases are discussed. The thesis finalizes with conclusions and recommendations on improvements of the software. A user guide for the FI module is found in Appendix C. This enables the user to have a quick yet informed start.

2

Passing vessel interaction

This chapter will give an overview of the relevant hydrodynamics for passing vessel interaction. Chapter 3 will go into deeper detail about the implemented physics and mathematics in the FlowInteraction module.

2.1. General axis convention

In hydromechanics a coordinate system with a surge, sway and heave direction is used. These directions correspond with the x, y and z direction of general coordinate systems. The rotations around these axis are referred to as: roll, pitch and yaw. All six degrees of freedom and their sign convention are depicted in figure 2.1. Unless explicitly stated differently, this convention is used throughout this thesis.

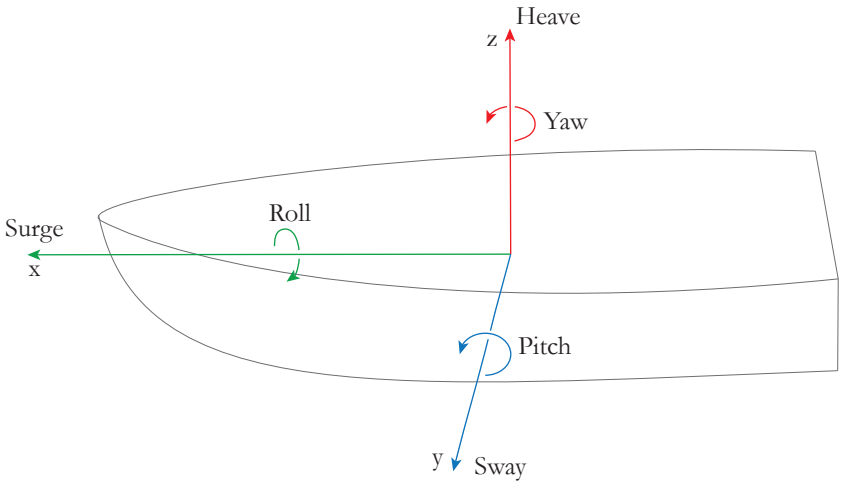

Figure 2.1: Ship axes convention: direction of the arrow is positive

2.2. Moored vessel behaviour

Moored ships in harbours and coastal waters may experience large motions, these can be induced by wind, waves and currents or passing vessels. In most cases the combined stiffness of a vessel and mooring system as a whole is relatively low in the horizontal plane. In the vertical plane buoyancy induces a much higher stiffness. A low stiffness leads to a low natural frequency, which may lead to resonant motions induced by passing ship effects. This is because slow passing vessels exert a low frequency loading on the moored vessel [13]. This is the reason that passing vessel interaction can lead to high mooring forces and unacceptable motions of the moored vessel. Therefore passing vessel software generally focusses on forces acting in the horizontal plane.

2.3. Vessel interaction

Dependent on the parameters of the passing event, different physical mechanisms are significant for the passing ship interaction. Previous research identified these mechanisms and methods to simulate these in a computational efficient way:

- During a slow passing event (Froude numbers lower than 0.3 [-]) moving through a continues harbour geometry at constant velocity; the primary wave system around the passing vessel is governing. The primary wave system refers to the non-dispersive wave around the passing ship. It is observed as a hight bow and stern wave, with a deep trough or drawdown through midships as explained by Tschirky et al [12]. Korsmeyer et al [6] showed that a double body flow (DBF) model describes this effect accurately;

- The influence of the harbour geometry on the interaction forces is significant. Pinkster [11] showed that the presence of a quay increases the surge force by approximately 80% and reduces the sway force and yaw moment by 60%. It is concluded that the passing forces on a ship moored in open water are not a good measure for the forces on a ship alongside a quay;

- In a complex harbour geometry long period wave activity can be triggered even in case of a slow passing event. The pressure field moving with the passing vessel can trigger this due to fluid velocities in the normal direction to the boundaries of the canal. A second trigger is a sudden change in the propagation speed or the harbour geometry, for example: a sudden change in water depth. This may lead to the release of some of the long period primary wave energy as free waves. These free waves can set off seiche activity. This is a long period standing wave in an enclosed or partially enclosed body of water. Pinkster [10] developed a method based on a DBF model in combination with a diffraction model to account for the long period wave influences. When the moored ship lays in a dock, as a notch sideways in the canal, these long period wave effects should not be neglected. The influence of the pressure field decays with $\frac{1}{r}$ (r is the passing distance), as a consequence the long period wave effects dominate the force interaction for large r;

- For a passing ship that has a Froude number higher than 0.3 [-], short period free surface effects are significant. A high Froude number indicates a relative high speed of the passing vessel in comparison to the water depth (or for deep water cases, in comparison to the vessels length). This was one of the conclusions derived from the ROPES JIP [13]. The interaction acting through the secondary wave system around the vessel is in such an event significant. The secondary wave system refers to wash wave effects in the wake of the passing ship;

- When a ship passes under a significant drift angle (a yaw angle of the passing vessel), viscous effects get significant. This is substantiated by findings in this thesis in Chapter 5. Bunnik [1] showed that the viscous effects due to drift angles till 15 degrees (negative or positive) can be estimated accurately using a RANS method without including free surface effects.

2.4. Double Body Flow

The double body flow (DBF) method is generally applied in a situation that the suction effects due to the primary wave are dominant. Korsmeyer et al [6] showed that a DBF model describes this effect accurately. Situations where free surface or viscous effects become significant cannot be simulated. This is because DBF models are implemented with potential theory and neglect free surface effects. In Chapter 3 one can find an elaboration on these assumptions.

Previous model approaches to passing vessel events based on the DBF method simulated passing events under the assumption of captive ships. This means that the motions of the ships under the acting external interaction forces did not move. For the passing ship this means that the ship passes with a constant velocity in a straight line. As a consequence the influence of the motions of the moored ship on the interaction forces are neglected. The motions of the moored ship are then calculated in two steps:

1. Capture the time history of the interaction forces, simulated on a restrained ship;

2. Couple the time history of the interaction forces to the equations of motion to find the ship response.

The FI module is based on a DBF model. Special about the FI module is: it does simulate the ship motions at every time step. This means that the influence of the changing position and velocity of the moored ship is taken into account in the simulated pressure field. In order to describe the response of the moored vessel accurately, radiation forces are important.

2.5. Radiation forces

In the FlowInteraction module not the entire Navier-Stokes equation is solved, it is assumed that the fluid domain can be described using potential theory. In Chapter 3 a more elaborate description is found of the assumptions and mathematics implemented in the module. In potential theory two of the neglected fluid properties is viscosity and compressibility. Due to this assumption no friction resistance and no turbulent behaviour of the fluid can be modelled. The linear radiation force components that can be simulated using potential theory are shown in figure 2.2.

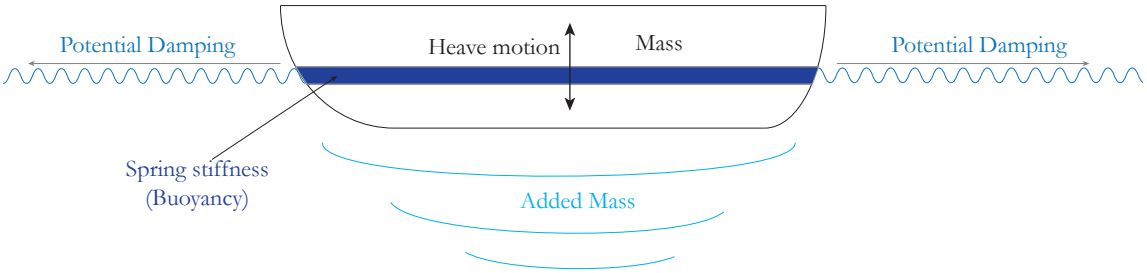

Figure 2.2: Linear fluid-body interaction forces potential theory

Potential damping is due to wave radiation induced by the body motions. Since a double body flow model cannot describe wave radiation, due to the mirroring assumption explained in Chapter 3, potential damping is not included in the FI module. Motion damping by viscous effects are in most cases neglected in motion calculations of offshore structures. The major part of the damping is caused by the wave damping. But viscous damping can be significant for rolling ships. This is because the potential damping for roll is generally relatively small [4].

Added mass refers to additional inertia due to fluid accelerating with the accelerating vessel. To accelerate mass, a certain amount of energy is needed which leads to a force. Added mass is for computational efficiency not taken into account in the FI module. In Chapter 3 this is elaborated on. The spring stiffness is due to the difference in buoyancy because of body motions. Note that it provides the stiffness in heave direction, but can also amount in the stiffness coefficients in roll or pitch direction.

In the two step approach introduced in the previous section; the radiation coefficients in the equations of motion are generally determined by a frequency domain diffraction calculation with a conversion to the time domain solution using the Cummins equation. This method is basically a conversion of the frequency domain solution to the time domain solution. Due to this approach the radiation coefficients are time invariant during the passing event. This leads to inaccuracies since they are influenced by the changing environment during the passing event.

2.6. Froude number

Important in the consideration of which force interaction mechanisms between the two vessels is significant is the dimensionless Froude number (Fn). The Froude number is defined as the ratio between the flow inertia and the external field: the external field in this case being gravity. The Froude number has a direct relation to the resistance of a ship due to generated waves. Further the Froude number is used to scale model tests from real situations. This is because the wave pattern around a partially submerged object moving through water is similar at equal Froude numbers.

$$\mathrm{Fn}_L = \frac{u_0}{\sqrt{gL_{pp}}} \tag{2.1}$$

$$\mathrm{Fn}_h = \frac{u_0}{\sqrt{gh}} \tag{2.2}$$

Equations 2.1 and 2.2 respectively show the formula for the deep water and shallow water Froude number. Here u_0 refers to the relative velocity between the water and the vessel, L_{pp} is the length of the vessel between perpendiculars, g is the gravitational constant and h is the water depth. In shallow water the wave propagation speed is restricted by the water depth in stead of the wave length (λ). This follows from the dispersion relation for waves. The dispersion relation states that the propagation velocity of shallow water waves is equal to $c_p = \sqrt{gh}$ (for $\lambda \gg h$). This implicates that the Froude number for shallow water is determined differently than for deep water. When the vessel is moving with the wave propagation speed the Froude number is one and referred to as critical.

3

Numerical modelling

This chapter gives a quantitative and qualitative description of the applied physics and mathematics in the FlowInteraction module. Firstly, an overview of the FlowInteraction module and its interface with aNySIM is provided. After this, the steps taken to determine the potential field are handled, followed by the manner in which the forces and the motions are determined from the potential field.

3.1. Functionality FlowInteraction

The FlowInteraction module is additional functionality to the modular aNySIM XMF programming. The module adds the functionality of simulating interaction between bodies and fluid. The simulated interaction forces are included in the equation of motion. Forces provided by other aNySIM modules are included in the equation of motions as well, for example: buoyancy forces. Figure 3.1 is a visual representation of the functionality of the FlowInteraction module and how it is incorporated in aNySIM.

Unique to this approach of calculating body-fluid interaction is the recurring calculation of the total potential field. The potential field is a description of the fluid domain determined using potential theory. The whole potential field is determined during each time step, here the motions calculated during the previous time step are taken into account. In combination with the already existing aNySIM programming, this leads to a uniquely complete simulation tool. This tool is able to describe the motions and the forces on moored vessels under operation due to passing vessel effects. In Appendix C the restrictions on the use of the FlowInteraction module and potential theory are discussed.

3.1.1. Equation of motion

The dynamic behaviour induced by these FI forces is determined by already operational functionality. Properties of the simulated body, for example: mass, moment of enertia, body dimensions etc.; are input to the simulation. Two force terms, which are generally part of a hydrodynamic equation of motion, are not included by the FI module in the equation of motion:

- **added mass:** this is neglected (see section 3.4). The influence of body accelerations on the forces provided by the FlowInteraction module are not taken into account;
- **potential damping:** this is energy transfer from the body to the water by making waves. The waves propagate from the body, taking energy with it, thus energy is transferred from the body to the fluid domain. This energy moves to infinity and does not get transferred back to the body since the wave propagates away: damping the motions of the body. Since here the fluid is incompressible and the free surface is a mirror plane, flat and rigid, no waves are radiated and thus this mechanism for damping is not simulated.

Because the velocities and accelerations during a passing vessel event of large vessels are generally low, these terms are assumed to be negligible. If need be, these factors can be determined separately by means of diffraction software and then added through a hydrodynamic database file. A downside of this approach is that added mass and damping are influenced by the environment, which changes for a moving body with a

changing environment. In diffraction software a non-varying environment is assumed. Consequently added mass and potential damping are, in that case, constant for the whole simulation.

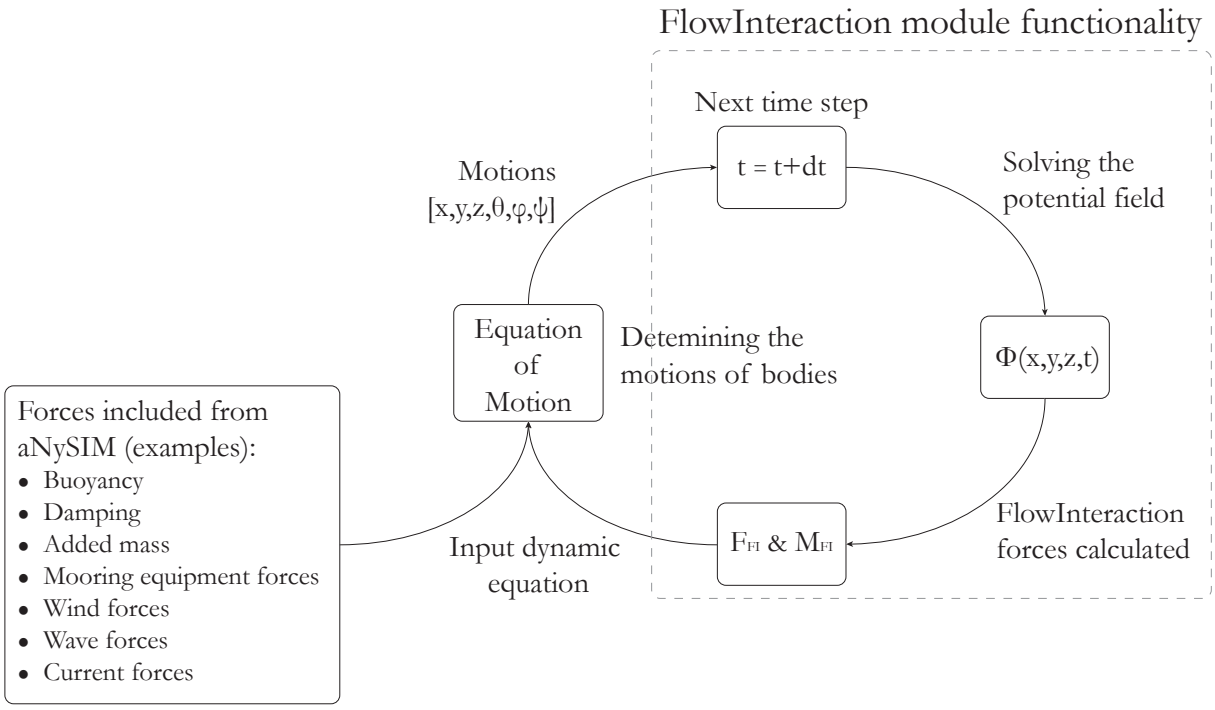

Figure 3.1: Overview of the additional functionality of the FlowInteraction module

3.2. Potential Theory

The FI module is based on potential theory. In potential theory the fluid domain is assumed to be continuous and rotation free. These characteristics of a potential flow are the reason that it can be solved at the edges of the flow domain (at a stream line), without having to pay attention to the fluid domain itself. The following assumptions lay at the fundamentals of potential theory:

- **Principle of continuity:** mass flowing into a control volume has to flow out at the same instant, the net mass flow is zero;
- **Incompressibility of fluid:** the fluid is assumed to be incompressible. This assumption leads to the continuity equation as in equation 3.2, which is the Laplace equation. The velocity is now proportional to the mass flow;
- **Inviscid and non-rotational fluid:** the flow does not rotate at first instance and will not start to do this due to its inviscid property. Only laminar flows are modelled through this theory.

$$u = \frac{\partial \Phi}{\partial x}, \quad v = \frac{\partial \Phi}{\partial y}, \quad w = \frac{\partial \Phi}{\partial z} \tag{3.1}$$

By definition of the velocity potential, equation 3.1 is true: the directional partial derivative of the velocity potential, equals the fluid velocity in that direction. In equation 3.1, the gradient of the potentials leads to the fluid velocities in x-, y- and z-direction, expressed as u,v and w. Substituting this identity into the continuity equation gives us the Laplace equation (see equation3.2). The velocity potential, $\Phi(x, y, z, t)$, always satisfies Laplace his condition.

$$\nabla^2 \Phi = \frac{\partial^2 \Phi}{\partial x^2} + \frac{\partial^2 \Phi}{\partial y^2} + \frac{\partial^2 \Phi}{\partial z^2} = 0 \tag{3.2}$$

3.3. Determining the potential field

Potential theory is applied to a three dimensional 0^{th} order panel method. This means that a geometry is approximated by multiple panels, these panels are acting as source sheets with a constant source strength, $\sigma(t)$ [m/s], over the panel. In order to solve the potential field, the strength of these sources need to be determined. Boundary conditions are imposed on the flow to find a unique solution of the source distribution on the panels. In this section the steps taken to find the solution to the potential field is explained. The following is discussed in this section:

- Different coordinate systems used during the simulation;
- Boundary condition and mathematical expression for the velocity potential;
- Influence analysis and the solution to the potential field.

3.3.1. Coordinate systems

Three different types of coordinate systems are used in the FI module. Between these coordinate systems transformations occur during the simulation. The used coordinate systems are:

1. **Panel local coordinate system:** this coordinate system is defined on each panel. In this coordinate system the influence parameters (section 3.3.3) are determined. The orientation of the local axis system per panel is defined as follows: the collocation point of the panel $(x_0, y_0, 0)$ is defined as the origin of this coordinate system. The corners of the panel are defined in these axis as $(x_1, y_1, 0) \cdots (x_4, y_4, 0)$. Figure 3.2 shows a panel with the local coordinate system on it. The z-axis is in normal direction, the x and y axis are orthonormal vectors to this direction;
2. **Body fixed coordinate system:** the body fixed coordinate system has its origin in the CoG of a simulated body. It translates together with the body it is fixed too. The advantage of this type of coordinate system is that rotations of the body around its CoG can be expressed easily, since this is a rotation around the origin of the coordinate system;
3. **Earth fixed coordinate system:** this coordinate system is earth fixed. The origin defines the global coordinate point (0,0,0). In this coordinate system all moving bodies are described by tracking the motions of the origins of the body fixed coordinate systems. Assuming that the bodies are rigid enables the summation of additional panel motions through body rotations. Analysing multiple bodies, with free motions, during the simulation creates need for this type of coordinate system. Relative motions of multiple bodies with respect to each cannot be described in body fixed coordinate systems.

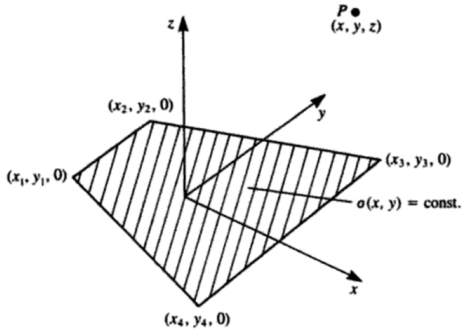

Figure 3.2: Quadrilateral panel with constant source strength and its influence on point P [5]

Note, in figure 3.2 the assumption is made that the edges of the panel are assumed to lay in a flat horizontal plane with origin at z_0=0. A twisted panel can be taken into account, yet its twist will be neglected. The twisted panel is decomposed in two (or more) panels which will have a mean normal and a mean centroid. These will be determined at the start of the influence analysis (see section 3.3.3) defining the z-direction and the origin of the local axis system.

3.3.2. Boundary Condition

The linear property of potential theory enables us to describe total velocity potential as a superposition of multiple partial velocity potentials. In this case the total potential, $\Phi_{tot}(x,y,z,t)$, is a superposition of the free stream potential, $\Phi_\infty(x,y,z,t)$, which describes the free stream of the fluid and a perturbation potential, $\Phi(x,y,z,t)$, describing the perturbation of the fluid by the body (see equation 3.3).

$$\Phi_{tot}(x,y,z,t) = \Phi(x,y,z,t) + \Phi_\infty(x,y,z,t) \tag{3.3}$$

With this knowledge the used Neumann boundary condition is quantified in equation 3.4. Qualitatively it states: 'the hull of the vessel is water tight' which is equivalent to no net normal velocities of the fluid at the surface of the panel. This boundary condition is satisfied at the collocation point (the centroid) of each panel on the body.

$$\nabla(\Phi_m + \Phi_\infty) \cdot \bar{n}_m = -(\bar{u}_m + \bar{\omega} \times \bar{r}_m) \cdot \bar{n}_m \tag{3.4}$$

where:

$\bar{u}$ is the translational velocity vector of the body of which panel m is a part [m/s];

$\bar{\omega}$ is the rotational velocity vector around the CoG of the body of which panel m is a part [rad/s];

$\bar{r}_m$ is the radius vector from the CoG of the body to the collocation point of panel m [m];

$\bar{n}_m$ is the normal vector of panel m expressed in the earth fixed coordinate system [-].

3.3.3. Influence analysis

For the next step in the simulation the expression for the perturbation potential needs to be derived. Katz and Plotkin [5] provide this formulation of the perturbation potential as equation 3.5.

$$\Phi(x,y,z,t) = -\sigma(t) \cdot \frac{1}{4\pi} \cdot \int_S \frac{dS}{\sqrt{(x-x_0)^2 + (y-y_0)^2 + z^2}} \tag{3.5}$$

where:

$\sigma(t)$ is the source strength [m/s];

x,y,z is the x,y,z-coordinate of the point of evaluation of source strength σ [m];

dS is the surface area of the panel with σ [m^2].

From this equation it is evident that the formulation of the perturbation potential consists of a source strength and a geometric term describing the surface area of the panel and the decay of the source strength (scatter) in space. Note that this description satisfies the Laplace equation (3.2). Solving the integral in equation 3.5 leads to the expression in equation 3.6 provided by Hess and Smith [3]. This expression of the perturbation potential is applicable to each panel.

$$\Phi(x,y,z,t) = -\sigma(t)\cdot\frac{1}{4\pi}\left\{\left[\frac{(x-x_1)(y_2-y_1)-(y-y_1)(x_2-x_1)}{d_{12}}\ln\left(\frac{r_1+r_2+d_{12}}{r_1+r_2-d_{12}}\right)\right.\right.$$

$$+\frac{(x-x_2)(y_3-y_2)-(y-y_2)(x_3-x_2)}{d_{23}}\ln\left(\frac{r_2+r_3+d_{23}}{r_2+r_3-d_{23}}\right)$$

$$+\frac{(x-x_3)(y_4-y_3)-(y-y_3)(x_4-x_3)}{d_{34}}\ln\left(\frac{r_3+r_4+d_{34}}{r_3+r_4-d_{34}}\right)$$

$$\left.+\frac{(x-x_4)(y_1-y_4)-(y-y_4)(x_1-x_4)}{d_{41}}\ln\left(\frac{r_4+r_1+d_{41}}{r_4+r_1-d_{41}}\right)\right]$$

$$\left.+|z|\left[\tan^{-1}\left(\frac{m_{12}e_1-h_1}{zr_1}\right)+\tan^{-1}\left(\frac{m_{23}e_2-h_2}{zr_2}\right)+\tan^{-1}\left(\frac{m_{34}e_3-h_3}{zr_3}\right)+\tan^{-1}\left(\frac{m_{41}e_4-h_4}{zr_4}\right)\right]\right\} \quad (3.6)$$

Variables d_{ij}, r_k, m_{ij}, e_k, h_k and r_k are defined in equations 3.7, 3.8 and 3.9. These values are substitutes for additional variables to keep equation 3.6 clear and understandable. Note that the second part of equation 3.6 (the part between braces) describes the decay of the source strength over a distance to point (x,y,z). In this representation of the equation the panels are assumed to be square, yet the panel code works with polygons with an arbitrary amount of vertices (in equations 3.7, 3.8 and 3.9, i, j, k take values from one to the amount of panel vertices).

$$d_{ij} = \sqrt{(x_j-x_i)^2+(y_j-y_i)^2} \qquad \begin{cases} i = 1,2,3,4 \\ j = 2,3,4,1 \end{cases} \quad (3.7)$$

$$m_{ij} = \frac{y_j-y_i}{x_j-x_i} \qquad \begin{cases} i = 1,2,3,4 \\ j = 2,3,4,1 \end{cases} \quad (3.8)$$

$$\left.\begin{array}{rcl} r_k & = & \sqrt{(x-x_k)^2+(y-y_k)^2+z^2} \\ e_k & = & (x-x_k)^2+z^2 \\ h_k & = & (x-x_k)(y-y_k) \end{array}\right\} k = 1,2,3,4 \quad (3.9)$$

If point (x,y,z) is far from the collocation point of panel n, then the influence of the panel element with an area S is approximated by a point source. This approximation improves computational efficiency. The term far is defined as a distance of more than four times the average panel diameter. Equation 3.6 is in that case simplified to equation 3.10, with S the surface area $[m^2]$ of the influencing panel.

$$\Phi(x,y,z,t) = -\sigma(t)\cdot\frac{S}{4\pi\cdot\sqrt{(x-x_0)^2+(y-y_0)^2+z^2}} \quad (3.10)$$

The intensity (influence) of the source reduces with $\frac{1}{r}$, in which r is the absolute distance between the centroid of the panel and the point where the potential is evaluated.

Influence coefficients

Short recap, the perturbation potential is described as function of the source strength and a space dependent part. This can be seen in equation 3.5. To solve the potential field the source strength on each panel needs to be determined. A unique solution for the source strengths is found by imposing the boundary condition, equation 3.4, to the collocation point on each panel. To solve this problem, the interaction between panels needs to be quantified. This is done by means of influence coefficients. The influence coefficient of one panel on another is a value that says something about the remaining strength (decay over space) of the source strength on a panel over a specified distance (x,y,z). The influence coefficient equals the expression for the gradient of the perturbation potential divided by its source strength, this is shown in equation 3.11. Note that the definition of A_{mn} is chosen to be drawn from the gradient of the potential, this is convenient

when applying the Neumann boundary condition.

$$\nabla\Phi(x,y,z,t)\cdot\vec{n}_m = \sum_{n=1}^{N} A_{mn}(x,y,z,t)\sigma_n(t) \quad \rightarrow \quad A_{mn} = \frac{\nabla\Phi_{mn}\cdot\vec{n}_m}{\sigma_n} \tag{3.11}$$

The total potential value on any point in the fluid due to the fluid perturbation by a body, is the sum of each source strength times the influence coefficient. To solve the equation at the panels on which a boundary condition is imposed, the total potential at the collocation point of this panel needs to be determined. Index mn refers to which panels are analysed. Index n refers to the panel which contributes to the total perturbation potential value at the collocation point of the panel with index m. The interaction between all simulated panels is described by these influence coefficients. Note that the coordinates (x,y,z), where the potential is evaluated, are described in the local coordinate system of the influencing panel. This, in practice, needs an additional transformation from the local coordinate system on panel n to the global coordinate system, since $\vec{n}_m$ is the normal vector of panel m in the global coordinate system.

Free surface

Mirroring of the event over the x and y plane of the global coordinate system is used to enforce a zero flux through the free surface. Because of the induced symmetry around the mirroring plane, this plane is simulated as a streamline. A streamline cannot be crossed by other streamlines, making it a rigid flat surface. This mirroring plane will act as the free surface. Not imposing the kinematic and dynamic boundary conditions on the free surface minimizes the computational effort. The downside is the neglect of all free surface effects. This mirroring technique is what defines a double body flow model. Figure 3.3 provides a visualization of the mirroring technique. Employing the free surface as a mirror practically means that every body is simulated twice (one time in the real and one time in the mirrored fluid domain) which effectively enables the problem to be solved in one fluid domain without a fluid border.

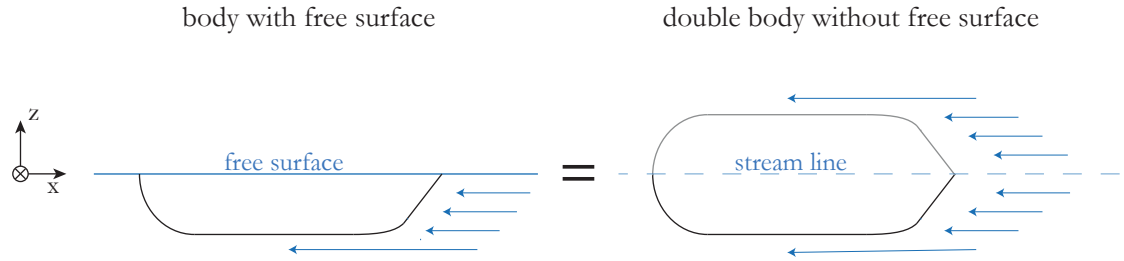

Figure 3.3: Mirroring technique

A set of linear equations

The positions of all panels in the simulation are known. The influence between different sources is determined by means of influence coefficients. Now the only unknown term in the expression of the perturbation potential, see equation 3.5, is the source strength on the panels. Substituting the expression for the perturbation potentials in the boundary condition, equation 3.4, leads to equation 3.12. The free stream potential is written to the right hand side of the equation. Here together with the motions of the panel, it determines the relative fluid velocity a panel encounters. Equation 3.12 shows a discrete linear set of equations. One equation for every panel, each equation being a superposition of the influences of all sources having to satisfy the right hand side. There are N unknowns and N equation, therefore there is a unique solution to this problem.

$$\frac{1}{2}\cdot\sigma_m + \sum_{n=1}^{N} A_{mn}\sigma_n = -\nabla\Phi_\infty\cdot\bar{n}_m - (\bar{u}_m - \bar{\omega}\times\bar{r}_m)\cdot\bar{n}_m \qquad \text{for} \qquad n\neq m \tag{3.12}$$

where:

m is the index of the analysed panel [-];

n is the index of the influencing panel [-];

N is the amount of panels in the simulation [-].

Note that in influence coefficient A_{mn} is already derived from the gradient of the perturbation potential, this is shown in equation 3.11. Influence A_{mm} is the self influence of the panel, this equals in every case $\frac{1}{2}$.

3.3.4. Solving the potential field

The sum in equation 3.12 is written in matrix and vector form, this leads to the expression shown in equation 3.13. This equation is solved to find a solution for the unknown source strengths on the panels. The expressions for the variables used in equation 3.13 are found in equations 3.14, 3.17 and 3.18.

$$\mathbf{A} \cdot \vec{\sigma} = \vec{V} \tag{3.13}$$

In this equation the following matrices and vectors are defined:

$\mathbf{A}$ is the influence matrix describing the influence of panels on each other [-];

$\vec{\sigma}$ is the source strength vector containing all the source strengths, the row index indicates at which panel they are located [m/s];

$\vec{V}$ is the vector containing the fluid velocity that a panel encounters due to panel motions and free stream [m/s]. It is equal to the right hand side of equation 3.12.

To find the influence matrix $\mathbf{A}$, first to two different $(N \times N)$-matrices are defined: one matrix containing the influence coefficients of the real panels on other real panels, $\mathbf{A_{RR}}$, and one matrix containing the influence of the mirrored panels on the real panels, $\mathbf{A_{MR}}$. The total influence matrix is the sum of these two matrices. Note that the real panels and there source strengths have indices from $1 \cdots N$ while the mirrored panels have indices from $1' \cdots N'$.

$$\mathbf{A} = \left[\mathbf{A_{RR}} + \mathbf{A_{MR}}\right] \tag{3.14}$$

$$\mathbf{A_{RR}} = \begin{bmatrix} A_{11} & \cdots & A_{1N} \\ \vdots & \ddots & \vdots \\ A_{N1} & \cdots & A_{NN} \end{bmatrix} \tag{3.15}$$

$$\mathbf{A_{MR}} = \begin{bmatrix} A_{11'} & \cdots & A_{1N'} \\ \vdots & \ddots & \vdots \\ A_{N1'} & \cdots & A_{NN'} \end{bmatrix} \tag{3.16}$$

The vector containing all the source strengths, defined in equation 3.17, has N entries as well. Due to the symmetry, the source strengths on the mirrored and real panels are equal.

$$\vec{\sigma} = \begin{bmatrix} \sigma_1 \\ \vdots \\ \sigma_N \end{bmatrix} \qquad \text{because,} \qquad \begin{bmatrix} \sigma_1 \\ \vdots \\ \sigma_N \end{bmatrix} = \begin{bmatrix} \sigma_{1'} \\ \vdots \\ \sigma_{N'} \end{bmatrix} \tag{3.17}$$

The fluid velocity a panel encounters is shown in equation 3.18. One might recognize this as a vector containing as elements the right hand side of equation 3.12.

$$\vec{V} = \begin{bmatrix} -\nabla\Phi_\infty \cdot \bar{n}_1 - (\bar{u}_1 - \bar{\omega} \times \bar{r}_1) \cdot \bar{n}_1 \\ \vdots \\ -\nabla\Phi_\infty \cdot \bar{n}_N - (\bar{u}_N - \bar{\omega} \times \bar{r}_N) \cdot \bar{n}_N \end{bmatrix} \tag{3.18}$$

3.4. Forces and Moments

The velocity potential field describing the fluid domain is known. Now the forces acting on the simulated bodies are evaluated. Using Bernoulli equation for unsteady potential flow, shown in equation 3.19, pressures in the fluid are determined. The deduction of this equation follows from the Euler equations for inviscid and incompressible flow and can be found in Offshore Hydrodynamics [4].

$$\rho_w \cdot \frac{\partial \Phi}{\partial t} + \frac{1}{2} \cdot \rho_w \cdot (\nabla \Phi)^2 + p + \rho_w \cdot g \cdot z = C(t) \tag{3.19}$$

where:

$\frac{\partial \Phi}{\partial t}$ is the unsteady part of the pressure equation [Pa], this term provides the fluid inertia forces;

$(\nabla \Phi)^2$ is the kinematic part of the pressure equation [Pa]. Note that by definition of the velocity potential the gradient of the potential equals the fluid velocity;

p is the pressure [Pa];

$g \cdot z$ is the hydrostatic part of the pressure equation [Pa]. This pressure is not provided by the FlowInteraction module but by another module of aNySIM as buoyancy;

$C(t)$ this function depends only on time, not on position in the fluid domain. Consequently the Bernoulli equation applies to the whole fluid domain and not only along a streamline;

ρ_w is the density of the water [kg/m^3].

The forces (provided by the FlowInteraction module) are obtained by integration of the pressure at each panel over its surface area. When this is done, the forces acting on panels are expressed as forces and moments around the CoG of the simulated bodies. Substituting equation 3.3 into equation 3.19 and integrating it over the surface of the panel leads to equation 3.20. This is the equation used to find the force on each panel.

$$\mathbf{F} = -\iint_S p \cdot \bar{n} dS = -\iint_S \left\{ -\rho_w \frac{\partial \Phi}{\partial t} - \frac{1}{2} \rho_w (\nabla \Phi)^2 \right\} \cdot \bar{n} dS \tag{3.20}$$

The net force on a body is a superposition of the forces acting on the panels of that particular body. Moments are determined in the same manner. Equation 3.21 and 3.22 provide the expression respectively used to calculate the forces on and the moments around the CoG of each body. Note that the force has to be evaluated on each panel. The net moment and force on a body is a superposition of the separate panel forces.

$$\mathbf{F} = \rho_w \frac{\partial}{\partial t} \iint_S \{\Phi_\infty + \Phi\} \cdot \bar{n} dS + \frac{\rho_w}{2} \iint_S \left\{ (\nabla \Phi_\infty + \nabla \Phi)^2 \right\} \cdot \bar{n} dS \tag{3.21}$$

$$\mathbf{M} = \rho_w \frac{\partial}{\partial t} \iint_S \{\Phi_\infty + \Phi\} \cdot (\bar{r} \times \bar{n}) \, dS + \frac{\rho_w}{2} \iint_S \left\{ (\nabla \Phi_\infty)^2 + (\nabla \Phi)^2 \right\} \cdot (\bar{r} \times \bar{n}) \, dS \tag{3.22}$$

where:

$\bar{r}$ is the vector containing the distance between the collocation point of the evaluated panel and the CoG of the analysed body [m];

$\bar{n}$ is the normal vector of the panel [-];

dS is the surface area of the panel being evaluated [m^2].

Added mass

In the FI forces, determined by equation 3.21, the unsteady part provides the inertia forces. This term consists of a part dependent on the velocity and a part dependent on the accelerations of the body. Inertia forces dependent on the acceleration of the body is referred to as added mass forces. All other inertia forces are referred to as cushion forces. The added mass force is neglected in the FI module, the cushion forces are taken into account.

The added mass is dependent on the acceleration, and the acceleration is on its term again dependent on the added mass force. The equation of motion and the FI calculation are solved in parallel loops, the accelerations can only be taken into account by the FI module if an iteration between the (by the FI module provided) added mass forces and the accelerations (provided by the equation of motion) is done. To avoid this iteration, the accelerations of the body are not included in the FI calculation: this implicates the neglect of added mass. This choice is justified because during a passing vessel event the accelerations of bodies are low.

3.5. Clipping of panels

The simulated bodies are free to move in six degrees of freedom. When the body moves in vertical direction it moves further into or out of the fluid domain. The free surface is in the calculation of the potential field merely a streamline, as explained in section 3.3.3, over which the moving body is mirrored. The body cannot cross the streamline, since then the bodies will collide. To solve this problem, the panels moving through the free surface are cut at the free surface. This means that a panel or a row of panels moving through the free surface vary in size over time. The collocation point has to be determined every time step before solving the potential field. The cutting of panels at the free surface will be referred to as clipping.

When a panel leaves the fluid domain, the expression for the source strength leaves the calculation. The consequence of this approach is that the source strength vector and thus the influence matrix changes in size over time. This is the reason that the time derivative of the source strength cannot be calculated as $\dot{\sigma}_0 = \sigma_1 - \sigma_0$, but is calculated from the separate derivatives of the influence matrix and the source strength vector.

3.6. Practical notes on implementation and functionality

This module is programmed having some additional functionality compared to other double body flow models used to determine passing vessel interaction. Some limitations follow from the implemented physics, or the approaches to account for free body motions in the simulation. Certain handles are implemented to specifically disable or enable some of the functionality of the FI module. These handles and other practical properties of the FI module are describes in Appendix C.

Captive vs free motion

In conventional programming in which passing vessel interaction is determined, the bodies in the simulation are kept captive. This refers to the fixed degrees of freedom of the bodies, in which the passing body generally has a fixed constant propagation speed over a straight line. Benefits of the conventional programming is that the whole event can be described in the body fixed coordinate system of the passing body. The down side of such a captive model is that an important assumption has to apply: 'the free motions of the vessels do not influence the potential field'. In the FI module the free motions of all bodies are taken into account for the determination of the potential field.

Twisted and triangular panels

The FI module, can deal with panels that have an arbitrary amount of vertices an even a twist in the panel: as long as they are not self-intersecting. Conventional programming often has restrictions concerning the geometry of panels, they only allow for quadrilateral panels. A twisted panel can be taken into account, but the twist will be neglected. A twisted panel is decomposed in two (or more) panels which will have a mean normal and a mean centroid. The twisted panel will after this be considered as a flat panel again, with a normal equalling the mean normal of the decomposed panels and the collocation laying at the weighted mean of these panels centroids as well.

Harbour and bottom geometries

Geometries of ships and harbour are taken into account by implementing panels on which the boundary condition is imposed. In the ROPES programming the mirror technique is used at the bottom as well, to account for shallow water effects. This double mirror implementation comes with the problem of infinite mirror series between the free surface and the bottom. It can be overcome by replacing the infinite mirror problem by a polynomial representation, as implemented in the ROPES software [9]. This polynomial solution was introduced by Grue and Bilberg [2].

Influence matrix taking memory

In the FI module the influence matrix is represented as a matrix-vector multiplication function and solved by a direct solution method. This manner of finding a solution takes a large work memory. Another option is to solve the potential field using iterative processes. The FI module, which is 32bit, has an available work space that allows for a simulation including maximal around 2000 panels. This is quite a restriction, it puts a constraint on the water depth and the amount of simulated bodies at once.

4

Verification

The mathematics introduced in Chapter 3, which is solved in the FlowInteraction module, needs to be verified. This chapter is a summary of the conclusions drawn based on multiple verification cases. These are documented in Appendix B. A more elaborate explanation of the encountered behaviour is found in this appendix. Chapter 5 will describe the validation cases and go deeper into how the simulated results correspond to the force measurement during the ROPES JIP.

4.1. Verification set-up

To verify the model as discussed in the previous chapter, a choice is made to use a barge of $100 \times 30 \times 20$ meters, which basically is a cuboid, as the body in the simulation. This simple geometry is chosen because it allows for predictability of the simulation results and a good reproducibility of the verification cases. Two panel distributions are used over the barge, we will refer to these as a coarse mesh and a fine mesh. The properties of this barge are found in table 4.1. Here the last two columns indicate the panel density on the hull. The average panel size on the coarse mesh is a little below 4×4 meters while the fine mesh is composed out of 2×2 meters panels.

Designation	Barge	Unit	Npanels Coarse	Npanels Fine
Length	100	m	25	50
Breadth	30	m	8	15
Height	20	m	5	10
Draft	10	m	-	-
Displacement	30 750	tonnes	-	-

Table 4.1: Geometric properties barge: panel sizes are approximately 4×4 m (coarse mesh) and 2×2 m (fine mesh)

4.2. Expected FI forces

To gain more insight in the forces provided by the FI module, equation 3.21 (restated in equation 4.1) is analysed. It shows how the provided forces are dependent on the velocity potential. From this it is clear that one part of the forces is dependent on the time derivative and one part on the gradient of the velocity potential.

$$\mathbf{F} = \rho_w \frac{\partial}{\partial t} \iint_S \{\Phi_\infty + \Phi\} \cdot \bar{n} dS + \frac{\rho_w}{2} \iint_S \left\{(\nabla\Phi_\infty + \nabla\Phi)^2\right\} \cdot \bar{n} dS \tag{4.1}$$

The perturbation potential can be expressed in terms of the influence matrix, the velocity vector $\vec{V}$ and the source strength vector. Here the derivative of the velocity potential is determined in terms of these vectors. This is done to gain insight into what simulated behaviour influences, via the velocity potential, the FI forces. Equations 4.2 and 4.3 show the expression for the time derivative and the gradient of the potential, where the velocity potential is expressed in terms of vectors defined in section 3.3.4. The influence vector $\vec{a}$ is defined in

equation 4.4. Note that the difference with respect to the influence coefficients A_{mn}, defined in section 3.3.3, is that $a_m(x,y,z)$ is not determined from the gradient of the perturbation potential.

$$\frac{\partial}{\partial t}\Phi(x,y,z,t)) = \dot{\vec{a}}(x,y,z,t)\vec{\sigma}(t) + \vec{a}(x,y,z,t)\dot{\vec{\sigma}}(t) \tag{4.2}$$

$$\nabla\Phi(x,y,z,t) = \nabla\vec{a}(x,y,z,t)\vec{\sigma}(t) + \vec{a}(x,y,z,t)\nabla\vec{\sigma}(t) \tag{4.3}$$

The free stream is neglected by the FI module, this is seen in verification case B.10.4. The identities shown in equation 4.4 are used for equations 4.2 and 4.3. After substituting the identities in equation 4.4 in equations 4.2 and 4.3, one finds equations 4.5 and 4.6.

$$\begin{array}{rcc} \vec{\sigma} & = & \mathbf{A}^{-1}\vec{V} \\ \dot{\vec{\sigma}} & = & \mathbf{A}^{-1}\dot{\vec{V}} + \left(\dot{\mathbf{A}^{-1}}\right)\vec{V} \\ \nabla\vec{\sigma} & = & 0 \\ \vec{V} & = & -(\bar{u}_m - \bar{\omega}\times\bar{r}_m)\cdot\bar{n}_m \\ \dot{\vec{V}} & = & 0 \\ \vec{a} & = & \frac{\Phi_m(x,y,z)}{\sigma_m} \end{array} \tag{4.4}$$

$$\frac{\partial}{\partial t}\Phi = \dot{\vec{a}}\mathbf{A}^{-1}\vec{V} + \vec{a}\left(\dot{\mathbf{A}^{-1}}\right)\vec{V} \tag{4.5}$$

$$\nabla\Phi = \nabla\vec{a}\mathbf{A}^{-1}\vec{V} \tag{4.6}$$

where:

A is the influence matrix as defined in section 3.3.4;

$\vec{a}$ is the influence (row) vector containing elements as defined in equation 4.4;

$\vec{V}$ is the fluid velocity vector that a panel encounters, this vector is defined in section 3.3.4.

Using equations 4.5 and 4.6 the FI forces can be analyzed in more detail. Both the unsteady term containing the time derivative of the velocity potential) and the kinematic Bernoulli term will be evaluated separately in the following paragraphs.

Influence of unsteady term on force interaction

The simulated events inducing an unsteady force term from equation (see equation 4.7) containing the time derivative of the velocity potential) is derived from the expression in equation 4.5. It is concluded that:

$$\mathbf{F}_{unsteady} = \rho_w \frac{\partial}{\partial t}\iint_S \{\Phi_\infty + \Phi\}\cdot\bar{n}dS \tag{4.7}$$

The unsteady Bernoulli term only leads to forces when multiple bodies with a nonzero velocity relative to each other are simulated (e.g. passing vessel events). The inertia forces based on the own accelerations of the body (read: added mass forces) are part of this force term as well, but are not included in the FI calculation. Note that the mirror condition implicates that there is always a real body and a mirrored body simulated. These bodies influence each other when a motion in the vertical plane is simulated. Only then, the real and mirrored body have a relative velocity with respect to each other.

This conclusion is explained by a brief explanation of the following vectors found in equation 4.5:

$\dot{\vec{a}}$ describes the change in influence over time between a panel and point (x,y,x). This vector is only not zero, $\dot{\vec{a}} \neq 0$, if there is a relative velocity between a point (x,y,z) and the panel. Only forces on simulated bodies are simulated, implicating that in practice this only amounts to a non-zero vector if a relative velocity between panels is simulated;

$\left(\dot{\mathbf{A}^{-1}}\right)$ describes the changing influence between all panels simulated in the fluid domain. Since the bodies are assumed to be rigid this amounts to the situation that $\left(\dot{\mathbf{A}^{-1}}\right) \neq 0$ if there are multiple bodies in the simulation having a relative velocity to each other.

The other parameters in equation 4.5 are nonzero independent of the amount of bodies in the simulation. The unsteady force term describes the fluid inertial forces, but neglects the added mass forces due to own acceleration. The inertia forces, not dependent on the accelerations of the simulated body, will be referred to as cushion forces throughout this thesis.

Influence of kinematic term on force interaction

From equation 4.6 it can be concluded that the kinematic force component (see equation 4.8)is influenced by only three variables. Together they describe the velocity of the fluid at a chosen point in the fluid domain. The event is influenced by all bodies in the simulation: this force component can be nonzero even if only one body is moving in the horizontal plane. Varying fluid velocities lead to pressure variations in the fluid. This is the origin of the forces provided by this force term.

$$\mathbf{F}_{kinematic} = \frac{\rho_w}{2} \iint_S \left\{ (\nabla\Phi_\infty + \nabla\Phi)^2 \right\} \cdot \bar{n} dS \tag{4.8}$$

The velocity of fluid flow is influenced by the following events in a simulation:

$\mathbf{A}^{-1}$ is the position of multiple panels relative to each other, note that it is the inverse influence matrix;

$\vec{V}$ is the velocity of the panels on the body relative to the fluid;

$\nabla\vec{a}$ is the gradient of the influence at the point of interest.

It can be stated that the kinematic force component leads to forces in case of a asymmetric flow field around a body. This leads to two often seen hydrodynamic effects:

- **Squat effect:** the fluid flows faster underneath the body inducing a low pressure. The body is pulled deeper into the water;
- **Bank suction effect:** an asymmetric flow pattern around the body is induced, because at one side the presence of (static or dynamic) geometry disrupts the flow pattern. This asymmetric flow field leads to suction forces to the side of the second geometry. Bank suction effects generally refer to suction interaction between a quay or bank and a propagating ship. In this thesis the name will be used for ship-ship interaction induced by the kinematic Bernoulli term as well.

4.3. Verification of expected FI forces

The expectations listed shortly are verified and documented in appendix B. First the general implementation of the physics is verified. Secondly the properties associated with the FI module are treated. Then some seemingly non-physical behaviour and why it is simulated will be elaborated on. Implemented handles that enables users to exclude forces for computational efficiency are treated in Appendix C.

4.3.1. General implementation

The model is a potential theory based model. This means that the expression found for the fluid domain has to satisfy the Laplace equation at all time instants. A faulty implementation of the potential theory can result in a unsatisfied continuity equation. Verification case B.1 confirms that the Laplace condition is met.

Further the implemented mirror condition at the free surface enables us to solve the fluid domain without imposing the kinematic and dynamic boundary conditions on the free surface. A faulty implementation might lead to simulated errors. Verification case B.2 shows that the free surface is indeed a rigid flat surface with zero flux through it. This indicates a correct implementation.

4.3.2. Properties of module

From simplifications and handles implemented in the FlowInteraction module, described in Appendix C, certain force components acting on the simulated body are expected. These expectations were verified through a set of simulations found in Appendix B. The following behaviour is expected:

- **No fluid-body interaction in the horizontal plane:** Added mass and potential damping are not taken into account. These are the only forces acting in horizontal plane for an event simulated with potential theory. The verification case documented in section B.3 confirms this behaviour;
- **Squat forces:** A downward force underneath the barge due to the kinematic Bernoulli term should be simulated. The verification case documented in section B.3 confirms this expectation.
- **Bank effect:** Bank effects refers to force interaction between a ship and a bank or quay. It consists of suction forces due to the kinematic Bernoulli term and of cushion forces which are inertia forces:
  1. **Bank suction effect:** This effect is also described in section 4.2. From verification case B.10.1 it is hard to verify this force on itself, the kinematic Bernoulli forces blend with the inertia forces, the latter of the two being dominant;
  2. **Bank cushion effect:** Force interaction between two (or multiple) bodies because of accelerated fluid. This fluid inertia force is not related to the acceleration of the ship but rather to the relative velocity between two bodies. This mechanism for force interaction is tested during the validation cases in Appendix **??**, by simulating the passing vessel forces. Verification case B.10.1 confirms the functionality of this force term.
- **Asymmetric fluid flow induced yaw:** to prevent interference of FI forces on manoeuvring forces on ships in aNySIM, the yaw FI moment induced by sway and surge motions is disabled. Manoeuvring effects are already taken into account by empirically based coefficients in a manoeuvring model which is coupled as input to a ship in the simulation. Verification case B.10.3 confirms the expectation that yaw moments introduced by asymmetric fluid flow around a body is neglected.

4.3.3. Peculiar simulated behaviour

When motions are simulated in the vertical plane, referring to forces in the heave, roll or pitch direction, some peculiar behaviour is observed. An example is shown in figure 4.1, here the results of the simulated free heave oscillation of the coarse barge (table 4.1) is shown. In sub-figures (a) and (c) the FI forces acting on the barge are depicted, sub-figures (b) and (d) are the corresponding motions determined by aNySIM by finding a solution to the equations of motion. The applied initial excitation was -5 meters. The barge was only unrestrained in the heave direction. The difference between the two depicted simulated results is the time step size (dt=0.1 s versus dt=0.001 s), which has a significant influence in the obtained results. The unexpected behaviour observed in these simulated results is:

1. The simulated forces and motions in case of a time step of dt=0.1 s are damped, while no mechanisms to allow for damping are implemented in the FI module. When the time step is reduced to dt=0.001 s, the apparent damping is not simulated;
2. A smaller time step leads to spikes in the FI force results, this is clearly visible in figure 4.1c;
3. The mean value of the simulated FI forces is positive, as a consequence the barge emerges further out of the water then the applied excitation (see figures 4.1b and 4.1d). This is non-realistic behaviour.

This behaviour originates from different sources: time step size, discretization problems and the omission of the added mass force leading to non-physical behaviour. The complete verification case study is documented in Appendix section B.6.

Time step minimization

From figure 4.1 (and the full verification case study documented in Appendix section B.6) it is shown that the motions and forces decay over time for a small time step. This behaviour is not simulated when the handle squat is set to "false", indicating it only occurs when the FI calculation is executed.

$$F_{FI} - (m \cdot \ddot{z} + c \cdot z) = 0 \tag{4.9}$$

The solution to equation 4.9, which is the equation of motion solved during the simulation with all force terms written to the left hand side, is visualised for the shown simulated case in figure 4.2 (additional graphs shown in figures B.13c, B.13f and B.13k). If the equation of motion is solved correctly then equation 4.9 has a zero value at every instant in time. It is evident that the is equation of motion is not solved correctly. Some

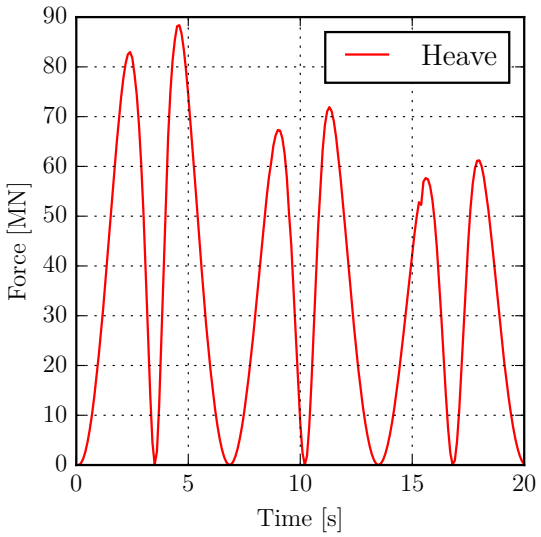

(a) FI force during free heave vibration (dt=0.1s)

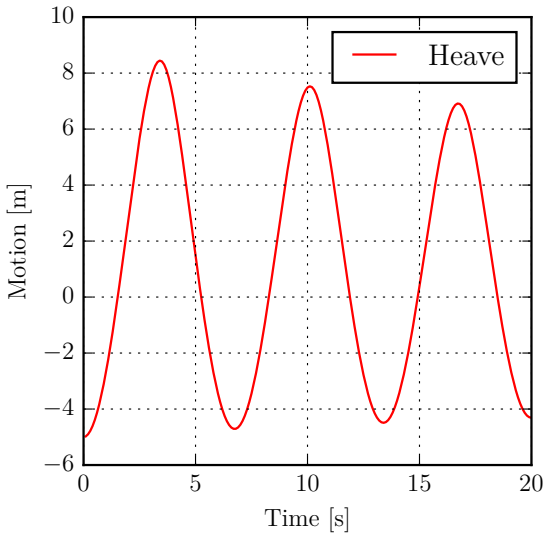

(b) Motions under the acting FI forces (dt=0.1s)

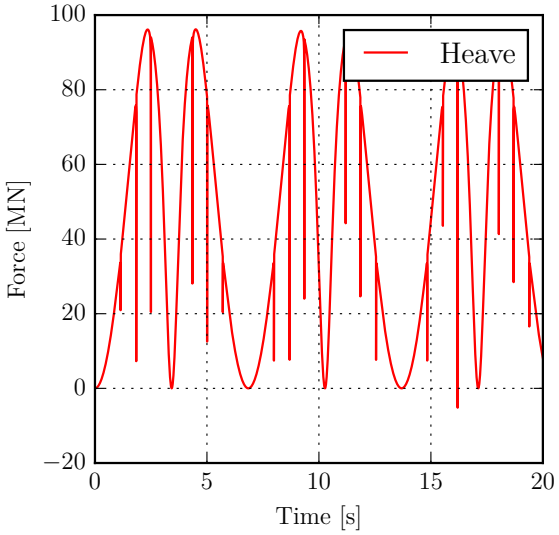

(c) FI force during free heave vibration (dt=0.001s)

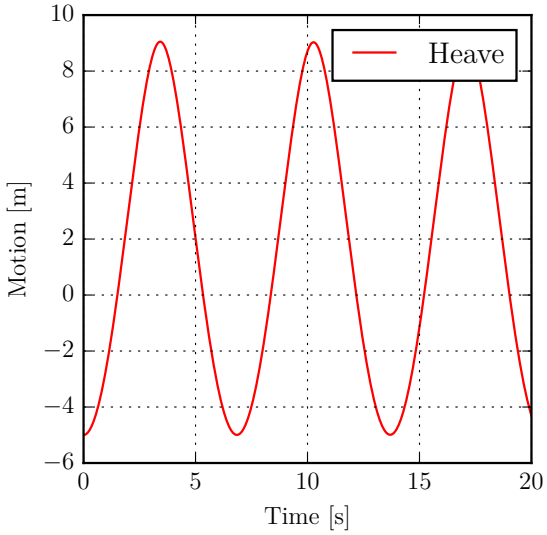

(d) Motions under the acting FI forces (dt=0.001s)

Figure 4.1: An initial excitation of -5 meters is applied to the coarse barge (table 4.1). The FI forces acting (in the heave direction) on the coarse barge due to the motions are found in (a) and (c) with the corresponding motions in (b) and (d). The difference between the two simulated case studies is the time step size: (a), (b) time step of dt=0.1 s and (c), (d) time step of dt=0.001 s. The time step size has a significant influence on the simulated results.

of the simulated FI forces are not accounted for in the motions of the body at a time step larger than 0.001 second. Energy seems dissipated because of this. The error in the solution of the equation of motion follows from a disabled automatic time step adaptation of the (Runge Kutta 2) ODE solver. The FI calculation and the equation of motion are solved in parallel. For time step synchronization purposes the automatic time step reduction is disabled.

Drop of forces

In figure 4.1, which is part of verification case study B.6, an unusual drop in FlowInteraction forces is seen. These spikes are observed in figure 4.2b as well. The behaviour manifests at simulations in which a small time step (e.g. dt=0.001 second) is applied in combination with bodies moving in the vertical plane. The part of the simulated geometry that moves through the free surface gets cut off, this is explained in section 3.5. From figure B.13l it is evident that the unexpected forces occur when a row of panel interfaces move through the

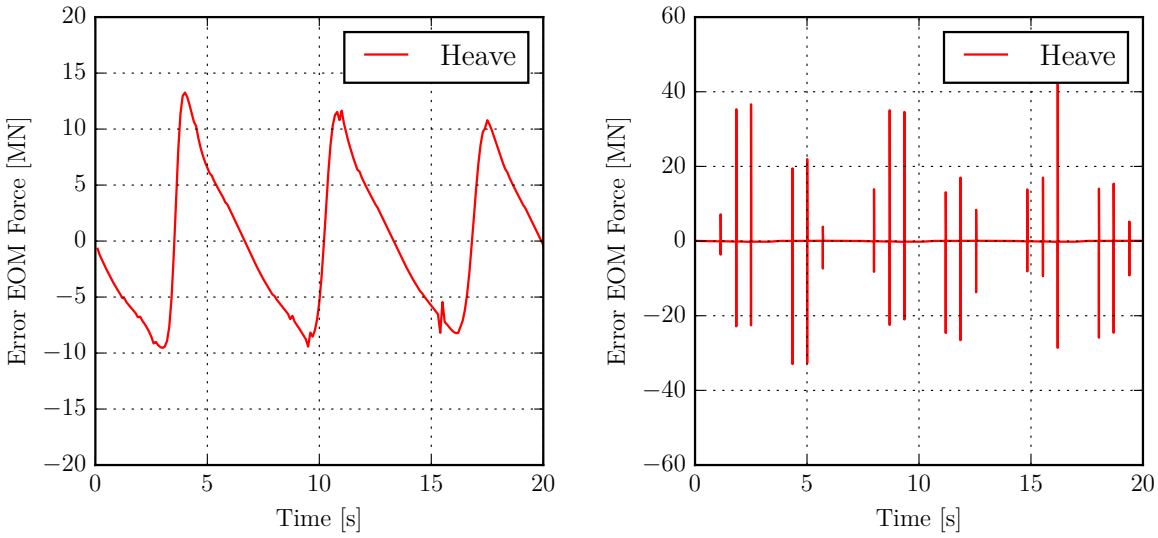

(a) Error solution of EOM free heave (dt=0.1s)

(b) Error solution of EOM free heave (dt=0.001s)

Figure 4.2: The solutions to equation 4.9. If the ODE solver solves the differential equation correctly, then the graph would be a line with zero value at every instant of time. The error in the solution for the time step of dt=0.1 s (sub-figure (a)) indicates that the time step size is to large. Sub-figure (b) shows that the time step size of dt=0.001 s is sufficient to solve the ODE accordingly.

free surface. The panel gets very small due to the clipping near the interface which leads to a numerical error. Verification case B.6 elaborates on this.

Inertia forces between mirrored and real panels

When a body moves through the vertical plane, the mirrored body and the real body influence each other. Mathematics indicates this by the relative velocity between the mirrored and real panel, see section 4.2. Figure 4.1 shows that influence between the mirrored and real panel is indeed present. The FI forces are positive while the kinematic Bernoulli term exerts a suction force. The positive forces are due to dominating cushion forces. The vertical motion allows $\left(\dot{\mathbf{A}^{-1}}\right)$ and $\dot{\vec{a}}$ from equation 4.5 to be non-zero and provide FI forces.

When added mass forces are taken into account, the positive mean induced by cushion forces are compensated. The mean of the simulated FI forces turn negative. The negative mean force is physical and provided by the negative mean force due to kinematic Bernoulli and added mass forces. This overall negative mean force indicates that added mass force has a small non-linearity present. Figure 4.4, which is part of verification case study B.5, substantiates this theory.

Behaviour unrelated to FI-module

Some behaviour encountered during the verification, which is not due to the FI implementation, should be noted. The following is quantified, yet the origin of the problem is not known. It is introduced through modules other than the FI module.

- **Shift of mean motion at forced oscillation:** verification case B.4 shows a negative shift in the mean of the motions of a forced vertical oscillation. The option to forcefully oscillate the barge is introduced through the handle forcedHeavePeriod and forcedHeaveAmplitude of the xsf::BodyOde module. The FlowInteraction forces are positive at any instant in time, see figures B.8 and B.9. This sign is contrary to the sign of the mean shift in motion.

  Figure B.10 shows that the shift in the mean of the forced oscillation is independent of the FI calculation. From this it is concluded that the behaviour is introduced through the already implemented programming. The motion shift seems to be caused by the first time step not being taken into account. The shift in the mean motion in case B.4 seems to be accurately predicted by the following expression $\bar{z} = -\frac{A_z}{2} \cdot \sin(\omega \cdot dt)$. In table B.4, the rule of thumb is verified for five scenarios with different amplitudes, time steps and frequencies. The time step needs to be sufficiently small in order to minimize this

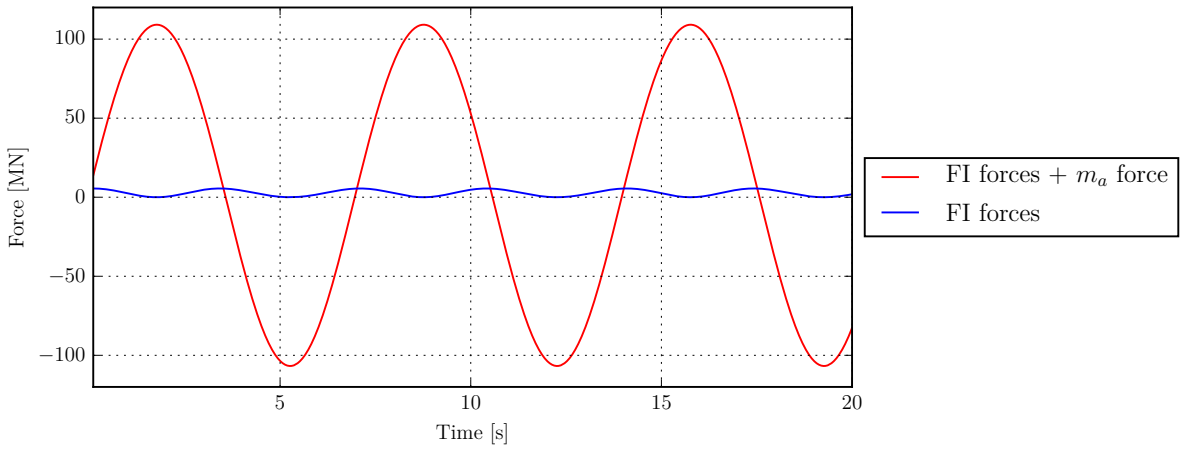

Figure 4.3: FI forces versus FI forces with added mass

Figure 4.4: Simulated results: An oscillating kinematic excitation is applied to the coarse barge (table 4.1) with an amplitude of 2 m and a period of 7 seconds. The FI forces acting on the barge are shown in blue. In red the FI forces with added mass included is shown, which was determined with the acceleration of the barge during the previous time step. The kinematic excitation means that no EOM is solved, consequently the additional forces were not of influence on the motions of the barge.

error;

- **Amplitude half of the applied rotation:** verification cases B.3 and B.8 show that the initial rotational angle before going into free rotational vibration is not equal to the amplitude of the following free vibration. In verification case B.9, in which the FI forces are set to zero, this behaviour is seen as well. From this it is concluded that this behaviour is not introduced through the FI module. The observed behaviour shows that the initial rotation divided by two is equal to the amplitude of the free vibration.

5 Validation

Validation of the FlowInteraction module is done by comparing results from the model tests done during the ROPES JIP with simulated results. In Appendix A information concerning these model tests is documented. The forces and moments acting in the horizontal plane on the moored vessel are evaluated. The results of the simulations and model tests are documented in Appendix **??**.

5.1. Validation setup

To ascertain validation of the FI model, the simulated results will be compared to the measurements done during the model tests which were part of the ROPES JIP. Measurement data from these towing tank tests is provided by MARIN. For the model tests Froude scaling was applied, Appendix A elaborates on the scaled dimensions. In this text the dimensions of the full scale events are stated.

Parameters of the ship models used during the model tests are shown in tables A.3 and A.4. These hull shapes are also used in the simulation. The dimensions of the canal are tabulated in table A.1. The passing distance, keel clearance and quay distance can be found in table A.2. The setup as used during the ROPES JIP model tests was recreated in the simulation. During the model tests the concerned ships were held captive. The loads acting on the ships was measured by a six component measurement frame. The passing ship was forced through the water with a different constant speed and drift angle per model test case. The drift angle refers to a yaw angle of the passing ship. The moored ship was held captive next to a vertical wall which acted as quay.

During the model tests the keel clearance of the passing ship only amounted to 1.04 meter. In order to simulate the bottom, a panelled body needs to be implemented at 14 meters depth. This causes a problem: the distance between to bodies should, as a rule of thumb, at least be the size of the panel. This implicates that a very fine mesh has to be applied on the hull of the passing ship and on the bottom, in order to simulate the situation. The FlowInteraction module cannot simulate this, because the available work memory is exceeded (see section 3.6). To compensate for this problem, the FI module approximates the influence of shallow water by the use of empirical coefficients. The simulation is done for a deep water situation and then multiplied by this shallow water coefficient. This shallow water coefficient is a constant factor dependent on the ratio between the water depth and draft. For validation, the scenarios tested during the ROPES JIP (depicted in tables **??** and **??**), are simulated without a bottom. Simulation results with and without the shallow water coefficients are validated versus the test data. In this way the accuracy of the shallow water coefficients and the trend of the force curve over time is separately validated.

5.2. Expectation

The assumptions made in the mathematical and physical modelling of the FI-modules indicate that certain behaviour will lead to deviations between simulation results and the model test results. The goal of this validation is determining where the line is drawn when it comes to this matter. The following physical mechanisms through which force interaction between the moored and passing ship is established are not all included and might become significant in some of the simulated events:

- **Wash waves:** The Froude number has a direct relation with the wave radiation of a vessel propagating through the water: an expression for the Froude number can be found in equations 2.1 and 2.2. This wave system around the vessel cannot be simulated by the FlowInteraction module. At higher Froude numbers ($Fr \geq 0.3$) the force interaction between the vessels through these so called wash waves are expected to become significant. For high Froude numbers the simulation results are expected to deviate from the model test results;

- **Viscous effects:** If the vessel is moving through the fluid under a drift angle, viscous effects in a real flow get significant. The angle of attack leads to flow separation causing a wake with turbulent fluid behaviour. Inside this wake the pressure is lower [4], this leads to higher interaction forces. The wake will occur on the sheltered side of the vessel;

- **Shallow water vs deep water:** Force interaction between passing ships is higher in a shallow water then in deep water. Since the ROPES JIP model tests were performed in shallow water and the simulations are performed for deep water, the simulated forces on the moored vessel should be significantly smaller in magnitude.

5.3. Evaluation

Two characteristics of the ship interaction are evaluated to validate the FlowInteraction module, namely the force magnitude and the development over time (shape) of the forces. Further the implemented shallow water coefficients to account for shallow water effects are evaluated.

5.3.1. Magnitude forces

From the simulation results of the simulated mooring force magnitude versus tested mooring force documented in Appendix **??**, it is clear that the forces acting on the moored ship in the towing tank test set up are larger than the simulated forces. This behaviour is expected for deep water simulations, yet it can be concluded that the empirical coefficients do not fully correct for this difference. Figures 5.1 and 5.2 help to establish more insight in how the magnitudes of mooring forces measured during the model tests, correlate with the simulated results. The difference between the figures is that the latter one is corrected by the shallow water coefficients. The shallow water coefficient is a factor dependent on water depth over draft, this is the reason that both figures are similar. In these figures the difference between the maximum and minimum values of respectively the simulated versus tested force magnitudes are shown on the vertical and horizontal axis. The simulated results in which 700 panels were used to describe each of the simulated geometries, are used for these figures. This is chosen because it is the most accurate approximation of the real hull shape.

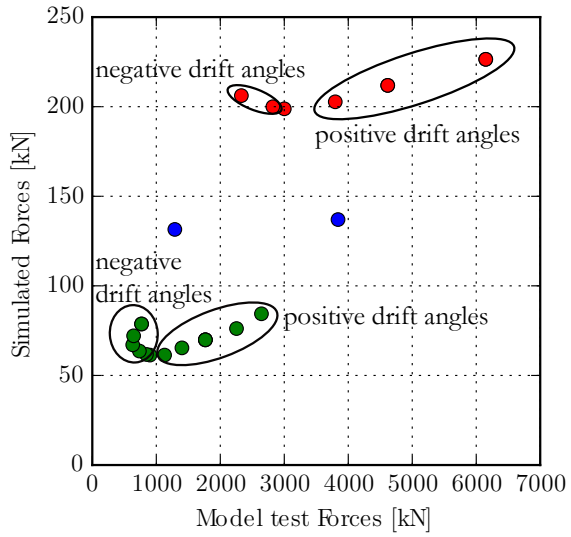

(a) Magnitude difference between max/min surge forces

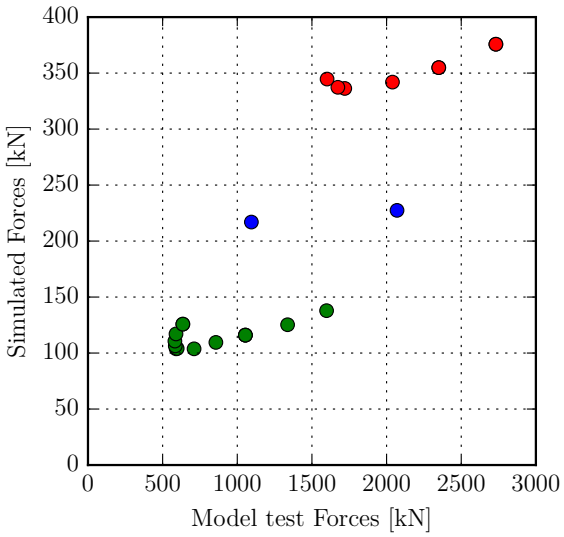

(b) Magnitude difference between max/min sway forces

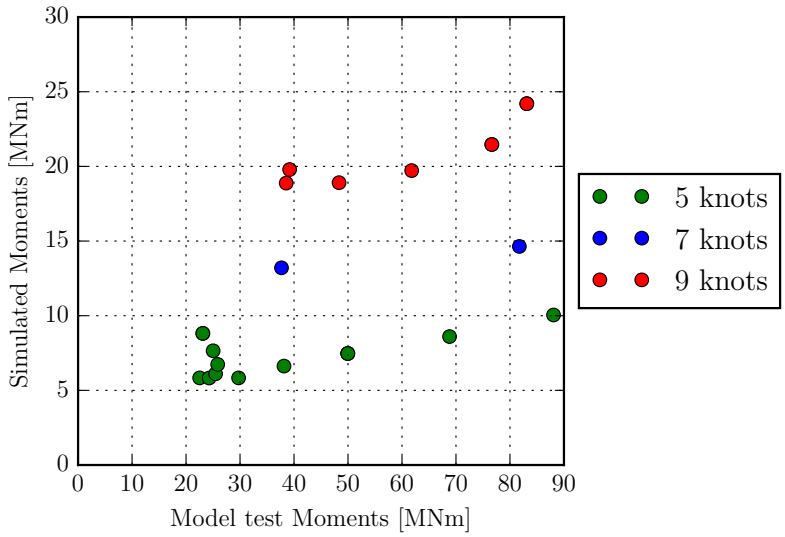

(c) Magnitude difference between max/min yaw moments

Figure 5.1: The absolute difference between the global maximum and minimum in the forces on the moored vessel during a passing event. Shallow water was not taken into account in the simulation, while the model test was done at a (full scale) water depth of 14 meters. The forces in (a) surge, (b) sway and moments in (c) yaw direction are evaluated separately.

If, in figures 5.1 and 5.2, the mooring force magnitudes measured during the model tests and the simulated magnitudes were the same, all dots would line up. To be more specific, if the influence of the drift angles would be the same in both simulation and towing tank test: the dots per passing velocity would be in line. This is not the case, as can be seen in figure 5.1a, where the negative and positive drift angles are circled. The scatter clearly shows in the mooring forces and moments in all directions of the horizontal plane. A general trend in force magnitudes is recognized:

- **Negative drift angles:** these are simulated with a bigger magnitude than in the case of no drift angle, yet a little smaller then the positive drift angle simulations. In the model test measurement, the magnitude of the mooring force was a little smaller for negative drift angles then in the case of the zero drift angle event. The simulation of the magnitude of mooring forces when an event is simulated with a negative drift angle is done incorrectly, as the magnitude grows while it should shrink;
+ **Positive drift angles:** these are simulated with a bigger magnitude than in the case of no or a negative

drift angle. From the model test measurements it is evident that this behaviour is as one would expect, yet a positive drift angle of 15 degree leads to mooring force magnitudes at least twice as high compared to the situation in which no drift angle is applied. This indicates that during the simulations, the full effect of this positive drift angle is not accounted for.

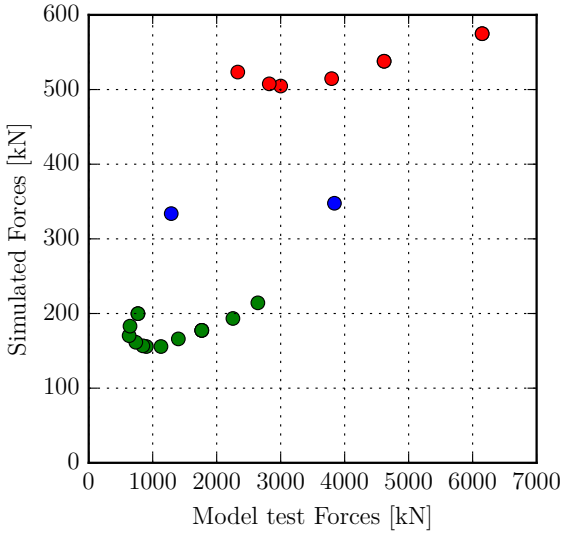

(a) Magnitude difference between max/min surge forces

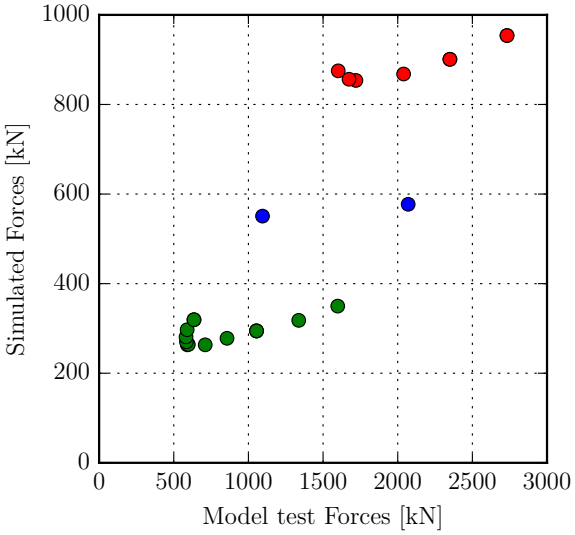

(b) Magnitude difference between max/min sway forces

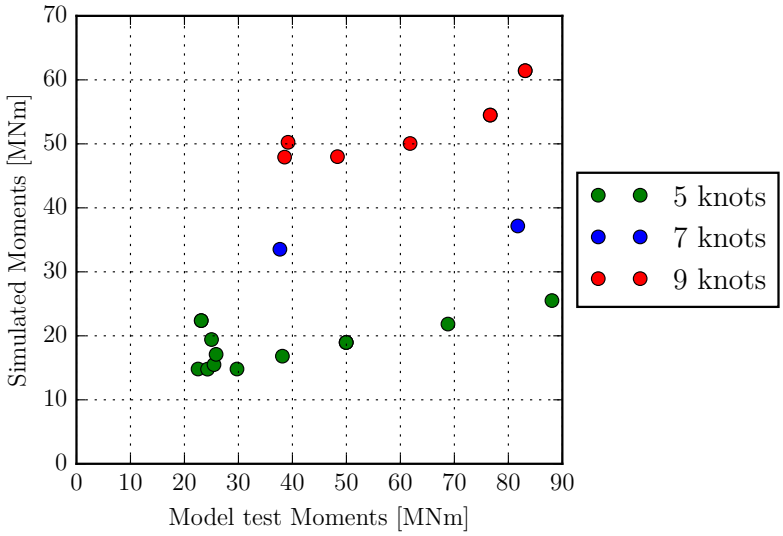

(c) Magnitude difference between max/min yaw moments

Figure 5.2: The absolute difference between the global maximum and minimum in the forces on the moored vessel during a passing event. Shallow water was simulated by applying the shallow water coefficient, the model test was done at a (full scale) water depth of 14 meters. The forces in (a) surge, (b) sway and moments in (c) yaw direction are evaluated separately. The shallow water coefficients do not account for full shallow water effect.

5.3.2. Force development

From the documented force graphs in Appendix **??**, conclusions can be drawn concerning the simulated force development over time and how it compares to the measured forces. Firstly, the results from the model tests and simulations with no drift angle will be discussed, secondly the influence of drift angles, followed by mesh refinement and the fast time approximation is treated.

Passing speed and Froude number

The model test force measurements in the surge direction represented in figure 5.3 (the sway and yaw direction are depicted in figures **??** and **??**), show that for a passing ship moving at a speed of 5 knots (2.57 m/s) in 14 meters of water depth, no free surface effects are present. The influence of wash waves manifests by showing additional oscillations at the start and end of the time trace in the mooring force curve. This behaviour is clearly recognizable looking at the results of the measured test forces of the 9 knots passing speed event in figure 5.3 (more examples in figures **??** to **??**). A passing speed of 2.57 m/s in combination with a water depth of 14 m amounts to a Froude number (equation 2.2) of 0.22 [-]. This finding corroborates with the expectation that free surface effects are negligible for Froude numbers up to 0.3 [-], this is described in Chapter 2. When a ship passes without drift angle and a passing speed low enough to satisfy $Fn < 0.3$ [-], then the mooring forces are simulated with the same amount of maxima and minima occurring at the same instant of time compared to the measured forces from the model tests. The magnitude is not equal, this was already established in the previous section.

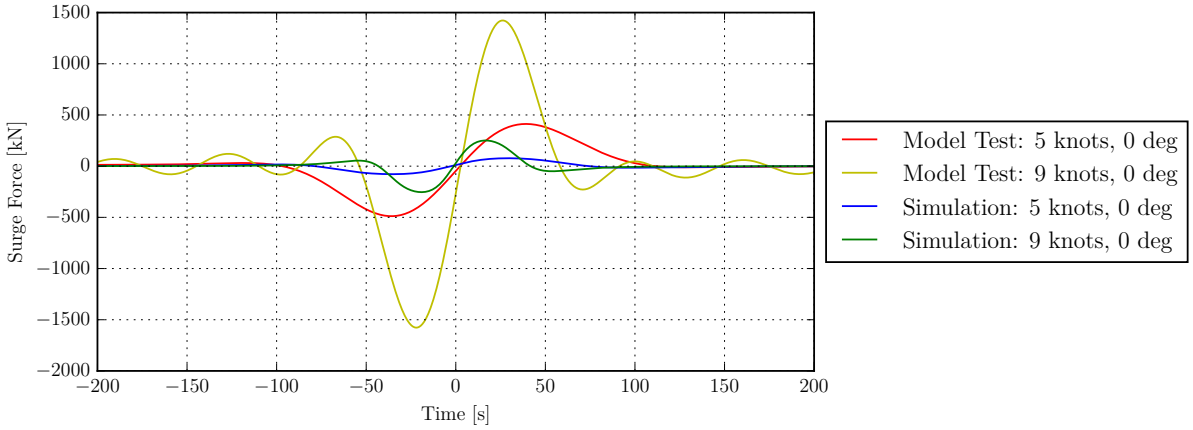

Figure 5.3: Passing ship interaction surge forces at passing speed 5 knots and 9 knots, both the model test and simulated results. Model test results: oscillations at the start and end of the time trace (for the 9 knots passing event) indicates the wash effects. The simulated results include the shallow water coefficient. The drift angle in these events is zero, both of the ship hulls are described by 700 panels.

From the test curve in figure 5.3 (the sway and yaw direction are depicted in figures **??** and **??**) it is evident that when a ship passes at a speed of 9 knots (4.63 m/s), in a water depth of 14 meters, free surface effects are important. The Froude number is 0.40 [-] in this case. This is higher than the Froude number indicated in literature, under which free surface effects can be neglected. In case of a simulated passing event without drift angle but a passing speed of 9 knots, the global maximum and minimum of the model test and simulation results have a small shift compared to each other.

Influence of drift angles

Passing events in which the ship was passing at a drift angle led to deviations in the development of the mooring forces during the model tests. This is evident from the documented figures with mooring forces in Appendix **??**. In figure 5.4 a comparison is made between a passing event where the ship passed with a drift angle of 9 and -9 degree at a passing speed of 5 knots. It is very clear that a negative and a positive drift angle have a different influence on the passing event. The trend that the influence of positive and negative drift angles have on the passing event, in terms of force development, is evaluated:

- **Negative drift angles:** in case of a negative drift angle the passing event gets stretched; it takes longer. The change of sign between the global maximum and minimum shifts to a later time instant then in the passing event without drift angle. If the negative drift angle grows above -6 degrees, the shape of the model test force curve is composed out of extra peaks with significant magnitude which are not simulated. The trend under a significant negative drift angle is simulated poorly, especially the shift of the global maxima and minima of the simulated results compared to the tested results;

+ **Positive drift angles:** a positive drift angle influences the force development less than a negative drift angle. The governing influence of a positive drift angle is the increase in force magnitude. For large

drift angles the development of the mooring force has the change of sign between the global maximum and minimum at an earlier moment in the passing event. This is shown by figure 5.4 (and figures **??** till **??** and by figures **??** till **??**).

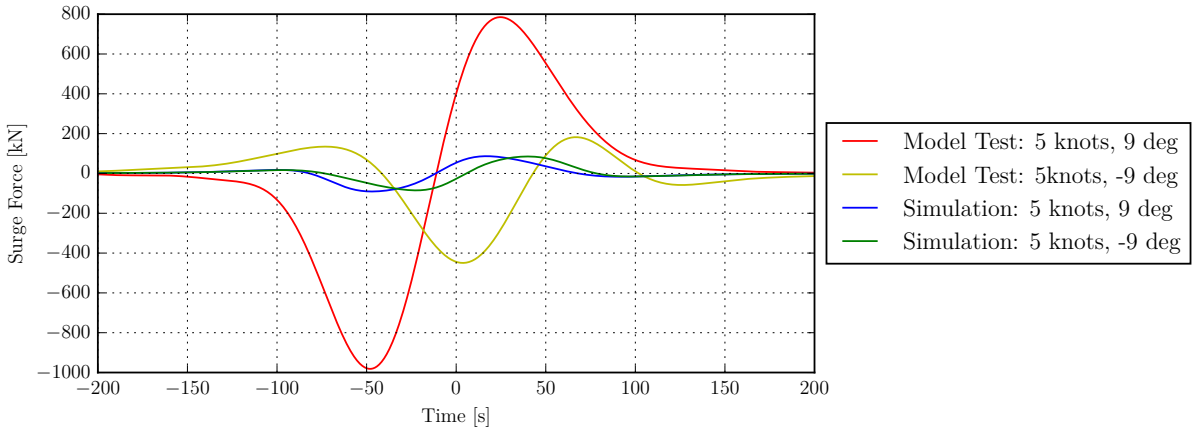

Figure 5.4: Passing ship interaction surge forces at passing speed 5 knots and a drift angle of ±9 [deg], both the model test and simulated results. The simulated results include the shallow water coefficient, both of the ship hulls are described by 700 panels.

Panel sensitivity

Simulation accuracy is influenced by the amount of panels used to describe a geometry. The more panels on a body, the closer the approximation will come to the outcome of a continuous problem. It can be stated that for the most accurate simulation results the amount of panels used to describe the body should be infinite. After a certain amount of panels the influence of a finer mesh on the results is negligible. From the results documented in Appendix **??** it is found that this convergence happens at less than 300 panels per body.

Fast time simulations - direct handle

The fast time (FT) simulation, which is done when the Direct handle is set to "true", has a big influence on the results. The simulation becomes much faster because the hull shape is approximated by 11 polygons. In section C.2 this handle is elaborated on. The results of the fast time simulations contain additional local maxima and minima, as evident from the results in Appendix **??**. These additional maxima and minima are explained by two mechanisms:

1. The first reason for inaccuracies in a very coarse hull mesh (as is the case during a FT approximation) is due to the implementation of a zero order panel method. The source strength is assumed to be constant over the whole panel, yet it is determined based on the condition in its collocation point. In general it can be stated that a smaller panel will be better approximated by a constant source strength than a larger panel. A simulation in which geometries are approximated with more panels leads to a more accurate source strength distribution over the whole geometry;
2. The second reason for inaccuracies of the FT approximation is due to decay of the source strengths over distance. In figure 5.5 the effect of mesh refinement in a two dimensional space is explained. On the left side in figure 5.5, a situation is sketched with two panels, on the right side this same length is modelled using four panels. The dotted rounded lines are the lines of equal source decay. These lines of equal decay are rounded since the source strength decays with $\frac{1}{r}$. Assume that these panels are located on the side of the passing vessel and that the blue line indicates the distance at which the passing vessel passes the moored vessel. When the ship passes by the moored vessel the influence of a finer meshed hull will develop more continuously and thus more smoothly, so that the source influence of the passing ship is more equally distributed over the hull of the moored ship.

The panel density on the hull before the FT algorithm is applied has influence on the FT simulated results. This is especially clear when the simulated results for shallow water events in Appendix **??** are evaluated. The applied algorithm to simplify the geometry is the reason for this. Appendix C elaborates on this.

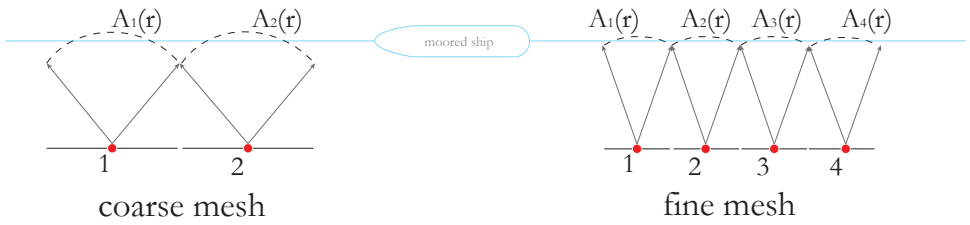

Figure 5.5: Direct handle; additional local minima and maxima in force interaction

5.4. Conclusion

The FlowInteraction module is a fast simulating module for simple passing events. The amount of panels in the simulation should be kept as low as possible within the required accuracy limits. The visualisation tool of aNySIM, in combination with the direct handle (for fast time simulations) is a convenient way of visualising the whole simulation in a matter of seconds and to visually verify if the input parameters are set correctly in order to describe the passing event as intended.

From the simulations it became clear that certain behaviour is not simulated as observed during the model tests. Based on the separate evaluation of the force magnitude and the force development over time, the following is concluded:

- **Shallow water coefficients:** Shallow water simulations result in a systematic underestimation of the mooring forces. The shallow water coefficients do not properly account for the influence of shallow water on a passing event;
- **Drift angles:** Drift angles in the FI module are not accounted for in a manner that corresponds with reality. For small drift angles between $-6 \leq \psi \leq 6$ [deg] the difference in mooring forces are kept to a minimum. At much larger drift angles ($\psi > \pm 6$) the growth in mooring force magnitude in the model tests is very different than in the simulations. A negative drift angle mostly affects the time history (shape of the curve) during the passing event. The governing differences in case of positive drift angles are in the magnitude of the mooring forces;
- **Froude number:** Events with a large Froude number are not simulated correctly through a double body flow model like the FI module. This conclusion corroborates with the theory stated in literature (see van den Boom et al [13]) that free surface effects get significant at passing events with a Froude number $Fn \geq 0.3$.

It is not recommended to use the FI module for shallow water calculations since this will result in a significant underestimation of the interaction forces. The use is further restricted to passing events happening at a Froude number lower than 0.3 and simulated drift angles between $-6 \leq \psi \leq 6$.

6 Conclusion

This chapter states the conclusions drawn based on the findings in this master thesis. Appendix C states practical recommendations for users of the module. Recommendations for further improvement of the module are included in this chapter. Chapter 7 states a discussion on the implemented physics in the FI module.

6.1. Main conclusions

The modular hydrodynamic simulation tool aNySIM, gains new functionality through the FlowInteraction module. This module extends the possibilities of aNySIM to the calculation of passing vessel interaction forces by means of potential theory. The aim of this module is the simulation of passing vessel events. In existing software the simulation does not allow for free motions of bodies. In these simulations it is assumed that the free motions of the vessels have no influence on the total force interaction. In the FI module, this assumption is not made. The implemented physics is assessed through various verification and validation cases. The research shows that the intended physics is implemented correctly in the FI module. It is able to simulate free motions using the double body flow method, but oscillations through the vertical plane often lead to non-physical behaviour. The main conclusions drawn from the work done in this thesis are discussed in the following paragraphs.

6.1.1. Inertia forces

Oscillations with significant accelerations through the vertical plane are dominated by added mass forces. If added mass is neglected, the event is dominated by non-linear cushion forces. The mirroring condition implicates that there is always a real body and a mirrored body simulated. These bodies only have a nonzero velocity relative to each other when motions in the vertical plane are simulated. Therefore, for a simulated event with a single body, the cushion forces are only simulated when the body moves in the vertical plane. It produces a mean over pressure under the geometry. This upward force leads to a non-physical response of the simulated body. Added mass and the kinematic Bernoulli term together compensate this mean upward force. The added mass force contains a small non-linear harmonic force term leading to a negative mean of this force.

6.1.2. Discretization error

A panel moving through the free surface needs to be clipped, to not interfere with the mirrored counterpart. When panels have a height to width ratio approaching zero, unstable behaviour is present. This manifests itself as spikes towards zero in the simulated FI forces. This discretization error is only present for small time steps. This allows the panel to get clipped very close to the interface between panels.

6.1.3. Time step minimization

For time step synchronizing purposes between the FI module and the ODE solver, the automatic time step reduction of the ODE solver is disabled. Oscillations through the vertical plane, where the FI forces are quadratic, are not solved at the usual time step choices. This might lead to seemingly damped behaviour. A manually set time step, set small enough, leads to a correct solution of the equations of motion.

6.1.4. Force interaction passing ships

From the validation cases it is concluded that the interaction forces are composed of the correct force terms. Drift angle effects and high speed passing events are not solved accordingly. This corroborates with expectations drawn from literature studies. The implemented shallow water coefficients do not account for the full shallow water effect.

6.2. Recommendation on further development

The recommendations for further development of the FI module are directly derived from the main conclusions:

- **Include added mass:** the dependency of the body accelerations on the added mass forces and vice versa has as a consequence that at every time step an iterative process is needed until the value found for the acceleration converges. In the current version of the FI module the added mass force is neglected, to implement it the accelerations of the body at that time step need to be included in the unsteady term of the FI forces. The potential damping cannot be simulated by a DBF model, this poses a problem and is discussed in Chapter 7. Because the iterative process to determine the added mass forces leads to a more time consuming simulation, the user should be free to choose whether to include it in the simulation or not. It is recommended to disable all self-inflicted forces on a body (the added mass, cushion and kinematic Bernoulli forces) in case the added mass force is not included, this to prevent the non-physical upward forces from being simulated. The interaction forces induced by the passing event can still be simulated when the self-inflicted forces are left out;
- **Solve clipping error:** the error in FI forces due to clipping leads to comparable spikes in the acceleration at the concerned time step. The time step is so small that this does not lead to a significant error in the response. If added mass is taken into account, this error in the acceleration is amplified. A possible solution: when a panel is clipped till less then 5% of its original height, include it with the panel it has the largest interface width. In this manner the panels will not get small enough to provide an error;
- **Activate the adaptive time stepsize of the ODE solver:** by enabling the automatic time step reduction of the ODE solver, the program becomes more user friendly. The whole problem does not need solving with a very small time step, which cannot be evaded when the adaptive time stepsize is disabled. Enabling it, is expected to lead to a faster simulation compared to one solved with a continues very small time step. The time step reduction will influence the time step in the FI module to keep them synchronized. For every automatic time step reduction of the ODE solver, the FI forces need to be re-calculated. Therefore it needs to be verified whether automatic time step reduction leads to a faster simulation;
- **FI shallow water applicable:** the harbour geometry is now simulated as a panelled geometry, this is computational inefficient since it increases the number of unknowns. This provides problems with available work memory in the current version. Two methods are proposed to take the harbour geometry in a more computational efficient manner into account:
    1. Reduction of the computational effort can be done by exploiting more symmetry effects. It is recommended to model the quay using the same mirroring principle as is currently used at the free surface. When a more complex quay shape needs to be simulated, it can be implemented as a panelled geometry. Shallow water effects can be taken into account by mirroring as well. A problem encountered when a zero normal flux through by mirroring over both the free surface and the bottom is that this leads to an infinite series of mirrored singularities which has a slow convergence for small water depths. Grue and Biberg [2] provided a polynomial expansion to replace the infinite mirror series. I recommend to look into this in more detail;
    2. The influence matrix represented as a matrix-vector multiplication function can be solved by a direct solution method (LU decomposition) or by an iterative solver. The computational effort involved with iterative solvers is quadratic in the number of unknows, while for direct solver the effort is a cubic function of the number of unknows [4]. Direct solvers are shown to be faster for a problem with a small number of unknowns, this is quantified by Journee as 300-600 unknowns [4]. For an iterative solver, the FI calculation is not limited any more by the available work memory. Since the FI module will employ multiple bodies and geometries, it is recommended to look into the use of an iterative solution method.

7

Discussion

7.1. Radiation forces

The double body flow method provides a good approximation of the fluid pressures induced by the primary wave flow around the passing ship in a very time efficient way, yet a lot of assumptions have to be made. The neglect of free surface effects poses a problem with finding the radiation forces. In the current applications of the DBF model radiation forces are found through a frequency domain diffraction calculation with a conversion to the time domain solution using the Cummins equation. As a consequence these radiation coefficients are time invariant, the significance of this assumption on the response of the moored ship during a passing vessel event is to this author's knowledge unknown.

The amount of assumptions for a DBF model makes it seem a rather inaccurate method. On the other hand, research has shown that the DBF method leads to good approximations of the interaction forces and during the ROPES JIP it was shown to lead to quite accurate estimations of the response of the moored ship [8]. The neglect of time variability of the radiation coefficients and the assumption generally made in frequency domain diffraction calculations of a constant (mean) wetted surface make that the DBF method is limited in its accuracy to estimate the response of the moored ship. By including a diffraction calculation directly in the time domain to find the radiation forces, the accuracy will presumabily be enhanced but it is expected to increase the simulation time. In order to make a definitive statement on this, it needs to be further investigated. It is discussable if the computational efficiency that is gained through the made assumptions in a DBF model, makes up for the inaccuracies. Based on results of previous research by Korsmeyer et al [6], Pinkster [11] and the ROPES JIP [8], [13], the author feels it is an acceptable trade off and a valid method to make a good and quick estimation of the response of the moored ship. Taking the motions of the moored ship into account might improve the accuracy of the DBF model, without loss of the time efficiency goal on which the choice for a DBF model is often based.

7.2. Influence of body motions in a DBF model on the interaction forces

Part of the ROPES JIP were multiple model tests to create a numerical approach based on the DBF method, solving the motions in a two step approach: first calculating a time trace of excitation forces and in a second step finding the response of the moored ship by coupling this to an EOM established using a frequency domain diffraction calculation with a conversion to the time domain by the Cummins equation (method discussed in Chapter 2). One of the conclusions of the ROPES JIP was that the calculation of the motions by this decoupling of interaction forces from the ship response leads to accurate results [8]. This conclusion was based on the following compared data:

1. Motion measurements from model tests, where the moored ship was moored with springs and dampers;
2. Captive model tests where the interaction forces were measured, the motions were derived in a second step by use of the Cummins equation;
3. The interaction forces were calculated using the DBF model called ROPES. Here the motions were derived in a second step by use of the Cummins equation as well.

The passing ship passed by in a straight line with a passing speed of 9 knots. The setup was as described in Appendix A. The motions determined by results from approach 2 and 3 agreed better in shape with each other then either of them did with the measured results of approach 1. After discussing this with the main author of the ROPES report [8]; we believe that the neglect of the influence of the motions of the moored ship on the interaction forces is part of the reason for this difference.

To the author's knowledge, no research on the influence of the motions of the moored ship on the interaction forces is available. The results of the above described comparison showed that mostly the timing of the calculated response was not same as the timing of the measured response. It would be very interesting to find out how significant the influence of the motions of the moored ship are on the interaction forces and in what situations this decoupling of interaction forces from the moored ship response is unacceptable. A proposed method to do this is to compare the results from:

1. Motions calculated by the FI module on an unrestrained moored ship, finding the solution to the moored ship response at every time step using a frequency domain diffraction calculation with a conversion to the time domain using the Cummins equation;

2. Calculate the time trace of the interaction forces on a fixed moored ship using the FI module. Then finding the response by coupling the time trace to the equations of motions (established by the Cummins equation).

In this approach; mooring system induced stiffness and damping have to be included in the equations of motion. The passing ship is recommended to be simulated following a straight path. The influence of the assumption of time invariant radiation coefficients is in this way excluded from the comparison. The difference between the two results will purely be due to the influence of the motions of the moored ship on the interaction forces.

A

ROPES model test data

To ascertain validation of the FI model, the simulated results will be compared to the measurements done during the model tests from the ROPES JIP. Measurement data from these towing tank tests is provided by MARIN. The events tested during these towing tests, are simulated with the FI module. For this validation the meshed hull shape of the same vessels is used. Froude scaling is applied for the ROPES model tests, see the test report [7] and figure A.3 for details about the test set-up. An brief overview of the ROPES JIP model tests executed by MARIN will be provided in this appendix.

A.1. Test set-up

The scale of the model test was based on the available models from the MARIN stock, resulting in a scale of 1:38. The unscaled water depth during the model tests was 14 meters, it was chosen to leave 25% keel clearance of the moored vessel and a keel clearance of 1.04 m of the passing vessel. The basin dimensions are to be found in table A.1. The vessels faced the same direction during these model tests.

Dimensions of Basin	Model Scale	Channel Size (real)	Unit
Length	220	8360	m
Channel width	15.8	600.4	m
Water depth	0.37	14.0	m

Table A.1: Properties of the canal as used during ROPES model tests [7]

During the model tests a container vessel was moored with its port side to the basin wall, which acted as vertical quay. The distance between the vessel side and the quay was 3 meters. The distance between the starboard side of the moored container vessel en port side of the passing vessel was 1.5 times the beam of the moored vessel, this corresponds to 48.45 meters. These parameters are summarised in table A.2.

Porperties passing event	Model Scale	Channel Size (real)	Unit
Keel clearance moored vessel	0.093	3.50	m
Keel clearance passing vessel	0.027	1.04	m
Passing distance	1.275	48.45	m
Quay-vessel side distance	0.0789	3.00	m

Table A.2: Properties of the vessel placement [7]

A.2. Scale models

Both models were made of wood and fitted with a single passive propeller and rudder. The passing vessel was a typical tanker shaped vessel with a large block coefficient and displacement. This model was rigidly connected to the basin carriage such that the loads acting on the passing vessel can be measured by means

of a six component measurement frame. Such a frame enables the measurement of all forces and moments acting on the vessel. The passing vessel can be rotated around the heave axis (yaw) inducing a drift angle. This was done to recreate navigation of large vessels through the harbour when large wind forces are present, since this might lead to small drift angles. This drift angle is chosen to be positive when the bow of the passing vessel is turned towards the moored vessel, this coincides with the defined coordinate system in this thesis. Table A.3 gives an overview of parameters of the passing vessel, a visualization is given in figure A.1.

Designation	Notation	Model scale	Prototype	Unit
Length between perpendiculars	L_{pp}	5.64	214.3	m
Breadth moulded on waterline	B	0.974	37.0	m
Draught at FPP	T_f	0.342	13.0	m
Draught at APP	T_a	0.342	13.0	m
Displacement mass in seawater	Δ	1.54	86.562	tonnes
Block coefficients	C_b	0.82	0.82	-

Table A.3: Passing ship model used in towing tank test during ROPES JIP [7]

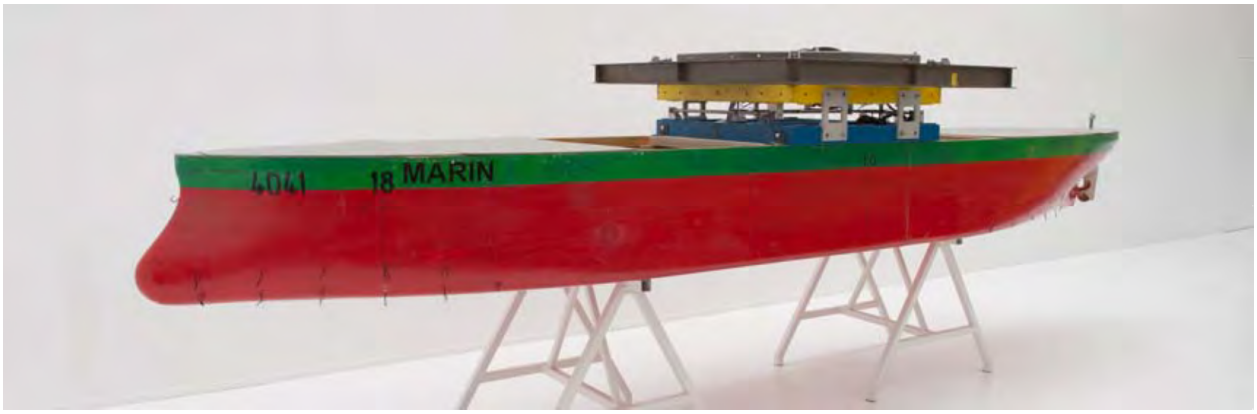

Figure A.1: Passing ship - tanker vessel [7]

The moored ship was a Korean standard container vessel, depicted in figure A.2. This vessel was hold captive during the event, at three meters (0.0789 scaled meters) from the quay, by the same mechanism as the passing vessel, measuring the forces and moment in all six degrees of freedom. The properties of this ship are summarised in table A.4. An overview of the whole setup is provided in figure A.3.

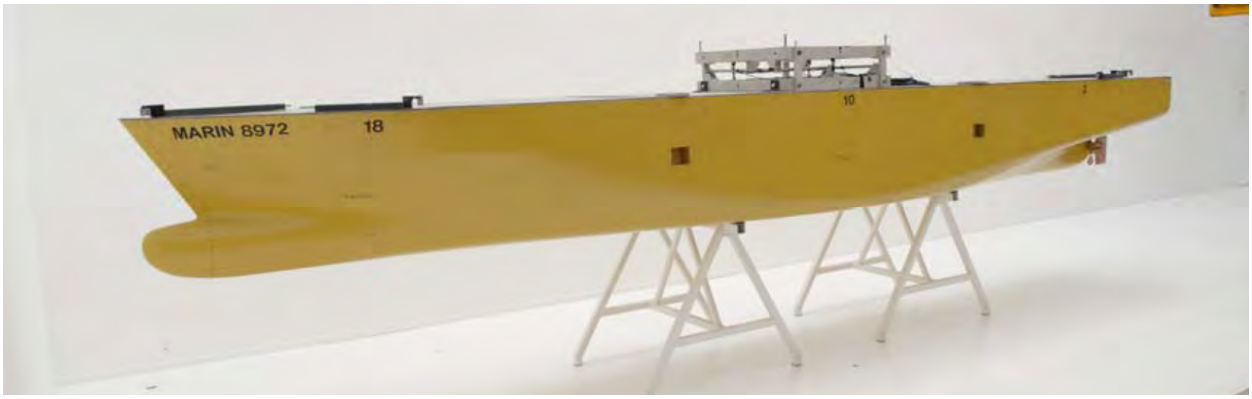

Figure A.2: Moored ship - Korean standard container vessel [7]

Designation	Notation	Model scale	Prototype	Unit
Length between perpendiculars	L_{pp}	6.06	230.1	m
Breadth moulded on waterline	B	0.566	32.3	m
Draught at FPP	T_f	0.29	11.2	m
Draught at APP	T_a	0.29	11.2	m
Displacement mass in seawater	Δ	1.00	56.334	tonnes
Block coefficients	C_b	0.66	0.66	-

Table A.4: Moored ship model used in towing tank test during ROPES JIP [7]

A.3. Data from model test

The measured properties of interest are the mooring forces in different passing events. The drift angle of the passing ship was varied between -15 and 15 degrees throughout the model tests. The exact passing velocities in combination with the passing drift angles are found in table **??**. Validation of the numerical model will be done based on this set-up and a panelled version of the above describes hull shapes. For validation purposes the moored ships will be simulated captive in the numerical model, this is done to recreate the event tested in the model test.

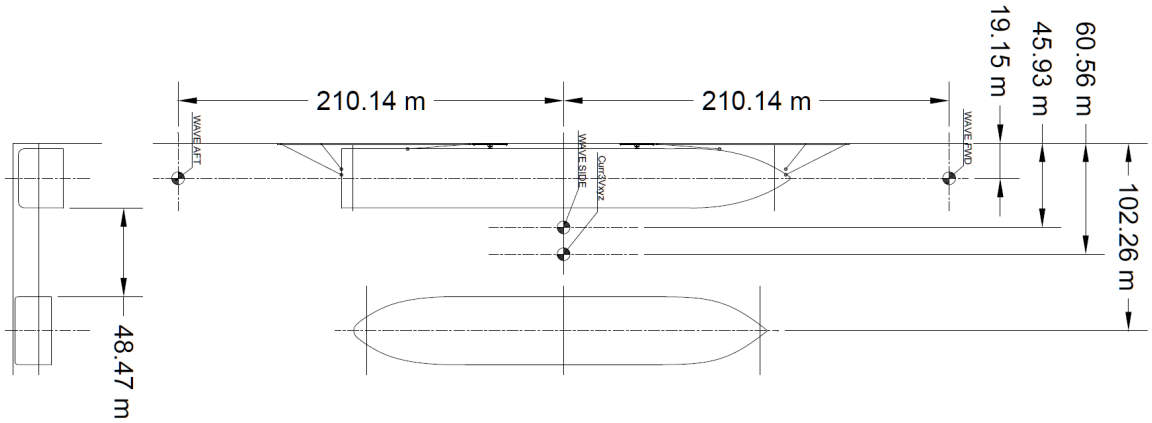

Figure A.3: Overview of the model test set up ROPES at MARIN [7]

A.3.1. Drift angle

Influence of drift angles is tested during the ROPES JIP because a vessel with a large exposed wind area (e.g. a large container ship) under high wind load and propagating with a low speed can be pushed under a small yaw angle. The broad range of drift angles is chosen because there is no data confirming a common drift angle. Based on observations of terminal personnel and observations during the ROPES JIP real scale measurements, these drift angles were observed. No extensive documentation on drift angles is available. Only 43 real passing events are documented in which the drift angles were measured. Tables A.5 and A.6 give an overview of measured drift angles during full scale measurements, respectively in August 2013 on the Caland Canal and in August 2012 on the Oude Maas river near Puttershoek (both in the Netherlands). A positive sign of the drift angle indicates a yaw angle at which the bow of the passing ship is turned toward the moored ship. From this data is concluded that drift angles between 3 and -3 degree are not exceptional, larger drift angles seem based on this data seldom encountered. Note that due to a small sample size this data cannot provide a sufficiently accurate conclusion about drift angles in general. Further the drift angles will vary per season and location, both measurement cases were executed during summer in the region Rotterdam.

Note that the drift angle is a result of a low propagation speed of the passing vessel and a large wind exposed area. When the propagation speed is higher then the drift angles will reduce, but the propagation speed will exceed the speed limits and regulations. Both speed and drift angle have a negative influence on the force interaction between ships.

Range ψ [deg]	$-2 \leq \psi < -1.5$	$-1.5 \leq \psi < -1.0$	$-1.0 \leq \psi < -0.5$	$-0.5 \leq \psi < 0$	$\psi = 0$
N observations	3	1	4	1	1
Range ψ [deg]	$0 < \psi \leq 0.5$	$0.5 < \psi \leq 1.0$	$1.0 < \psi \leq 1.5$	$1.5 < \psi \leq 2.0$	-
N observations	1	4	2	2	-

Table A.5: Drift angle observations August 2013 - Caland Canal [15]

Range [deg] ψ	$-3.0 \leq \psi < -2.0$	$-2.0 \leq \psi < -1.0$	$-1.0 \leq \psi < 0$	$\psi = 0$
N observations	2	2	0	0
Range [deg]ψ	$0 < \psi \leq 1.0$	$1.0 < \psi \leq 2.0$	$2.0 < \psi \leq 3.0$	$\psi = 4.8, 5.8, 10$
N observations	5	1	1	1,1,1

Table A.6: Drift angle observations August 2012 - Oude Maas river near Puttershoek [14]

B

Verification cases

This Appendix is an elaboration on chapter 4 and will describe the test done to support the statements made in Chapter 4. In these verification cases use is made of a barge: this because of the simple geometry for easy reproduction of the verification cases and good predictability of the simulated behaviour. Properties of this barge can be found in table B.1. When use is made of another geometry or panel density this will be explicitly stated. The forces evaluated in the verification cases are only the forces provided by the FlowInteraction module. Table B.2 shows the default setting of the FI handles in the verification cases, when different settings are applied this explicitly stated. The ODE is solved by a Runge Kutta 2 ODE solver, this is the default ODE solver used in aNySIM.

Designation	Barge	Unit	Npanels Coarse	Npanels Fine
Length	100	m	25	50
Breadth	30	m	8	15
Height	20	m	5	10
Draft	10	m	-	-
Displacement	30 750	tonnes	-	-

Table B.1: Geometric properties barge: panel sizes are approximately 4 × 4 m (coarse mesh) and 2 × 2 m (fine mesh)

Handle	**Input possibilities**	**Value**
enableVisualisation	"true"/"false"	"true"
soifactor	value	100.1
perturbCurrent	"true"/"false"	"true"
direct	"true"/"false"	"true"
squat	"true"/"false"	"true"
vmin	value	0
banksuction	"true"/"false"	"true"

Table B.2: Set simulation properties (FI handles)

B.1. Laplace Equation

Objective: Verify if the Laplace continuity equation is satisfied;

- **Result:** As expected;
- **Objects:** Single barge (coarse mesh);
- **Simulation time:** 203 seconds (29 periods) with a time step of 0.1 second and 0.01 second;
- **Criteria:** The fluid domain should satisfy the Laplace equation, this is a consequence of the applied potential theory. The measurement points are defined in the shape of a cube. The length of the ribs are

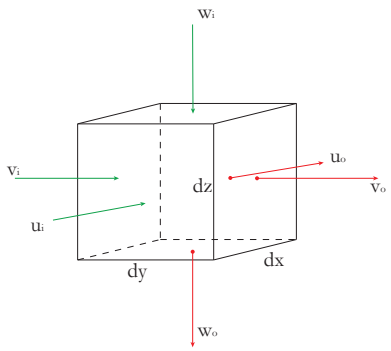

Figure B.1: A control volume with a fluid flowing in and out from 3 sides with velocities $u_{in}, u_{out}, v_{in}, v_{out}, w_{in}, w_{out}$

reduced over three simulations, this to see if the solution converges to zero. Further the influence of time step reduction is evaluated.

During this simulation a small control volume underneath the barge is monitored, while a oscillatory kinematic excitation is applied to the barge with a period of 7 seconds and an amplitude of 2 meters. The barge is simulated as single body in a semi-infinite fluid domain. The barge is restrained in all directions except for the heave direction. The control volume is placed three meters underneath the hydrostatic equilibrium of the keel of the barge. The coordinates of the measurement points are (in the earth fixed coordinate system) in the three different simulated events:

- [-0.5;-0.5;-13.0], [-0.5;0.5;-13.0], [-0.5;0.5;-14.0], [-0.5;-0.5;-14.0], [0.5;-0.5;-13.0], [0.5;0.5;-13.0], [0.5;0.5;-14.0], [0.5;-0.5;-14.0]
- [-0.05;-0.05;-13.0], [-0.05;0.05;-13.0], [-0.05;0.05;-13.1], [-0.05;-0.05;-13.1], [0.05;-0.05;-13.1], [0.05;0.05;-13.0], [0.05;0.05;-13.1], [0.05;-0.05;-13.1]
- [-0.005;-0.005;-13.01], [-0.005;0.005;-13.0], [-0.005;0.005;-13.01], [-0.005;-0.005;-13.01], [0.005;-0.005;-13.0], [0.005;0.005;-13.01], [0.005;0.005;-13.01], [0.005;-0.005;-13.01]

The Laplace equation (3.2) states the fluid flowing into the control volume should be at any instant equal to the out flowing fluid. The expression in equation B.2 is graphically represented in figure B.2. Here the measurements from the surface of the control volume, which is visualised in figure B.1, are used to verify if equation B.2 is satisfied. Per plane nine measurement points are present, symmetrically placed on the ribs and in the center of the plane. The ribs of the control volume are varied between 1 meter, 0.1 meter and 0.01.

$$\frac{du}{dx} + \frac{dv}{dy} + \frac{dw}{dz} = 0 \tag{B.1}$$

$$\frac{u_i - u_o}{dx} + \frac{v_i - v_o}{dy} + \frac{w_i - w_o}{dz} = 0 \qquad dx, dy, dz \rightarrow \frac{1}{\infty} \tag{B.2}$$

Conclusion

For $dx, dy, dx \rightarrow \frac{1}{\infty}$: the Laplace equation converges towards 0 [s^{-1}], meaning that equation B.2 is satisfied. For larger ribs the solution oscillates with a significant amplitude around zero, this is due to the low density of measurement points on a relative large plane. Time step reduction is shown to have no influence on the results.

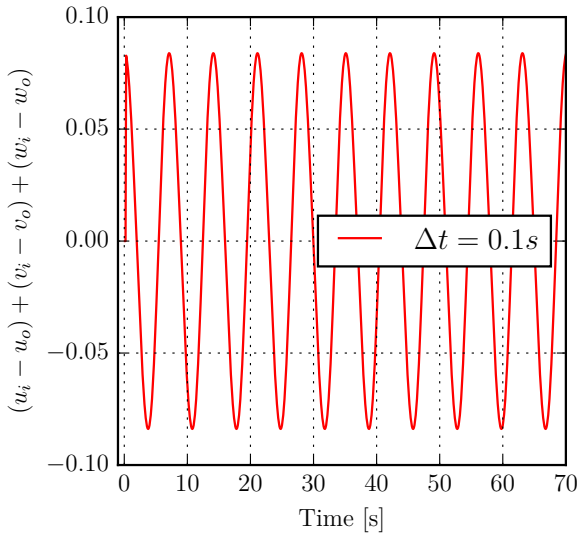

(a) Laplace check with dt=0.1 second, ribs of 1 meter

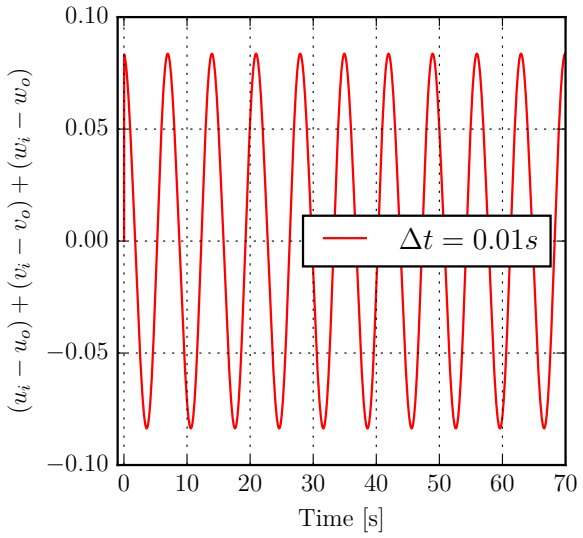

(b) Laplace check with dt=0.01 second, ribs of 1 meter

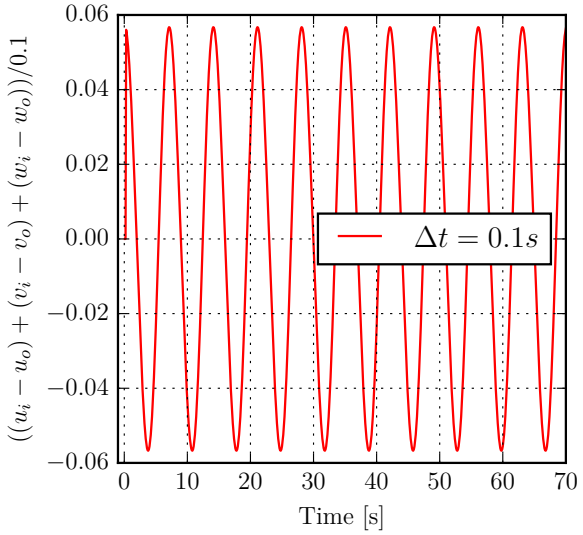

(c) Laplace check with dt=0.1 second, ribs of 0.1 meter

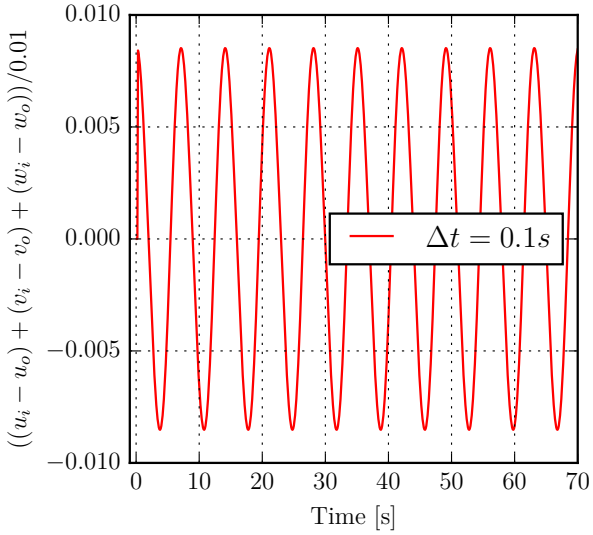

(d) Laplace check with dt=0.1 second, ribs of 0.01 meter

Figure B.2: Verification of the Laplace equation: the control volume cannot accumulate mass. For a small control volume the amplitude of the simulated results converges to zero.

B.2. Mirror condition

Objective: Assessment of the mirror condition;

- **Result:** As expected;
- **Objects:** Single barge (see table B.1 - coarse mesh);
- **Simulation time:** 203 seconds (29 periods) with dt=0.01 second;
- **Situation:** the barge is simulated as single body in a semi infinite fluid domain, a kinematic oscillatory excitation in the heave direction is applied, with a period of 7 seconds and amplitude 2 meters, the barge is restrained in all directions except or the heave direction. Ten measurement points on the free surface (z=0) are chosen, the coordinates and maximum and minimum simulated fluid velocities

normal to the free surface are shown in table B.3. From this table it is clear that zero fluid flux through the free surface is simulated (except for some numerical noise);

- **Criteria:** If the mirror assumption is valid and implemented correctly then zero fluid flux will be simulated through the free surface.

Coordinate (x;y;z)	min $\frac{\partial\Phi}{\partial z}$	max $\frac{\partial\Phi}{\partial z}$
(0;-16;0)	-2.22045e-016	4.44089e-016
(0;16;0)	-4.44089e-016	4.44089e-016
(0;-17.5;0)	-5.55112e-016	4.16334e-016
(0;17.5;0)	-3.88578e-016	5.55112e-016
(0;-19;0)	-3.33067e-016	4.16334e-016
(0;19;0)	-4.16334e-016	3.05311e-016
(0;-21.5;0)	-4.44089e-016	2.77556e-016
(0;21.5;0)	-2.84495e-016	4.57967e-016
(0;-23;0)	-3.67761e-016	2.98372e-016
(0;23;0)	-2.98372e-016	3.747e-016

Table B.3: Min. and max. flux through free surface

B.3. Horizontal translation

Objective: Verify if the FI forces acting on the propagating barge;

- **Result:** Correct;
- **Objects:** Single barge (see table B.1 - coarse mesh);
- **Simulation time:** 200 seconds with a time step of 0.1 second;
- **Situation:** The barge is simulated as single body in a semi infinite fluid domain. The barge is in static equilibrium at the start of the simulation. The first 50 seconds of the simulation a constant force is applied to the CoG of the barge of 30750 kN, which is chosen to satisfy $m \cdot a = F$, for an acceleration of 0.1 m/s^2. After 50 seconds a Lua Script will interfere and remove the force from the barge, leaving it only subjected to the interaction with the water;
- **Criteria:** No potential damping nor added mass terms taken into account in the FI module. A lack of FI forces in horizontal plane will lead to an eventual velocity of 5 m/s. The fluid flowing underneath the barge will flow at higher velocity underneath the body then fluid at the reference point, it is expected that a suction force will work on the barge in vertical direction.

B.3.1. General analysis

The body is simulated unrestrained in six DoF. Figure B.5 visualises the simulation results. Figures B.5a, B.5b and B.5e indicate that there is no fluid-body interaction in the horizontal plane. This meets the expectation since no added mass and potential damping is present in the FI module. A squat force is present, this corresponds with the expectations as well. The results concerning rotations and moments, see figure B.5c and B.5d, are initially not expected and further analysed.

A note has to be made regarding the apparent damping of the rotations of the barge, visible in figure B.5d. This is due to an insufficient time step of the Runge Kutta 2 ODE solver, verification case B.6 elaborates on this.

Suction forces

Figure B.5a, B.5b and figure B.5e show that the forces in horizontal plane are zero, this is as expected. The kinematic Bernoulli force pulls the barge down with approximately 10 MN. To verify this force, an estimation is made of how fast the water flows underneath the barge, evaluated with the barge as reference point. Equation B.3 is the expression used to determine the suction force. The calculation is done for a stationary situation when the barge is propagating with 5 m/s, at this velocity the simulated suction force is 10 MN.

Through equation B.3 the solution $v_0 = 5.61$ m/s is found. The fluid flows 0.61 m/s faster underneath the barge then around it. This is a realistic value.

The draw down of the barge due to this suction force is evaluated, equation B.4 provides the expression used. When applied one finds that the draw down under this force is equal to $\Delta z = -33.15$ cm. Figure B.5b confirms this finding. The oscillations of the barge around its newly obtained equilibrium are due to an initial overshoot due to inertia.

$$F = \int \Delta p dS = \frac{1}{2} \cdot \rho_w \cdot \left(v_0^2 - v_\infty^2\right) \cdot L \cdot B \tag{B.3}$$

$$\rho_w \cdot g \cdot \nabla_0 = \rho_w \cdot g \cdot \nabla_1 - 10^7 \qquad \rightarrow \qquad \Delta z = -\frac{10^7}{\rho_w \cdot g \cdot L \cdot B} \tag{B.4}$$

where:

v_∞ is the undisturbed fluid velocity, with the barge as reference point [m/s];

v_0 is the mean velocity of the fluid under the barge, with the barge as reference point [m/s];

L, B respectively the Length and the Breadth of the barge [m];)

ρ_w is the density of sea water [1025 kg/m^3];

Δz difference in depth of CoG of the barge [m];

∇_0, ∇_1 respectively displaced volume at start of simulation and displaced volume after reaching a velocity of 5 m/s [m^3].

Pitch moment

Figure B.5c and B.5d depict the FI moments acting on the barge during the simulation. The pitch moment exercised on the barge due to the kinematic Bernoulli force, seems non-physical and needs some additional elaboration. Figure B.6 shows the results of different simulations in which the barge is restrained in the pitch direction, the heave direction and an event in which both DoF are fixed. From this it is clear that when the barge cannot heave or pitch, the FI moments are zero. So both the heave and the pitch motion in combination with the surge velocity influence the simulated FI-moments. This is shown in figures B.6a, B.6b and figures B.6c, B.6d. The total FI-moment as seen in figure B.5c is a combination of both the influences. The influence of both motions on the generation of FlowInteraction moments can be explained by an asymmetric fluid velocity distribution around the y-axis underneath the barge:

pitch: A pitch rotation introduces three mechanisms through which the FI-moment is induced. An initial rotation gets amplified because the centre of buoyancy and the centre of gravity do not line up under this inclination. Secondly, the force resulting from the kinematic pressure always has a working direction perpendicular to the surface. This inclination also allows for a very small horizontal FI-force component which exerts a moment around the CoG. Since the rotations are very small, these two mechanisms are contributing only a little to the moment. Figure B.5c shows a maximum pitch angle (after reaching a constant speed) of only 0.10 degrees.

The governing mechanism through which the second order Bernoulli forces exerts a moment is based on a uneven distributed fluid velocity underneath the barge. In figure B.3 streamlines underneath the barge are drawn. The pitch angle pushes the streamlines closer together at the end of the barge, this means a higher fluid velocity at the stern of the barge then at the bow. This mechanism is expected to be dominant. It has to account for a FI moment with magnitude 2 MN. This means that the kinematic Bernoulli forces of 10 MN needs an arm towards the CoG of 0.2 m. We consider the barge to be composed of two equal parts divided by the y-axis of the barge. The total force acting on the barge should be equal to 10 MN, but the distribution should allow for a shift in application point of the mean force of $r = 0.2$ m. Equation B.5 and B.6 are used. This leads to an average velocity on the first halve of $\bar{v}_1 = 5.59$ m/s and on the second half of $\bar{v}_2 = 5.63$ m/s. Note that, in the used equation, the assumption is made that the fluid velocity on both sides is constant with a step in fluid velocity at the middle. The force is dependent on v^2 which means that if the velocity changes linear over the length of the barge, the force

will quadratically. The average force on both sides will then not apply at 25 meters from the middle. The in equation B.6 used arm of 25 meters will change to the point of application of both weighted average forces. Since the difference in fluid velocity is very small compared to total velocity, the influence of this non-linearity is neglected for this approximation. The small difference in average velocity make it a very realistic explanation;

heave: The heave motion also induces a variation in fluid velocity underneath the barge. The magnitude of the FI-moment induced by this motion is approximately equal to the moment induced by the pitch rotations. The velocities change underneath the barge due to heave oscillations is explained by superposition of streamlines as is visualized in figure B.4. When the fluid motions induced by the oscillation are summed with the fluid motions underneath the barge due to the surge propagation of the barge, it is found that on one side these counteract while on the other side these motions collaborate. This difference in velocities over the panels leads to a force distribution that induces a moment.

A note has to be made on these theories. While the FI-moments are in the MNm, the simulated body is very large and heavy. This means that the moments only lead to small rotations in pitch direction. A pitch angle of 0.1 degrees will in practice not be noticed by those on the vessel. The initial rotation is introduced through the functionality that allows to apply the driving force, during the first 50 seconds, to the CoG of the barge. This is presumably a small numerical error in application point of this force leading to a rotation.

$$\frac{1}{2}\cdot\rho_w\cdot\left(\frac{\bar{v}_1^2+\bar{v}_2^2}{2}-v_\infty^2\right)\cdot L\cdot B = F_{FI} \tag{B.5}$$

$$\frac{25+r}{25-r}\cdot\bar{v}_1^2=\bar{v}_2^2 \tag{B.6}$$

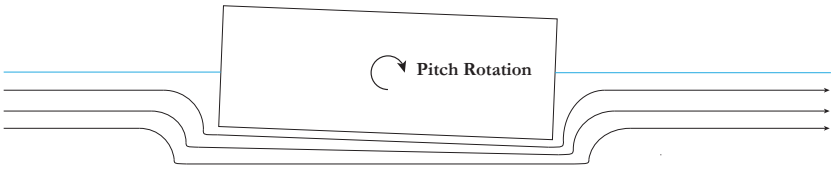

Figure B.3: Streamlines when propagating in surge direction with pitch rotation

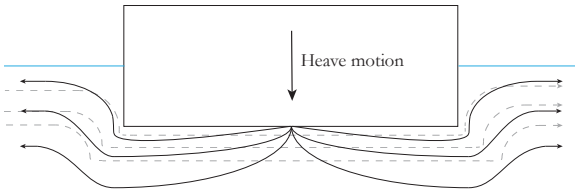

Figure B.4: Streamlines due to heaving (black lines) to be superposed with surge propagation streamlines (grey lines)

Decay of rotation

In figures B.5c and B.5d a small decay in FI moments and rotations over time is seen. A simulation time step reduction from dt=0.1 second to dt=0.01 second changes this behaviour. This is seen in figure B.7. The equations of motion are not solved accordingly due to an insufficient time step for the Runge Kutta 2 solver. Verification case B.6 elaborates on this.

B.3.2. Conclusion

The motions are simulated in accordance with the implemented physics. A small pitch moment induced through combined heave and pitch motions while the body is propagating in surge direction. The expectation of no simulated added mass and damping is confirmed. The squat forces are simulated correctly.

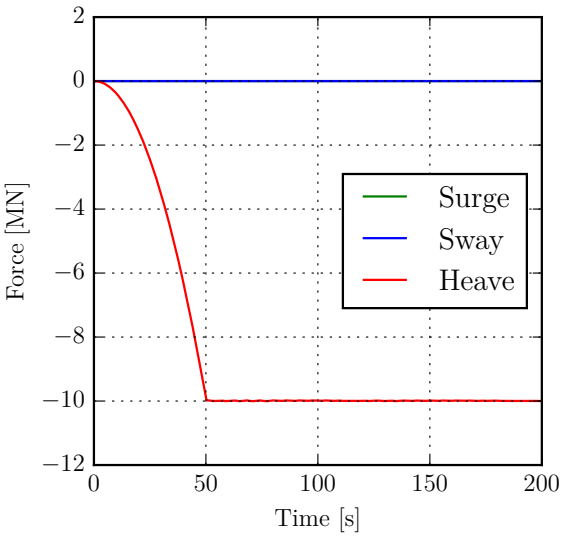

(a) FI force on unrestrained barge

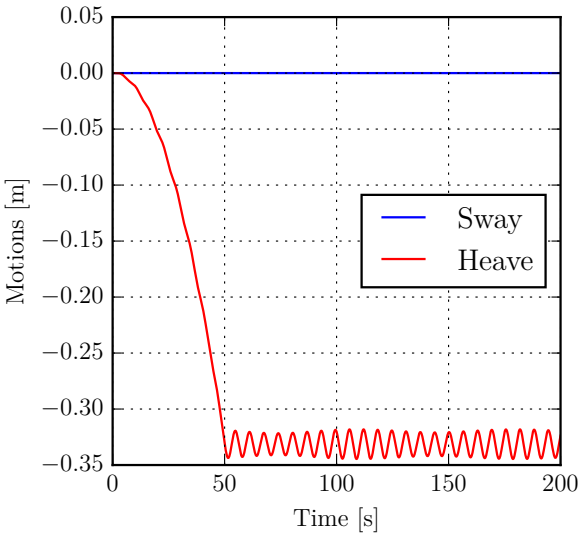

(b) Motions of unrestrained barge

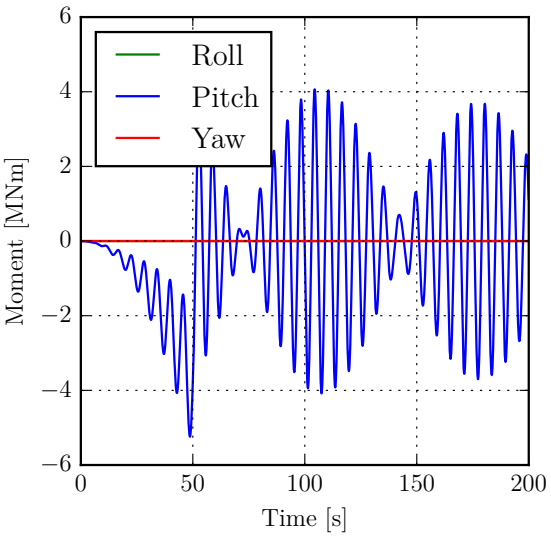

(c) FI moment on unrestrained barge

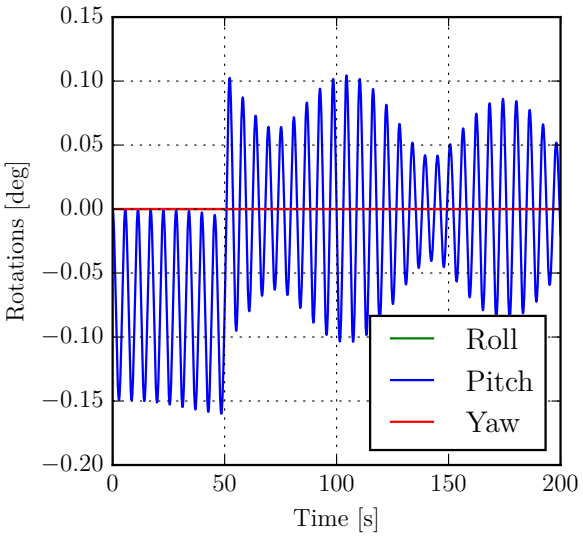

(d) Rotations of unrestrained barge

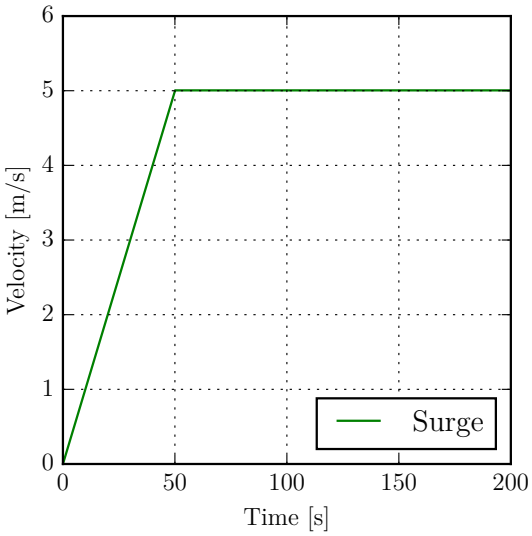

(e) Velocity of unrestrained barge

Figure B.5: Simulated unrestrained barge forcefully accelerated with 0.1 m/s^2 till 5 m/s. The simulated time step dt=0.1 second. Results of (a),(c) FI forces and moments acting on the barge. Sub-figures (b), (d) are the motions of the barge and (e) is the propagation speed of the barge.

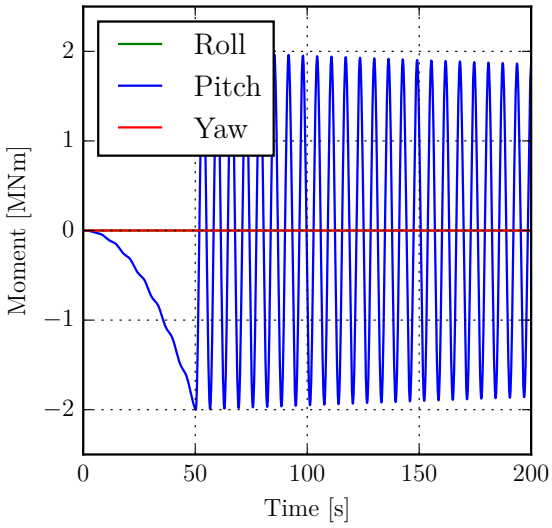

(a) FI pitch moment induced by heave motion

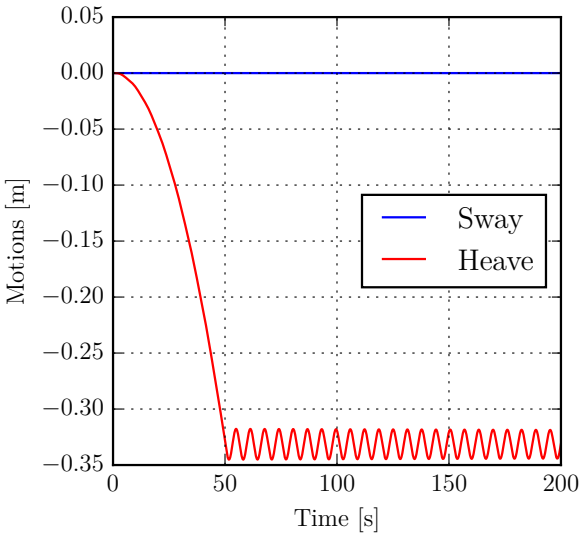

(b) Heave motion inducing FI pitch moment

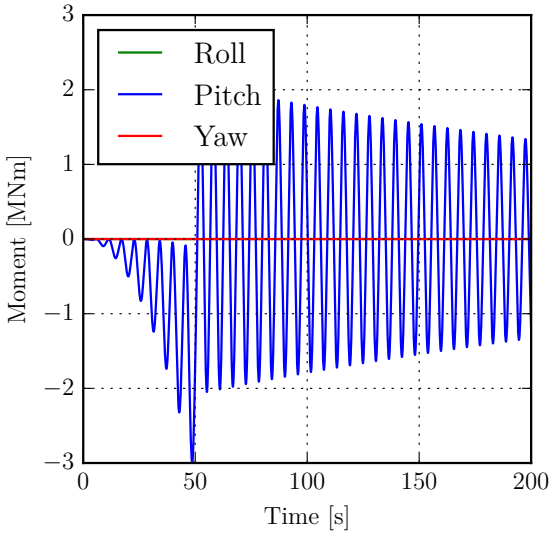

(c) FI pitch moment induced by pitch rotation

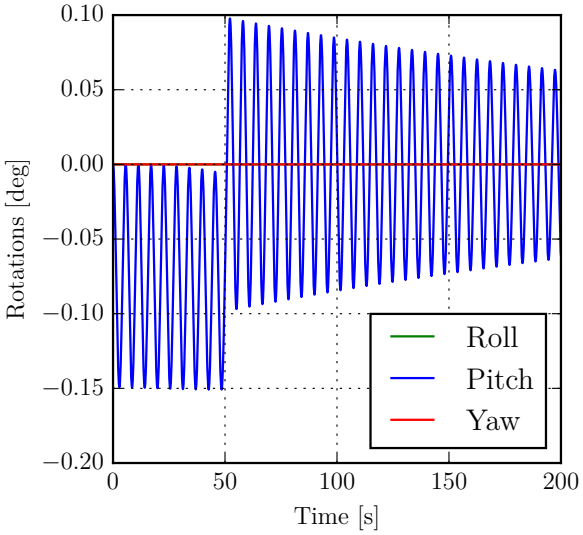

(d) Pitch rotation inducing FI pitch moment

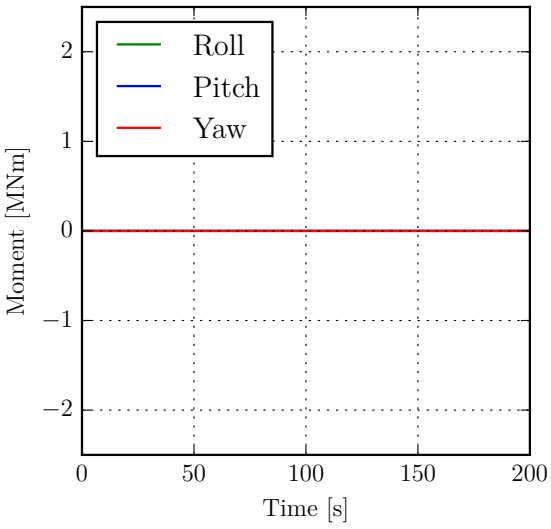

(e) FI moment through other DoF than heave and pitch

Figure B.6: Evaluation of separate influences of the heave motion and the pitch rotation on the pitch moment on the (in the surge direction) propagating barge. (a), (b) are results for the fixed pitch rotation; (c), (d) are results for the fixed heave translation; (e) results when both DoF are fixed.

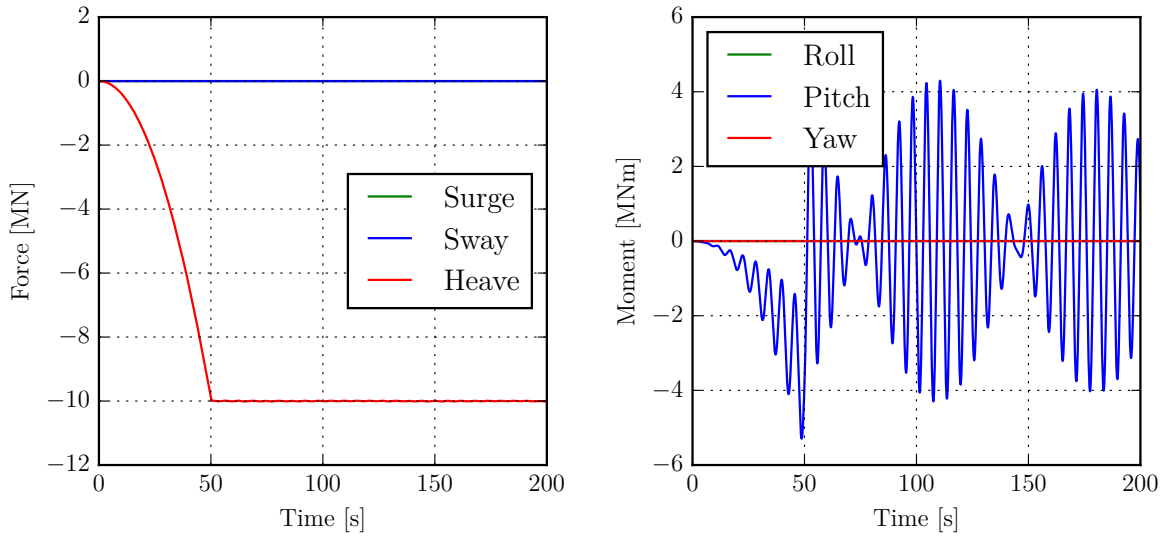

(a) FI force on unrestrained barge - dt=0.01s

(b) FI moment on unrestrained barge - dt=0.01s

Figure B.7: A barge, free to move in 6 DoF, is forcefully accelerated with 0.1 m/s^2 till 5 m/s. The simulated time step dt=0.01 second. Influence of time step reduction (compare to figure B.5).

B.4. Kinematic excited heave oscillation

Objective: Verify the interaction forces on the barge with a single frequency oscillatory kinematic excitation in heave direction;

- **Result:** As expected - with some explanation;
- **Objects:** Single barge (see table 4.1 - coarse mesh);
- **Situation:** The barge is simulated as single body in a semi-infinite fluid domain. A kinematic oscillatory excitation in the heave direction is applied to the barge, with an amplitude of 2 meters and a period of 7 seconds. The FI forces acting on the barge are shown in figure B.8. A shift of the mean motion is seen when a time step of 0.1 second is applied, this is evident from figure B.8b. The simulation is repeated with a time step of 0.01 second, from figure B.8d it seems that the shift is not simulated.

  The simulation is repeated with a smaller amplitude, now 0.02 meters and a shorter period of 1 second. The time step size is reduced as well. The results are documented in figure B.9;
- **Criteria:** Single body-fluid interaction in heave direction is expected, these are the non-linear kinematic Bernoulli and cushion forces.

B.4.1. General analysis

The results obtained from the simulation, depicted in figure B.8, show positive forces with a frequency twice the frequency of the velocity of the barge. These resulting FI forces are positive, the kinematic Bernoulli term leads to negative forces. Further a negative shift in mean motion is simulated, this seems to be influenced by the choice of time step size. Figure B.10 indicates that when the FI forces are not simulated, this negative shift in mean motion is still present.

Time step minimization

A time step reduction has a positive influence on the unexpected mean shift of the applied motion. No equations of motions are solved, the applied oscillation should not be influenced by the FI forces. This expectation is substantiated by the fact that the FI forces provide a mean force in the positive heave direction, while the mean motion shift is in the negative heave direction. When the squat handle is set to "false", as is done in the simulation providing the results of figures B.9c and B.9d, the mean shift is still present. This indicates that the shift in motion is not an error directly associated with the FI module.

The size of the time step seems directly related to the shift in the mean motion. After evaluation the five simulation of which the results are shown in figures B.8 and B.9, a relation is qualified. The error seems to correspond to the expression stated in equation B.7. It is to equal the value of the first time step of applied oscillation divided by two. In table B.4 this equation is verified. Note that the column 'approximation' is determined with equation B.7 while the $\bar{z}$ follows from the simulated results.

$$\bar{z}_{shift} = -\frac{A_z}{2} \cdot \sin(\omega \cdot \Delta t) \tag{B.7}$$

Case	T_0 [s]	dt [s]	A_z [m]	$\bar{z}$	Approximation
small amp	1	0.05	0.02	-0.0031	-0.003090
small amp	1	0.025	0.02	-0.0016	-0.001564
small amp	1	0.001	0.02	-0.0001	-0.0000628
large amp	7	0.1	2	-0.0898	-0.08963
large amp	7	0.01	2	-0.009	-0.008975858

Table B.4: Mean shift in motion at forces vertical oscillation, rule of thumb

Positive FI-forces

The forces simulated by the FI module are positive. The kinematic pressure forces following from the fluid velocities underneath the barge is a negative force. The negative kinematic force is seen in verification case B.3 as well. The reason for the positive forces follows from section 4.2. Here it is explained that the unsteady Bernoulli term, will provide a force when two or more bodies with a relative velocity to each other are simulated. Because the bodies are mirrored, see section 3.3.3, a relative velocity between the body and the reflection is simulated when motions in vertical plane are present.

This force is in this thesis referred to as cushion force, this is an inertia force to the accelerations of the fluid but not related to the accelerations of the barge. Imagine: the barge is moving with a constant velocity deeper into the water. Now water has to be put into motion to allow the barge to descent deeper into the water. The barge will never fully descent in this thought experiment. The water particles, moving away to make place for the barge, have to be accelerated. This leads to inertia forces, even though no body accelerations are present. In real situations, this event would be dominated by the added mass force, making this observation very counter intuitive. The neglect of added mass leads to non-physical behaviour. Verification case B.5 substantiates this theory.

Mesh refinement

By simulating this event using the barge with the fine mesh (see table 4.1), the results of the simulation change. Two properties are clearly visible. Firstly the forces are slightly lower in case of a finer mesh grid on the barge. A finer mesh leads in general to a more continues source strength distribution an thus a better representation of the real situation. Yet in this case at the top of each force peak a dent or spike in the forces is clearly visible. This is due to clipping. In this finer mesh, at the height of the hydrostatic equilibrium point two rows are divided. Every time that a peak is seen in the FI forces, a row of panels is cut off very close to the interface. Every time this happens a drop in the FI forces is observed. In verification case B.6 a more elaborate explanation is provided.

B.4.2. Conclusion

Two important properties are found in this verification case. The first one states that kinematic applied heave oscillation has an error dependent on the time step chosen. The relation between the chosen time step and the error in mean motions of the forced oscillation is quantified with equation B.7. A second observation indicates that the forces simulated by the flow interaction module, when significant motions through the vertical plane are present, contain inertia forces. These inertia forces are quadratically related to the velocity of the barge. Verification case B.5 will go into deeper detail. A finer mesh distribution on the hull of the simulated barge leads to a significant longer simulation time, the simulated FI forces are slightly lower. A discretization error is seen when the panel row gets cut off very close to the interface between two panel rows. Verification case B.6 elaborates on this.

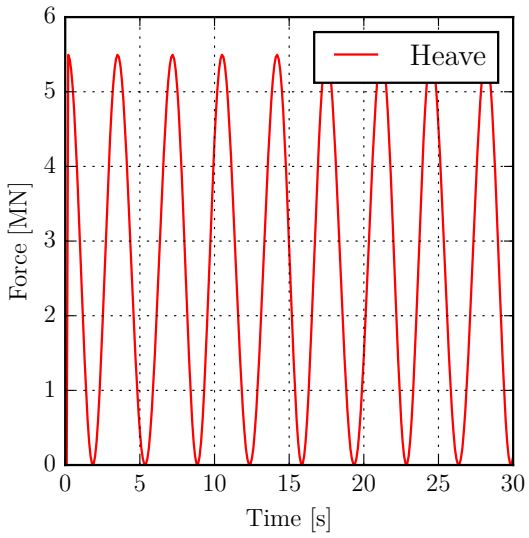

(a) FI forces acting on coarse barge (dt=0.1s)

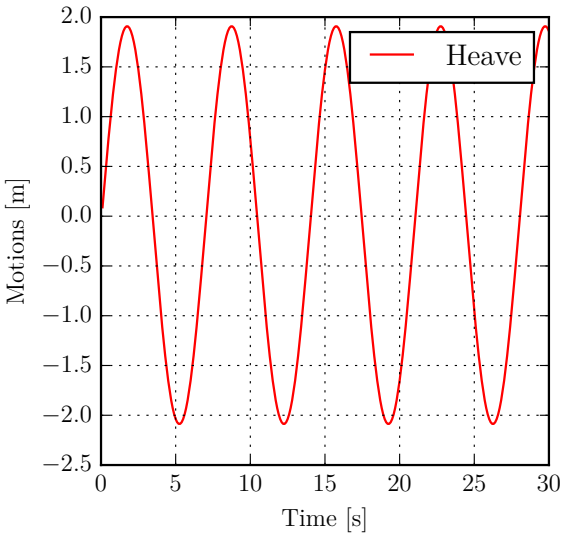

(b) Motions of coarse barge (dt=0.1s)

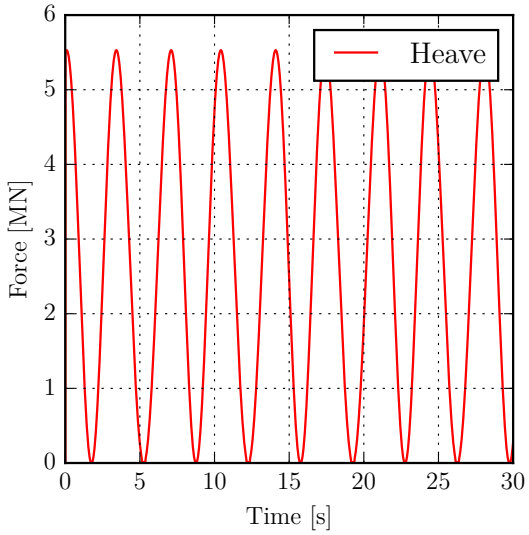

(c) FI forces acting on coarse barge (dt=0.01s)

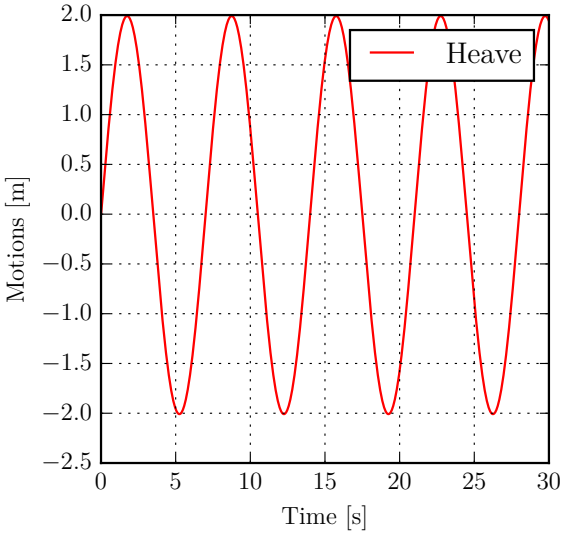

(d) Motions of coarse barge (dt=0.01s)

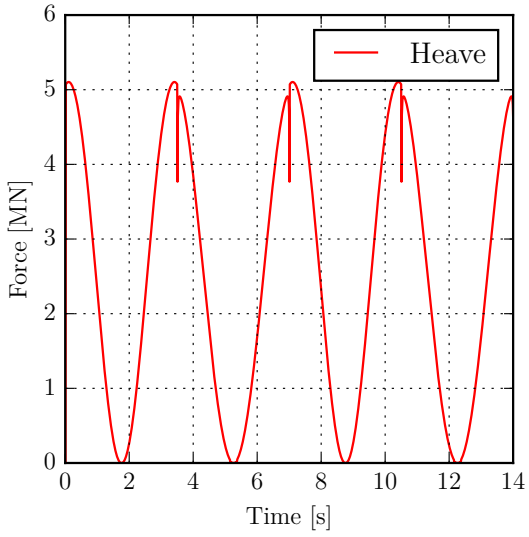

(e) FI forces acting on fine barge (dt=0.01s)

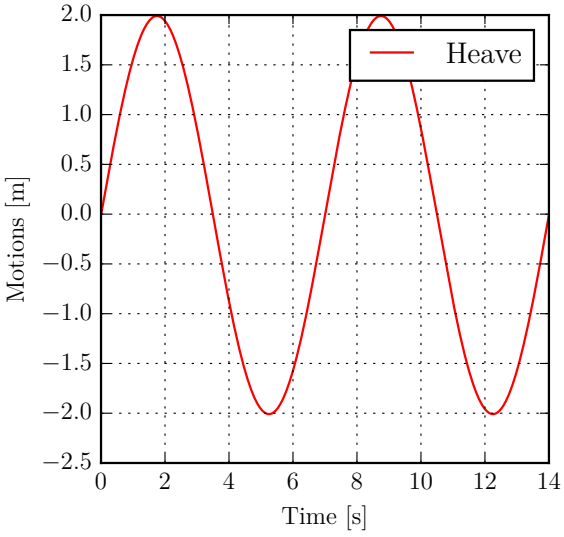

(f) Motions of fine barge (dt=0.01s)

Figure B.8: Simulated results of kinematic excited barge oscillating in the heave direction with a period of 7s and an amplitude of 2m. The influence of time step reduction and the density of the panel distribution on the hull is evaluated.

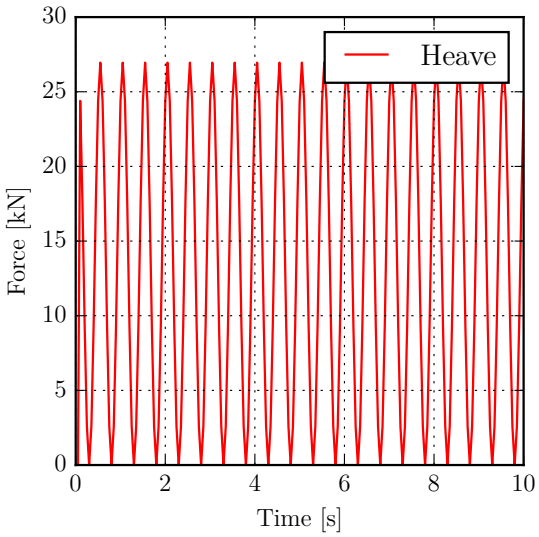

(a) FI forces acting on coarse barge (dt=0.05s)

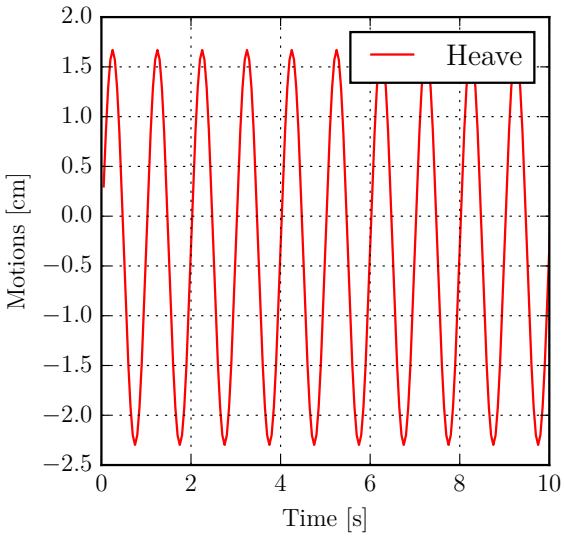

(b) Motions of coarse barge (dt=0.05s)

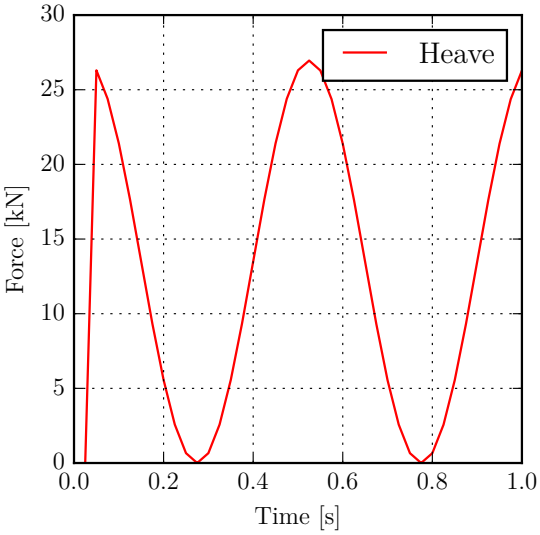

(c) FI forces acting on coarse barge (dt=0.025s)

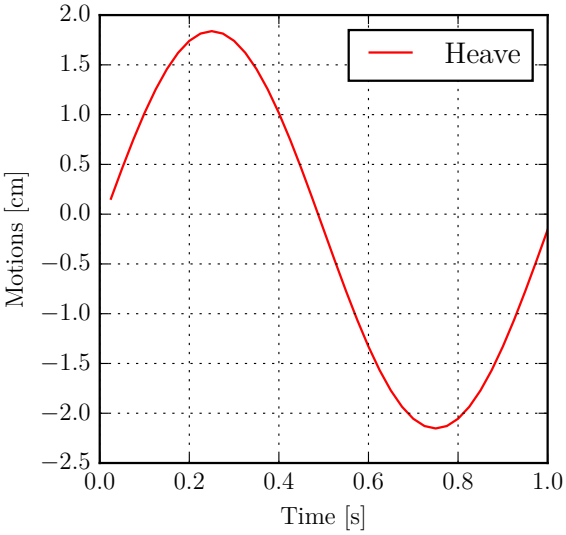

(d) Motions of coarse barge (dt=0.025s)

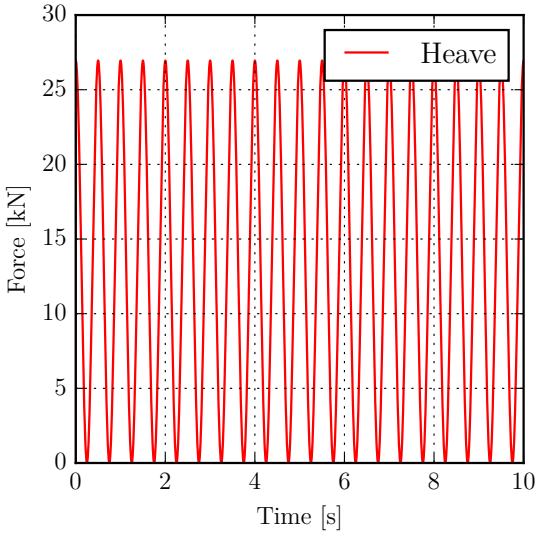

(e) FI forces acting on coarse barge (dt=0.001s)

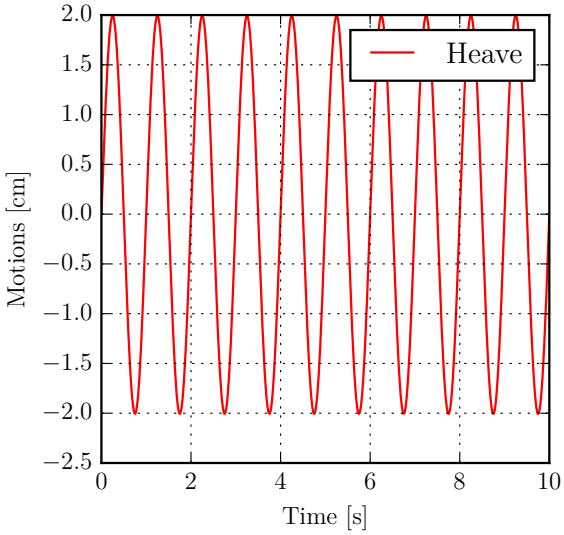

(f) Motions of coarse barge (dt=0.001s)

Figure B.9: Simulated results of kinematic excited barge oscillating in the heave direction with a period of 1s and an amplitude of 0.02m. The influence of time step reduction is evaluated.

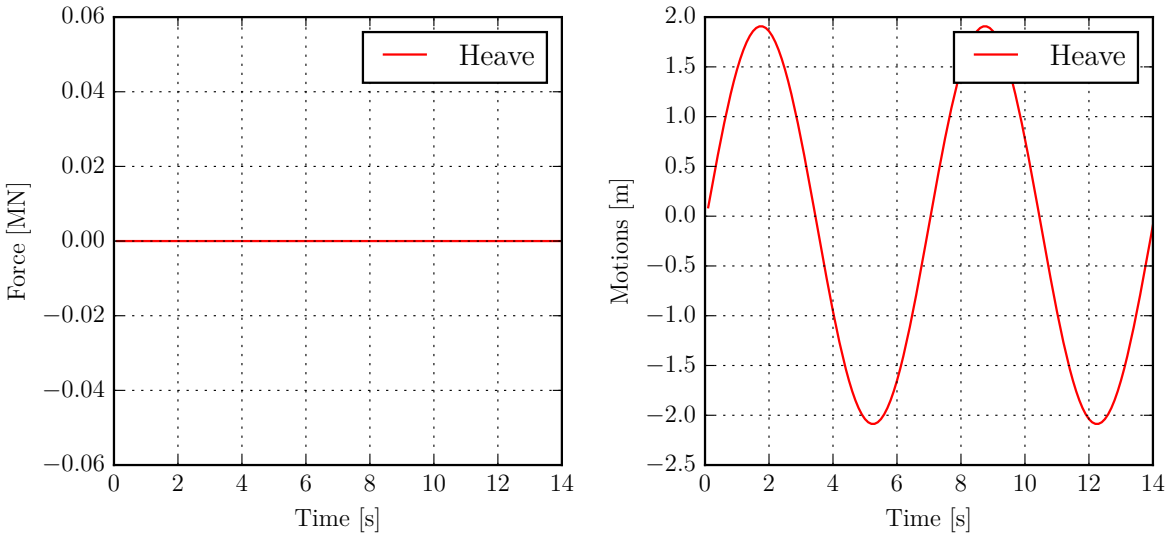

(a) FI forces - dt=0.05s

(b) Motions - dt=0.05s

Figure B.10: FI forces acting on a kinematic excited heave oscillation with a period of 7s and an amplitude of 2m. The squat handle was set to "false". From this it is clear that the shift in the mean of the motion is not due to the FI calculation.

B.5. Kinematic excitation heave: influence of added mass

Objective: Evaluate the influence of added mass on non-physical behaviour when motions through the vertical plane are simulated;

- **Result:** As expected - with some explanation;
- **Objects:** Single barge (see table 4.1 - coarse mesh);
- **Situation:** The simulated event is the same event as in verification case B.4. The kinematic excited barge has an amplitude of 2 meters and a period of 7 seconds. The time stepsize is 0.01 second. The difference with the previous verification case is that the influence of added mass is taken into account in this simulation. The acceleration of the previous time step is used on the right hand side of the equation of motion to account for added mass. For a kinematic excited body this is not a problem, since the motion is not dependent on provided forces. But for a free motion this is shown to lead to an unstable simulation in most cases. The option to add hydrodynamic forces due to own accelerations to the simulation is included in the program to verify the expectation stated in section B.4;
- **Criteria:** The in verification case B.4 simulated results contained positive double frequent forces. If the added mass is included in the calculation this should be counteraction and lead to a net negative force. A small non-linear harmonic component is expected to be present in the added mass.

B.5.1. General analysis

Figure B.11a shows the simulated FI forces with and without added mass included. The blue line represents the FI forces over time without the accelerations of the barge taken into account. This force has double the frequency compared to the frequency of the motions of the barge and a positive mean of 2.76 MN. When the FI forces are complemented with the added mass force, the mean of the simulated force turns negative to -144.1 kN. This negative mean value is what was initially expected. The kinematic Bernoulli term induces this negative force component. It manifests itself only now that the cushion forces are compensated by the added mass force of the real body. The magnitude of the negative mean indicates that if the kinematic Bernoulli forces also partly compensate for the mean positive of the cushion force. For the added mass to compensate for a part of the cushion based inertia forces, a quadratic component should be present in the added mass forces. This indicates that the added mass is not constant for the frequency but is slightly dependent on the motion of the barge. This variation, leading to a non-linear harmonic term after multiplication with the acceleration, is dominated by the constant part of the added mass value which generates forces with the same frequency as the acceleration of the barge.

B.5.2. Conclusion

When the added mass is taken into account, the mean of the FI forces become negative. This indicates a small non-linear term in the added mass force. The negative mean force is due to a combination of the added mass force and the kinematic Bernoulli term. The expectation that the added mass force (combined with the kinematic Bernoulli force) compensates for the inertia force dependent on the velocity of the barge, as explained in verification case B.4, is confirmed.

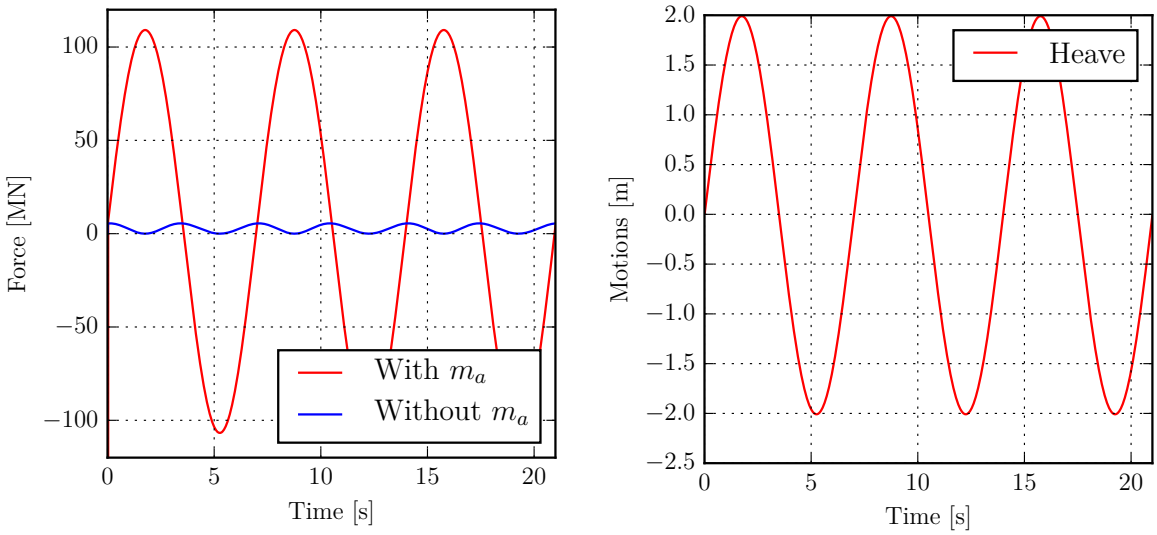

(a) FI forces acting on the barge (dt=0.01s)

(b) Motions of the barge (dt=0.01s)

Figure B.11: Kinematic excited barge in the heave direction with T_0 = 7 seconds and A_z = 2 meters. The FI forces acting on the barge with and without added mass taken into account are compared.

B.6. Free heave oscillation

Objective: Verify the interaction forces on the barge for a free heave oscillation;

- **Result:** Unexpected decay of forces and motions over time;
- **Objects:** Single barge (see table 4.1 - coarse and fine mesh used);
- **Situation:** The barge was simulated as the only body in a semi-infinite fluid domain. The barge had an initial excitation of -5 meters, this means that the keel of the barge was placed at a depth of -15 meters. At t=0 the barge was released and started to vibrate. The FI forces and the vertical motions of the barge are shown in figure B.13. Multiple variations in time stepsize are evaluated. The influence of mesh refinement is verified as well;
- **Criteria:** The barge should be in free vibration, the only FI forces working on the barge should be to the quadratic cushion and kinematic Bernoulli forces.

B.6.1. General analyses

Since no wave radiation is present in this module: the expectation is that no damping is present in the free heave oscillation motion. This expectation seems to be contradicted by the results of this simulation, documented in figure B.13. The apparent damping seems to be influenced by the chosen time step. The choice of time step also influences behaviour seen in figure B.13i. Here the forces seem to drop towards zero, six times per period. Further the FI forces have double the frequency compared to the frequency of the simulated motions, this behaviour originates from the same forces as explained in verification case B.4 and B.5.

It should be noted that the simulated motions of the barge are non-physical. The barge moves further up from the water than the initial excitation. In a real life situation this would contradict the law of energy conservation. Yet it does comply with the FI forces as they are simulated. The neglect of added mass allows for this non-physical behaviour of barge motions.

Time step minimization

The reduction of the time step has a significant influence on the apparent damping of the barge motions and FI forces. A time step of 0.1 second (figure B.13a and B.13b) shows a reduction of the initial dynamic force response of approximately 70% over the first 70 simulated seconds. A time step of 0.01 second shows a force amplitude reduction of approximately 20%. Figure B.13d and B.13e show the results of the simulation with a time step of 0.01 second. A simulation with time step dt=0.001 second, documented in figures B.13g and B.13h, confirms that time step minimization is the key to explain the unexpected behaviour.

The reason why time step minimization has such an influence on the simulated results is explained by figures B.13c, B.13f and B.13k. Here equation B.9 is plotted versus time, the expectation is that this is always zero over time. The equation of motion being solved in this simulation is expressed in equation B.8. In this equation m is the mass of the barge, c is the stiffness or buoyancy and F_{FI} is the force provided by the FI-module. The simulated FI forces and motions are known and so is the expression for buoyancy and mass of the barge. To check for errors in the solution of the equation of motion equation B.9 is applied, it equals zero if the dynamic equation is satisfied. From the results found in figures B.13c,B.13f and B.13k it is clear that for a smaller time step the equation of motion is solved with a smaller error. Mostly from figure B.13c it is evident that the integral area of the error over time per period is not equal to zero. If it was, an error in motions would be simulated but the decay of forces over time, as is seen in these simulation results, would not be present. It can be concluded that some of the simulated FI forces are not accounted for in body motions due to an insufficient time step of the Runge Kutta 2 ODE solver. To keep the time steps in the FI calculation and equation of motion synchronized, the automatic time step reduction was disabled by the programmer.

$$m \cdot \ddot{z} + c \cdot z = F_{FI} \tag{B.8}$$

$$F_{FI} - (m \cdot \ddot{z} + c \cdot z) = 0 \tag{B.9}$$

Clipping problem

There is some other inconsistent behaviour in the simulated forces, when the time step is reduced the behaviour manifests itself. In figure B.13i the behaviour is clearly visible in the forces provided by the FI module, six times per period the FI forces seem to shoot towards zero and back in just a few time steps. These peaks reveal in figures B.13f and B.13k as well, but now in two directions. This indicates that the inconsistency is found in the accelerations of the barge as well. The FI forces only contain negative peaks and the displacement has none as is clear from figure B.13, the positive spikes can only occur if they are present in the $m \cdot \ddot{z}$ force as well. Note that this inertia term is subtracted from the FI forces, thus the negative spikes provided by this term turn positive in the graph.

Each period exactly six vertical peaks are simulated, this is equal to the amount of panel rows that shift in and out of the water. Figure B.12 is a front view of the barge with the panel distribution. The red lines are the horizontal interfaces of the panels that move in and out of the water. Every time step the panels are cut at the free surface, only the panels in the fluid domain are included in the calculation of the FlowInteraction forces, section 3.5 elaborates on this. At the edges of the panel the fluid velocity is unstable, here the used mathematical expression turns infinite. Panels with a ratio between the width and height of $\frac{\Delta x_k}{\Delta y_k} \ll 1$ will lead instantaneous non-physical discretization errors. To confirm that the behaviour appears at the interface of two panel rows, figure B.13l is consulted. Here one period of barge motions is plotted in green, together with the solution to equation B.9 as is shown in figure B.13k. In red the interface height of the panels are drawn as horizontal lines. It is clear that the unexpected behaviour occurs at the same instant that a row of panels leaves or moves into the fluid domain, note that all three lines cross at the same time step. When the time step is minimized the chance of landing exactly on the interface between two panel rows grows and the error becomes more visible.

Fine vs Coarse mesh

The influence of a finer chosen mesh distribution versus a coarser mesh distribution (see table 4.1) on the barge is seen in the magnitude of the simulated forces. When a finer mesh is chosen, the forces are found to be smaller in magnitude. Figures B.13m, B.13n, B.13o and B.13p contain the results of the simulations

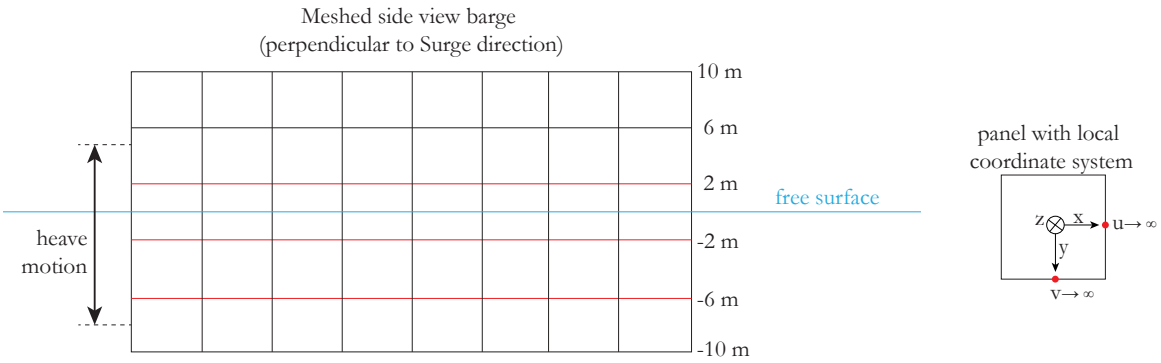

Figure B.12: On the left: a front view of the barge with panel distribution, red lines indicate the row borders moving into and out of the water. On the right: it is seen that calculation is unstable close to the panel border.

with a finer mesh distribution. The source strength is determined to satisfy the boundary condition at the collocation point of a panel and is assumed to be constant over that panel. The difference in simulated forces is explained by the fact that a finer mesh leads to a more continues source strength distribution and a better approximation of the real forces.

B.6.2. Conclusion

The damping in the simulation is a numerical error due to the Runge Kutta 2 ODE solver where time step adaptation is disabled. If the time step is manually chosen smaller the equation of motion is satisfied. This on its turn leads to another discretization error. This error, clearly visible in figures B.13f and B.13k, is due to the clipping of panels at the free surface. When panels get too small the source strength does not describe the full panel correctly any more.

A finer mesh distribution on the barge leads to smaller simulated FI forces, this complies with the behaviour seen in verification case B.4. The refinement of the mesh leads to significant longer simulation times.

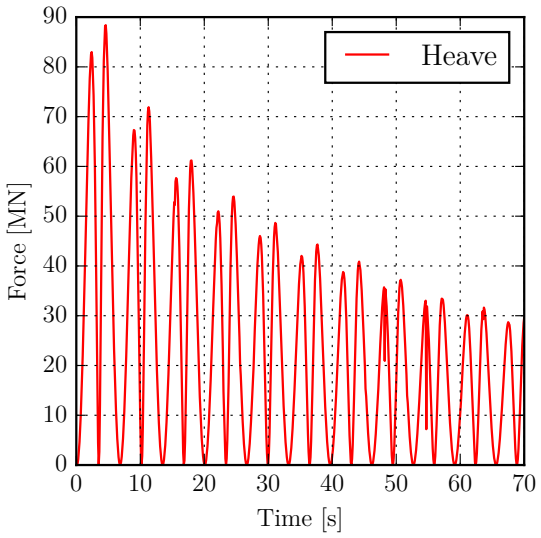

(a) Free heave osc. FI forces - dt=0.1 s, coarse mesh

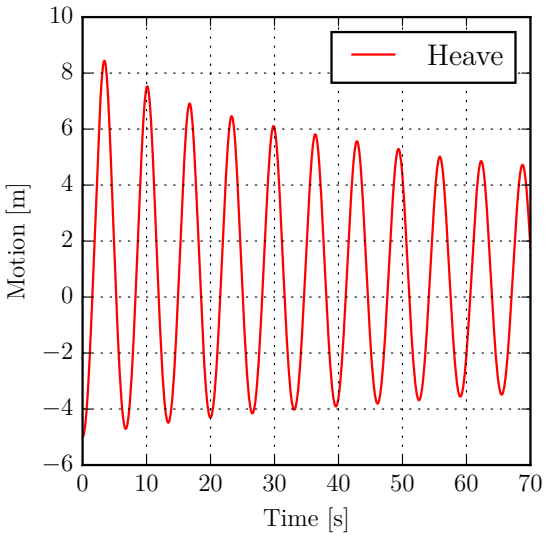

(b) Free heave osc. motions - dt=0.1 s, coarse mesh

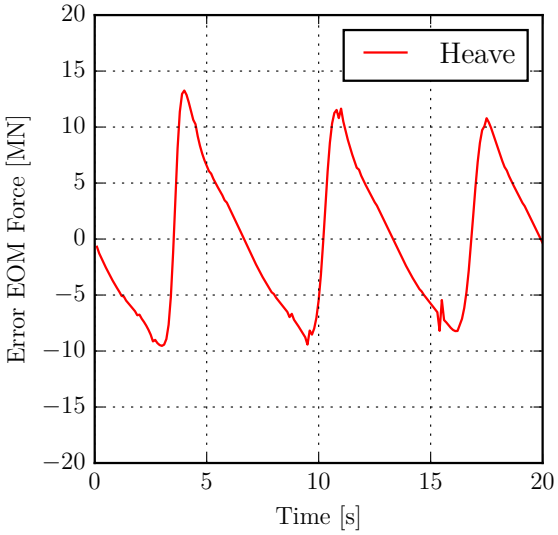

(c) Solution of EOM - dt=0.1 s, coarse mesh

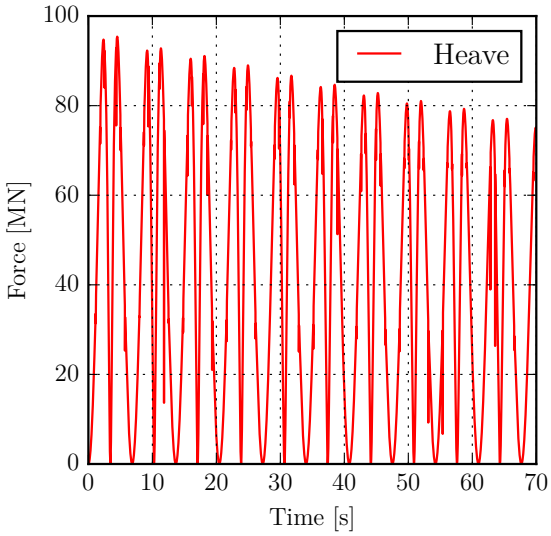

(d) free heave osc. FI forces - dt=0.01 s, coarse mesh

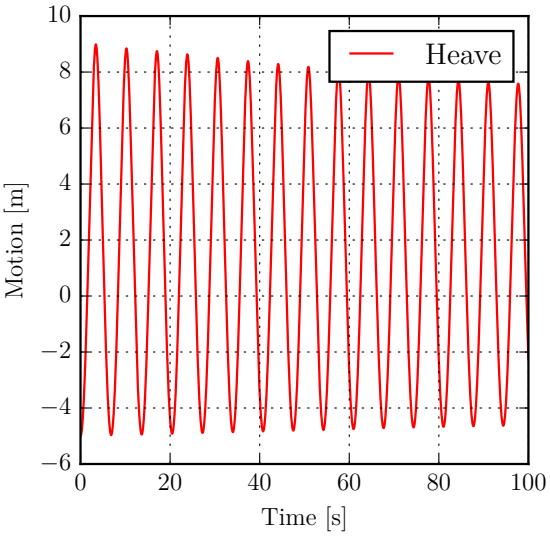

(e) free heave osc. motions - dt=0.01 s, coarse mesh

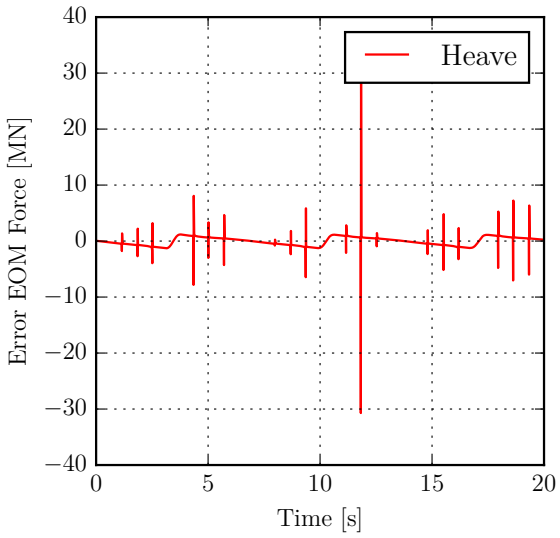

(f) Solution of EOM - dt=0.01 s, coarse mesh

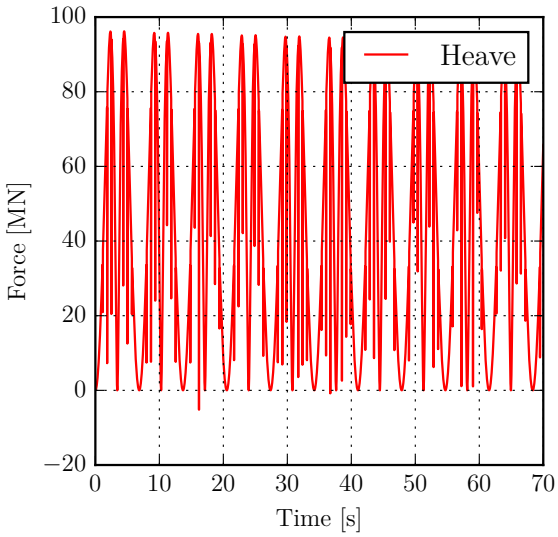

(g) free heave osc. FI forces - dt=0.001 s, coarse mesh

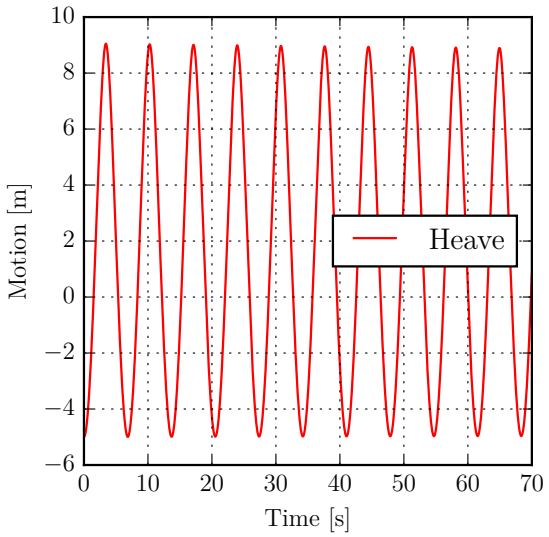

(h) free heave osc. motions - dt=0.001 s, coarse mesh

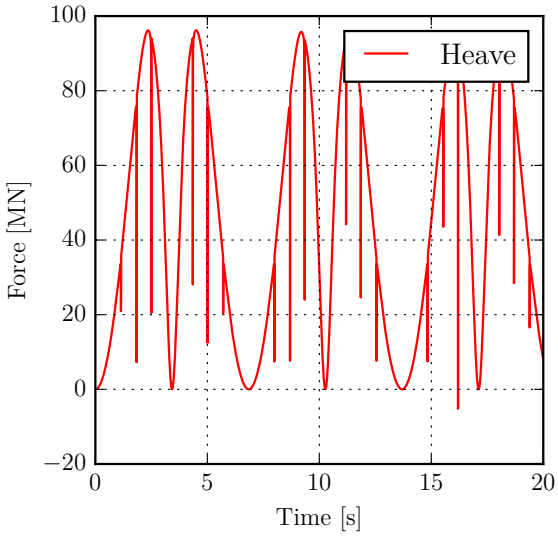

(i) zoom in of sub-figure g

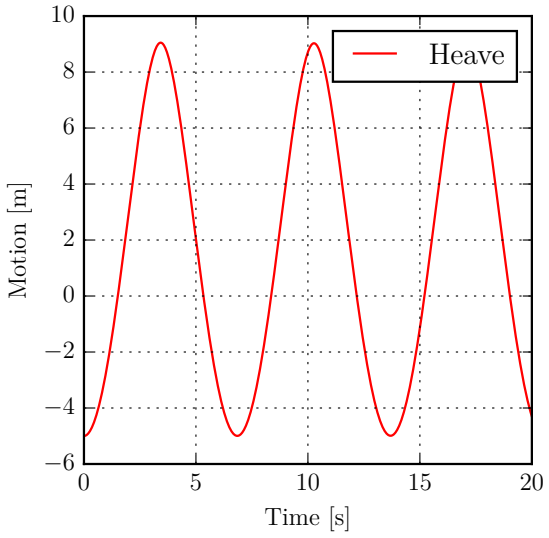

(j) zoom in of sub-figure h

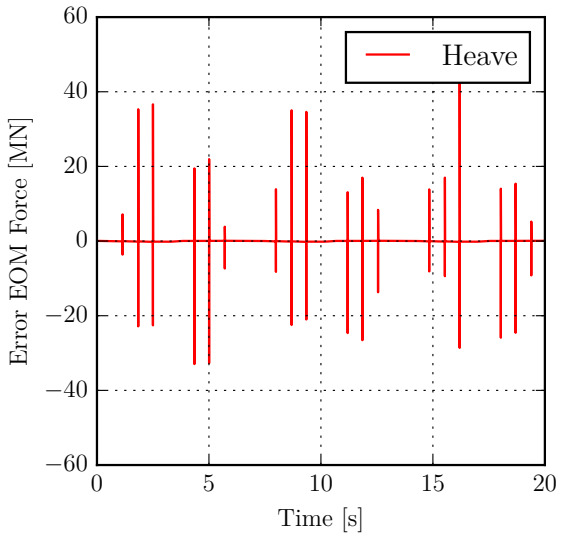

(k) Solution of EOM - dt=0.001 s, coarse mesh

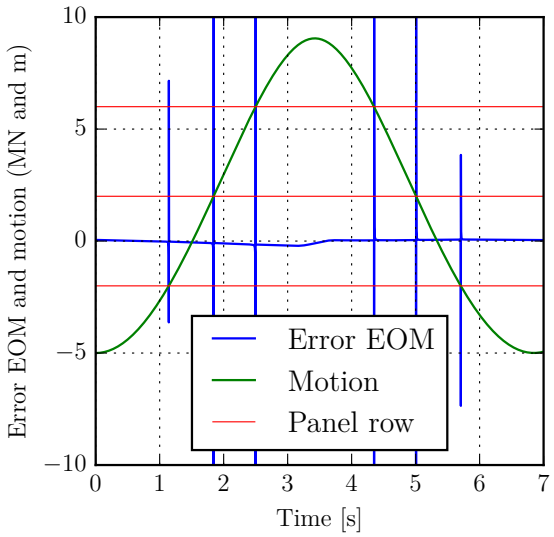

(l) Correlation FI-force drops and clipping of panel rows

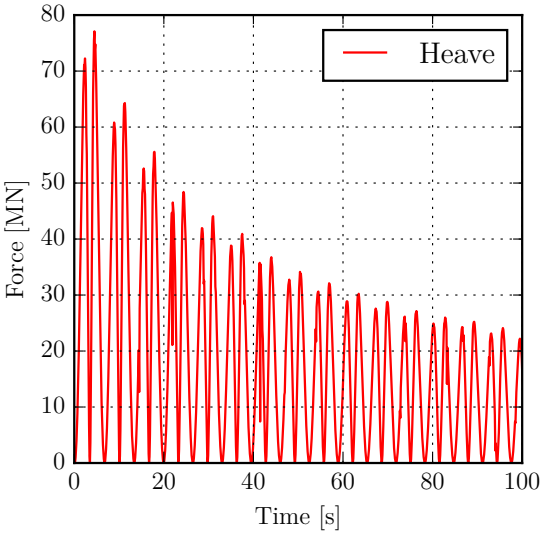

(m) free heave osc. FI forces - dt=0.1 s, fine mesh

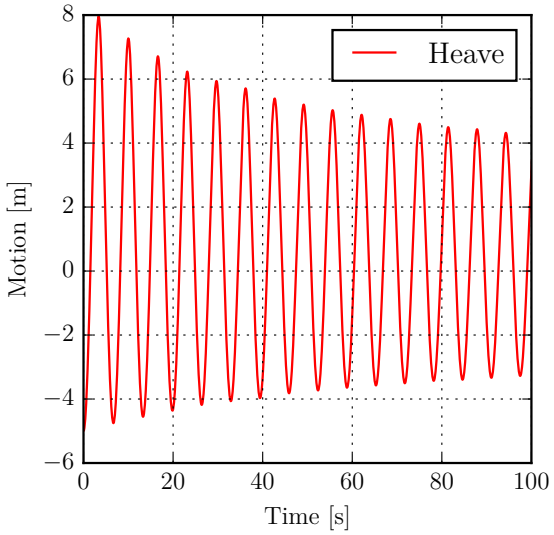

(n) free heave osc. motions - dt=0.1 s, fine mesh

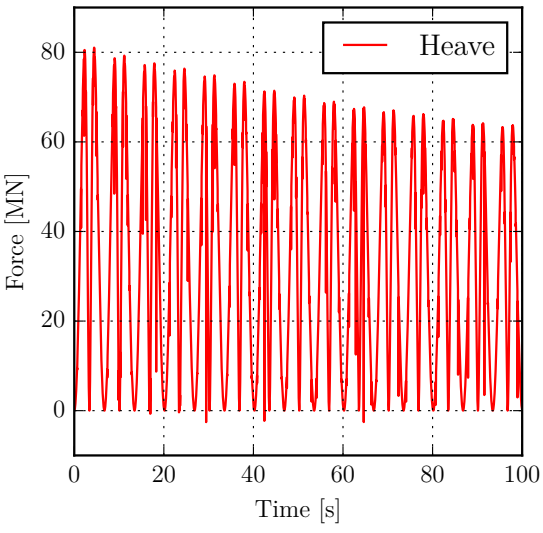

(o) free heave osc. FI forces - dt=0.01 s, fine mesh

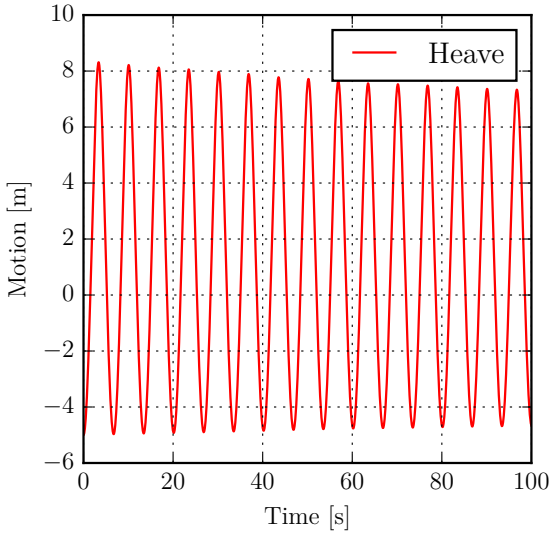

(p) free heave osc. motions - dt=0.01 s, fine mesh

Figure B.13: Heave oscillation - free vibration: different time steps and varied mesh grid on the hull of the barge are evaluated. The error in solving the EOM is shown in sub-figures (c), (f) and (k). (l) explains the clipping induced drop of FI forces.

B.7. Free heave oscillation - squat="false"

Objective: Verify the squat handle;

- **Result:** As expected;
- **Objects:** Single barge (see table 4.1 - coarse and fine mesh used)
- **Simulation time:** The simulation runs for 200 seconds with dt=0.05 second;
- **Situation:** A single barge simulated in a semi infinite fluid domain. An initial displacement of -5 meters was applied. The direct handle is set to "false";
- **Criteria:** No FI forces should be present, the barge should be in free vibration.

B.7.1. General analysis

The behaviour seen in verification case B.6 is influenced by the FI forces. The squat handle with value "false" sets the self-inflicting FI forces on the barge in heave direction to zero. All DoF except for the heave direction were restrained. The FI module should not provide forces and thus a free vibration of a mass-spring system: the spring being the buoyancy forces. Note that the buoyancy force, from which the restoring force coefficient is determined, is linear since the water plane area of the barge does not vary over height.

Natural frequency

To confirm that the simulated response is physical, the natural frequency was calculated in order to verify the simulated natural frequency. In figure B.14 it is shown that the simulated period of the motion is $\frac{70}{11} = 6.36$ seconds. In equation B.10 the dynamic equation of motion for this simulation is depicted. The natural frequency corresponding to this equation of motion is equal to equation B.11. Using the parameters of the barge as found in table 4.1, the expected natural frequency is; $\omega_n = \sqrt{\frac{30165750}{30750000}} = 0.99$ rad/s. This is equal to the simulated natural frequency: $\omega_n = \frac{2\pi}{6.36} = 0.99$ rad/s.

It is clear that the expected natural frequency and the simulated natural frequency match. Further the initial excitation is equal to the amplitude of the free vibration, this concurs with laws of energy conservation.

$$m \cdot \ddot{z} + c \cdot z = 0 \tag{B.10}$$

$$\omega = \sqrt{\frac{k}{m}} \tag{B.11}$$

B.7.2. Conclusion

After evaluation of figure B.14 and comparing it with figure B.13, it is clear that the squat handle works properly. No FI forces were simulated and the equation of motion was solved correctly.

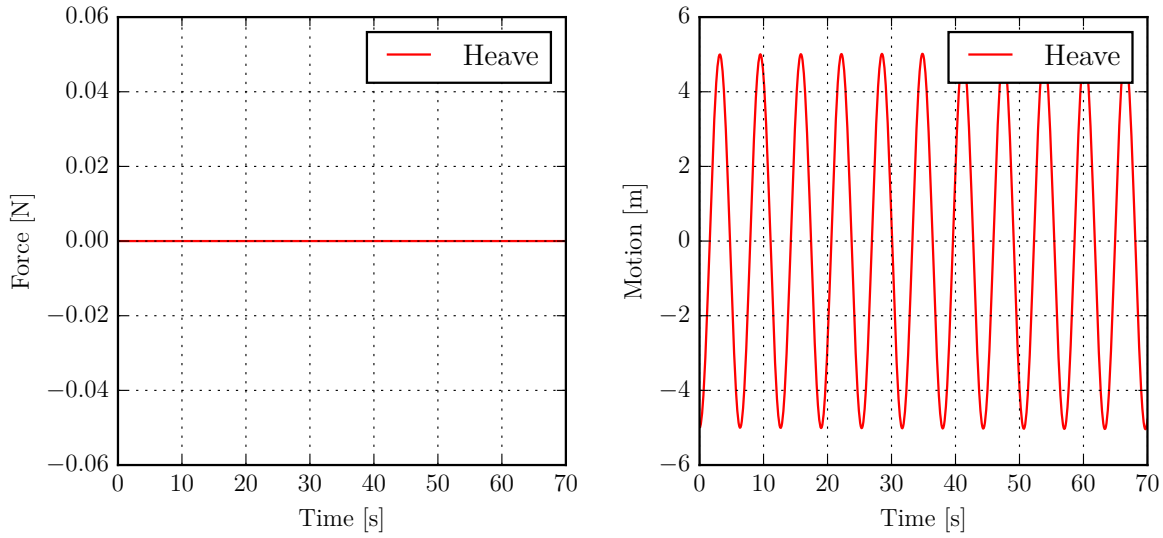

(a) Free heave osc. FI forces (dt=0.05s)

(b) Free heave osc. motions (dt=0.05s)

Figure B.14: Free heave oscillation, excited by an initial displacement of -5 meters. All self inflicting forces are disabled by setting the squat handle to "false".

B.8. Free roll oscillation

Objective: Verify free roll oscillation;

- **Result:** Unexpected amplitude compared to applied rotation - needs some explanation;
- **Objects:** Single barge (see table 4.1 - coarse mesh);
- **Simulation time:** The simulation runs for 200 seconds with dt=0.1 and dt=0.01 second;
- **Situation;** The barge is simulated as only body in a semi-infinite fluid domain. The simulation is excited by a 100 MNm roll torque for 10 seconds. After this time period the barge is released going into a free vibration. Table B.2 shows the FI handles chosen in this simulation;
- **Criteria:** The expectation is that for large rotational velocities the inertia (cushion) forces are governing.

B.8.1. General analyses

Figure B.15 shows the simulated FI forces and moments acting on the barge. The first 10 seconds a sway force was induced by the motion of the barge, initiating a motion in sway direction, figures B.15a and B.15b show this behaviour. When the barge is in free vibration the sway forces are still present but with a mean value of zero, only periodically influencing the sway motion. The heave motion seems to diverge as the roll motion converges, this indicates a transfer of energy from one motion to the other. Further the initial rotation is double the magnitude of the amplitude of the free vibration. This is not as expected, the amplitude of the oscillation should meet the amplitude of the initial rotation.

Sway and heave force

During the first roll rotation, the barge rolls to an angle of 14.40 degrees, a force is induced pushing the barge in negative sway direction. When the barge is released into a free vibration, this same force has a maximum again. These two maxima don't get compensated by any other force and the barge starts to sway. When the rotation of the barge turns negative, the sway force turns positive. The initial rotating of the barge leads to FI forces that push the barge one way. Because the initial amplitude is halved in the free vibration, a net sway force is present.

The barge rotates around the CoG, having one side of the barge move up through the free surface and one down from the free surface. As discussed in verification case B.4, the real geometry and its reflection interact

with each other. These inertia forces are dominant compared to the kinematic Bernoulli forces, this is substantiated by the conclusion drawn from verification cases B.4 and B.5 where inertia forces were governing as well. Note that in simulated fI forces in verification case B.3, where a rotation was part of the simulation as well, the kinematic Bernoulli term was governing. The difference with this simulation was the magnitude of the rotational velocity, which was in this case very much higher.

Further the roll rotation and the heave motion seem dependent. As the roll rotation decays, the heave motion grows. This behaviour was not induced by a insufficient time step, figure B.16 indicates this. A time step of dt=0.01 second in stead of 0.1 second was applied to the simulation. The decay in roll rotation over time was not an error in the solution of the equation of motion. This is different from verification case B.3 and B.6.

Initial amplitude

The amplitude of roll excitation was 14.40 degrees, this seems to be twice the amplitude of the free vibration. Energy conservation states that this is non physical behaviour, the initial excitation should match the amplitude of the free vibration. In verification case B.9 it was shown that this behaviour also manifests when the FI forces are set to zero. It is concluded that the loss of amplitude is not induced by the functionality of the FI module.

B.8.2. Conclusion

The simulated results show an instant loss in amplitude when the free vibration started. Verification case B.9 shows that this is not due to the FI module. The roll motions converges while the heave motion diverges, this strongly implies that both motions are coupled through the simulated FI forces. The positive heave force indicates that inertial (cushion) FI forces are significant. It is concluded that for large roll rotations (with high velocities) the cushion effect is governing. Verification case B.4 showed the same behaviour for heave motions. It can be generalized to: significant velocities, due to rotations or translations, through the vertical plane lead to large inertial forces. This complies with the mathematics in which the time derivative of the influence coefficients, which are related to relative velocities between panels, are taken into account.

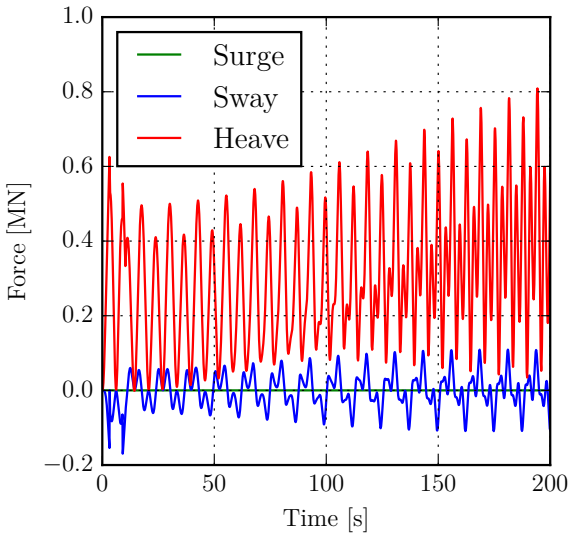

(a) FlowInteraction forces (dt=0.1s)

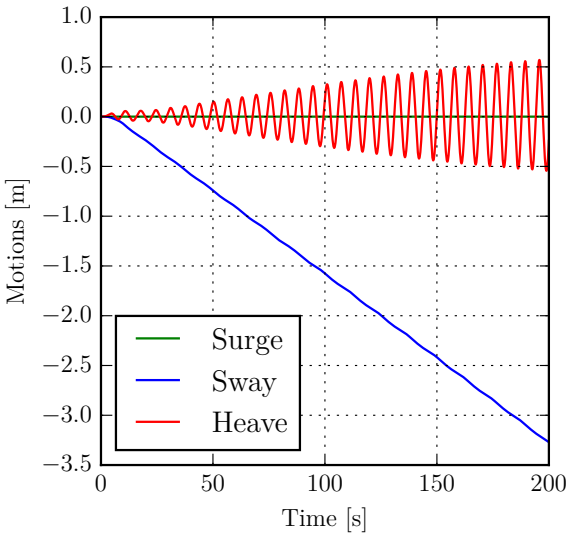

(b) Motions of the barge (dt=0.1s)

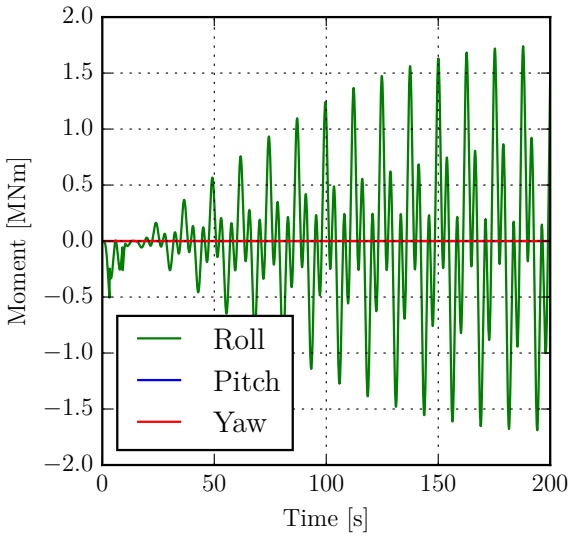

(c) FlowInteraction moments (dt=0.1s)

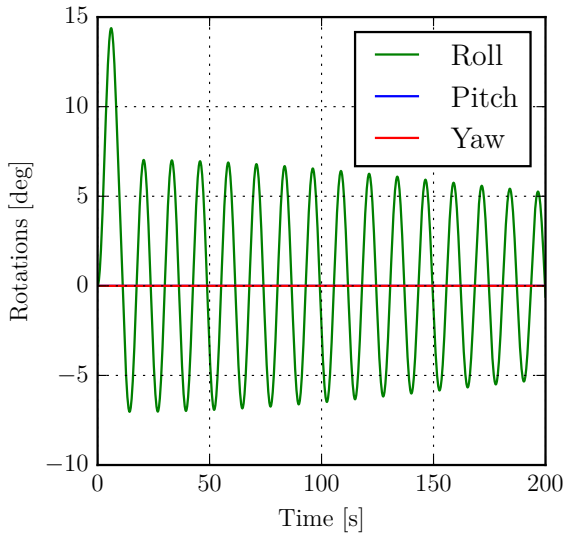

(d) Rotations of the barge (dt=0.1s)

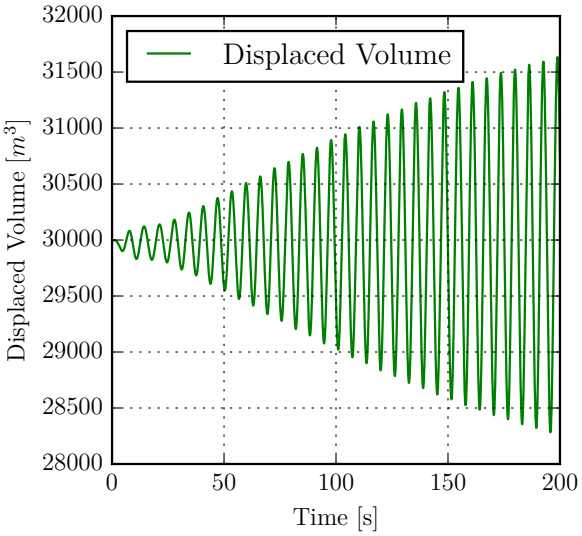

(e) Displace Volume over time (dt=0.1s)

Figure B.15: Simulated results of a roll oscillation - free vibration. The results are for a simulation time step dt=0.1s. The barge was unrestrained in 6 DoF.

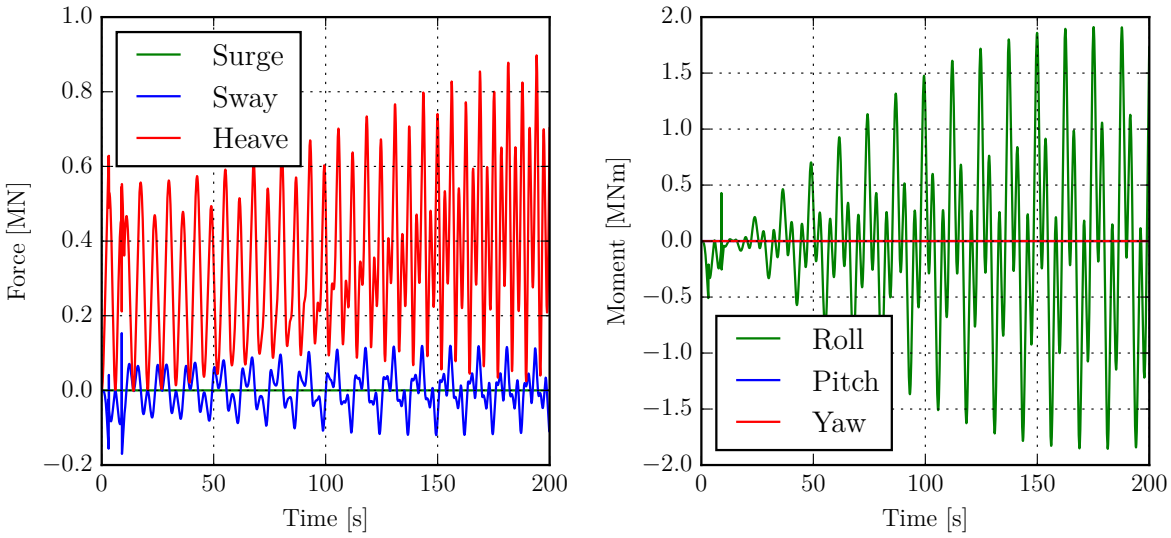

(a) FlowInteraction forces (dt=0.01s)

(b) FlowInteraction moments (dt=0.01s)

Figure B.16: Simulation results of a roll oscillation. The influence of time step reduction was analysed by comparing this figure with figure B.15.

B.9. Free roll oscillation - squat handle set to "false"

Objective: Verify if the loss of initial rotation as seen in verification case B.8 is due to FI forces;

- **Result:** The applied rotation is halved compared to the steady state amplitude of the vibration;
- **Objects:** Single barge (see table 4.1 - coarse mesh);
- **Simulation time:** The simulation runs for 200 seconds with dt=0.01 second;
- **Situation:** The barge is simulated as single body in a semi infinite fluid domain. The barge is excited by a 100 NM roll torque for the first 10 seconds of the simulation. After these ten seconds the barge is released to go into free vibration. Note that the difference with verification case B.8 is that the squat handle is set to "false", neglecting the FI forces. The rest of the handles are set as in table B.2;
- **Criteria:** An undamped free vibration in roll direction with an amplitude equal to the applied initial rotation.

B.9.1. General analyses

Figure B.17 indicates that no forces nor translational motions are present when the squat function is put to "false". This concurs with the conclusion drawn from verification case B.7 and confirms the functionality of the squat handle. More importantly, the applied initial angle of 14 degrees does not equal the steady state amplitude of the free vibration, this does not concur with the law of energy conservation. Since in this case no FI forces are simulated, this behaviour is introduced by other modules in the aNySIM programming. The applied amplitude seems to be divided by two compared to the steady state amplitude.

conclusion

The amplitude of the free vibration is only half the amplitude of the applied initial excitation. This behaviour is seen in verification case B.3 and B.8 as well. Since no FI forces are simulated in this event, it can be concluded that this error is introduced through other modules within the aNySIM programming.

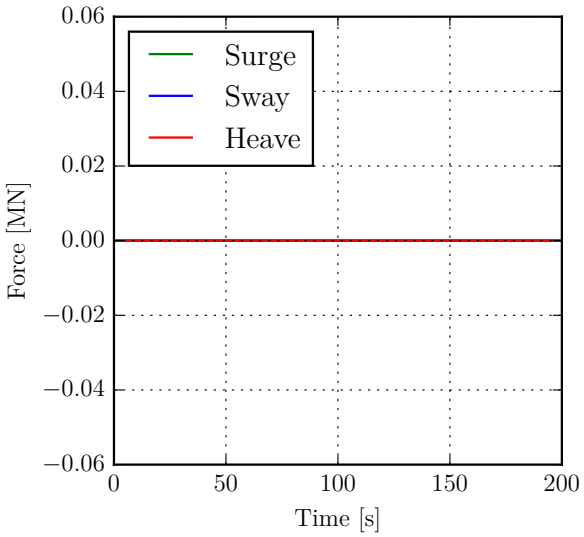

(a) FlowInteraction forces (dt=0.01s)

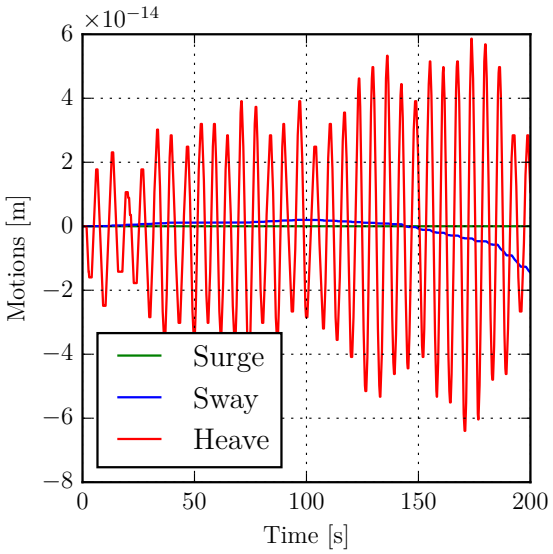

(b) Motions of the barge (dt=0.01s)

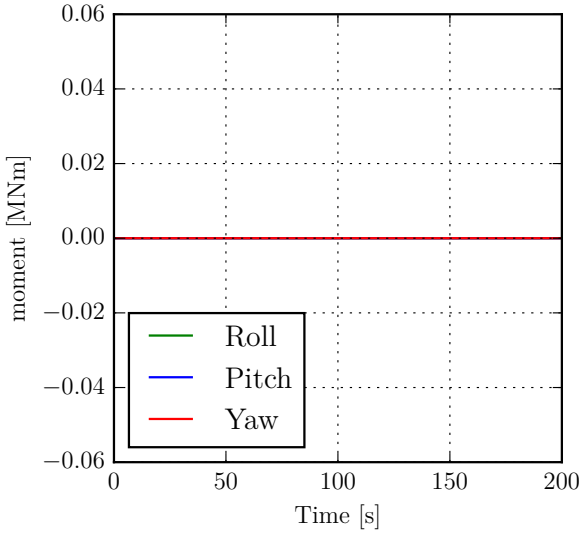

(c) FlowInteraction moments (dt=0.01s)

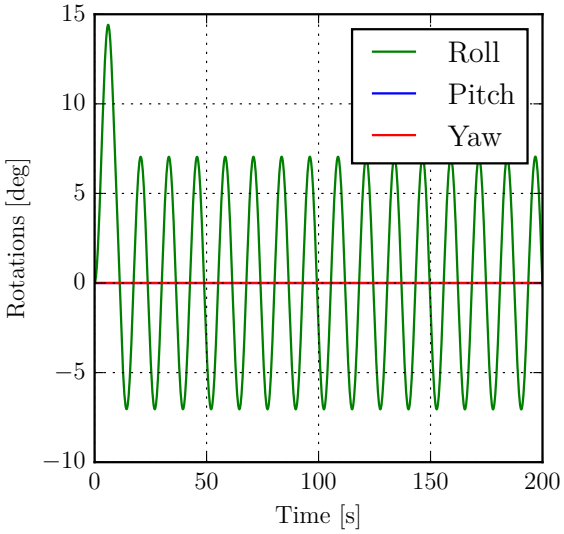

(d) Rotations of the barge (dt=0.01s)

Figure B.17: Simulated results of a free roll oscillation. The squat handle is set to "false" in order to verify if the steady state amplitude is equal to halve the initial amplitude.

B.10. FI handles and implemented properties

The functionality of the FI handles and properties of the FI module are verified in this section. In every subsection the approach to verification, the result and the evaluation of that handle or property is described.

B.10.1. Bank effect

Objective: Verify if the bank effect is simulated correctly;

- **Result:** As expected;
- **Objects:** Barge with coarse mesh (table 4.1) and a geometry functioning as quay (table **??** - 300 panels);
- **Simulation time:** 50 seconds with dt=0.01 second;
- **Situation:** the barge is simulated to move parallel to the quay with a constant velocity of 5 m/s. The passing distance is 15 meters between the starboard side of the barge and the port side of the quay.

The vessel passes on the left side of the quay (this is in the positive region of the sway axis). The quay is simulated as 14 meters deep and 400 meters long, with its center being at the global coordinate systems origin. The barge moves, measured from the CoG, from x=-125 to x=125 in the global coordinate system. The FI handles are set as in table B.5. The passing barge is restrained, it only moves in surge direction with a pre-defined velocity;

- **Criteria:** With the squat forces set to zero, only interaction forces should be simulated. The barge is not free to move, forces and moments in all six DoF should be present. Only in surge direction the FI forces are expected to be zero since the fluid will accelerate and decelerate before and behind the barge equally. The simulated value that is not zero in surge forces is because barge is noticing the effects the ends of the quay.

Figure B.18 shows the FI forces and moments acting on the passing barge. The lines in sub-figure (a) are forces in the surge, sway and heave direction shown in respectively green, blue and red. Note that the positive heave force is a product of the bank effect, since the squat handle is set to false this cannot be through the self-inflicted kinematic Bernoulli forces. The positive sway force means that the barge is pushed away from the quay. Suction forces introduced through the kinematic Bernoulli term are part of this interaction, yet it is clearly dominated by the inertia forces since a net overpressure between the barge and the quay is present. From the validation cases in Appendix **??** it is clear that when the vessels lay abreast the interaction forces between passing ships are dominated by the same force term.

Handle	Input possibilities	Value
enableVisualisation	"true"/"false"	"true"
soifactor	double	100.1
perturbCurrent	"true"/"false"	"true"
direct	"true"/"false"	"true"
squat	"true"/"false"	"false"
vmin	double	0
banksuction	"true"/"false"	"true"

Table B.5: Set simulation properties (FI handles)

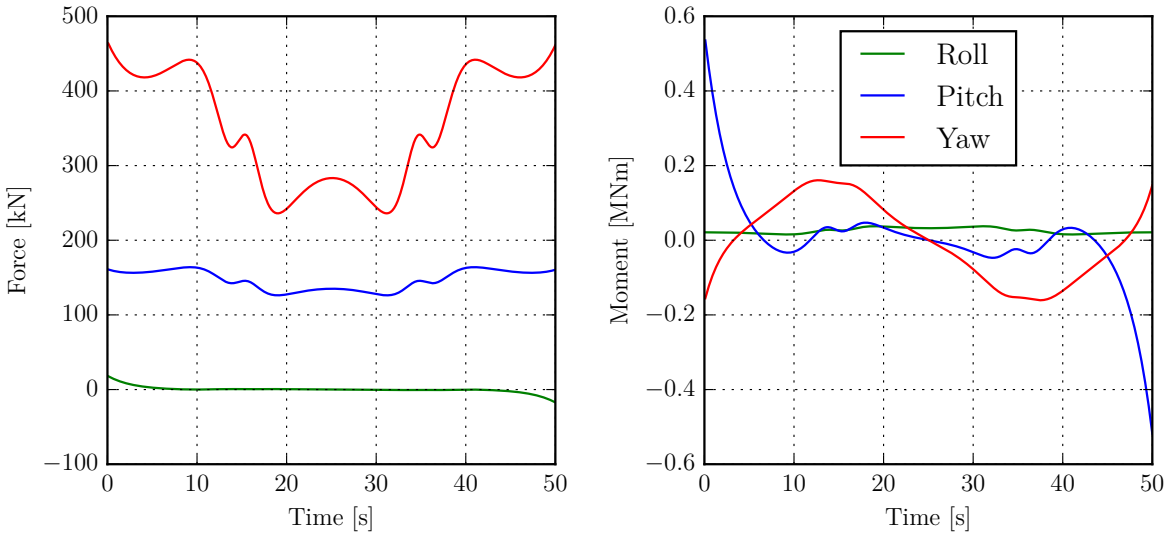

(a) FI forces on the passing barge (dt=0.01s)

(b) FI moments on the passing barge (dt=0.01s)

Figure B.18: Evaluation of the bank effect.

B.10.2. Banksuction handle

Objective: Verify the banksuction handle;

- **Result:** As expected - the bank suction handle works as intended;
- **Objects:** Barge with coarse mesh and a quay (300 panels) (table 4.1 and table **??**);
- **Simulation time:** 14 seconds with dt=0.01 second;
- **Situation:** the barge is simulated to move along side the quay with a constant velocity of 5 m/s. The passing distance is 15 meters. The quay is simulated as 14 meters deep and 400 meters long, with its center being at the global coordinate systems origin. The barge moves, with its CoG, from x=-125 to x=125 in the global coordinate system. The FI handles are set as in table B.5. All the DoF of the barge are fixed except for the forward velocity;
- **Criteria:** the same simulation is done in verification case B.10.1, only now with the banksuction handle set to false. Functionality of the banksuction handle dictates that no FI forces are simulated in this case.

Handle	Input possibilities	Value
enableVisualisation	"true"/"false"	"true"
soifactor	double	100.1
perturbCurrent	"true"/"false"	"false"
direct	"true"/"false"	"true"
squat	"true"/"false"	"false"
vmin	double	0.000
banksuction	"true"/"false"	"false"

Table B.6: Set simulation properties (FI handles)

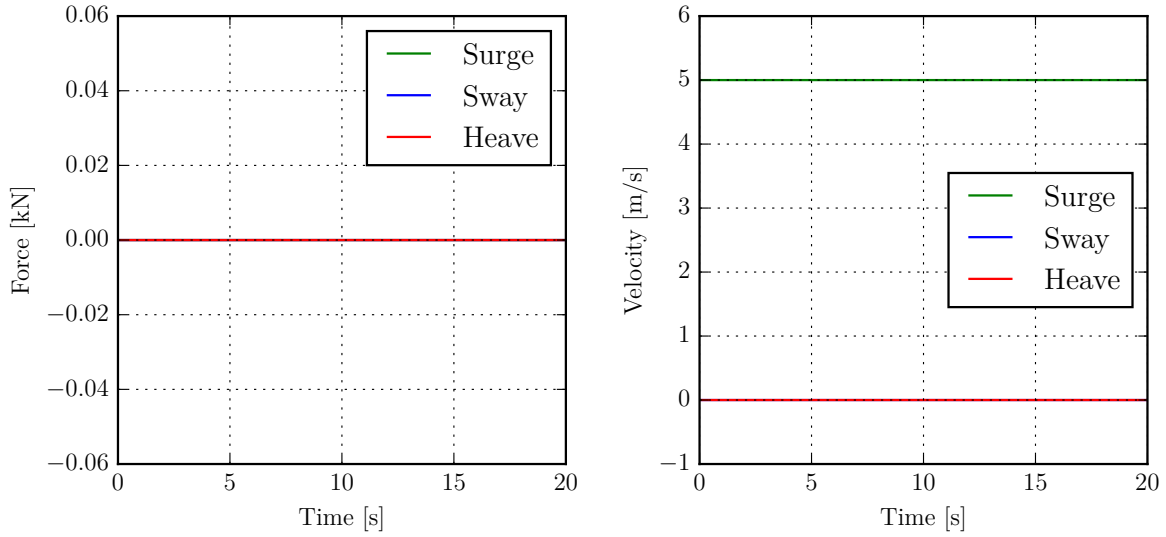

(a) FI forces acting on barge

(b) Motions of the barge

Figure B.19: Verification of banksuction handle

B.10.3. Manoeuvring induced yaw

Objective: Verify manoeuvring induced yaw;

- **Result:** As expected;
- **Objects:** Single barge with coarse mesh in a semi infinite fluid (table 4.1);
- **Simulation time:** 50 seconds with dt=0.01 second;

- **Situation:** the barge is simulated as single body in a semi infinite fluid domain, it moves along the x-axis with a constant velocity of 5 m/s. The barge propagates under a fixed yaw angle of -30 degrees. The FI handles are set as in table B.7. All the DoF of the barge are fixed except for propagating velocity;
- **Criteria:** Because the forward barge under a yaw angle will induce a non-symmetric fluid flow around itself, it leads to yaw moments. Yet the yaw induced by a vessel non-symmetrical geometry over the line of propagation is accounted for by empirical manoeuvring models in aNySIM. The FI module has to neglect these moments and not simulate them. This is implemented by the programmer of the FI module.

Handle	Input possibilities	Value
enableVisualisation	"true"/"false"	"true"
soifactor	double	100.1
perturbCurrent	"true"/"false"	"true"
direct	"true"/"false"	"true"
squat	"true"/"false"	"true"
vmin	double	0
banksuction	"true"/"false"	"true"

Table B.7: Set simulation properties (FI handles)

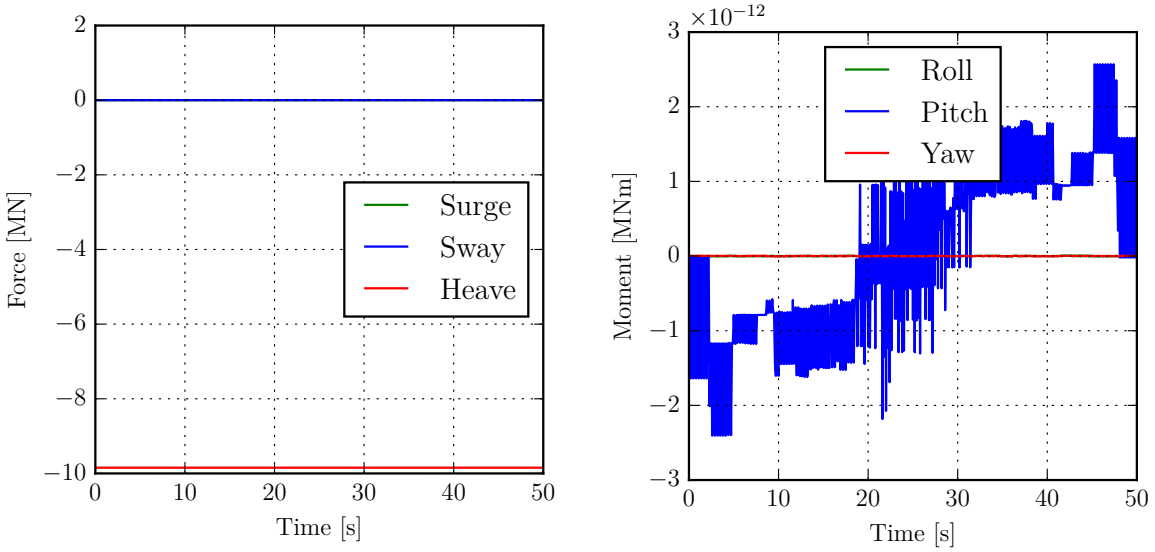

(a) FI forces acting on the barge (dt=0.01s)

(b) FI moments acting on the the barge (dt=0.01s)

Figure B.20: Simulated results of yaw induced by unsymmetrical flow around barge. The property works accordingly. The heave suction force due to the kin. Bernoulli forces is simulated as well, this is shown in sub-plot (a).

B.10.4. Influence current-vessel

Objective: Verify the current-vessel flow interaction forces;

- **Result:** As expected;
- **Objects:** Single barge with coarse mesh in a semi infinite fluid (table 4.1);
- **Simulation time:** 200 seconds with dt=0.1 second;
- **Situation:** The barge is simulated laying still in the fluid domain. It is unrestrained in all degrees of freedom. The free stream flows with a velocity of 5 m/s parallel with the surge direction. The settings of the FI handles are shown in table B.8;

- **Criteria:** The free stream should be entirely neglected by the FlowInteraction module (see section C.2.)

Handle	Input possibilities	Value
enableVisualisation	"true"/"false"	"true"
soifactor	double	100.1
perturbCurrent	"true"/"false"	"true"
direct	"true"/"false"	"true"
squat	"true"/"false"	"true"
vmin	double	0

Table B.8: Set simulation properties (FI handles)

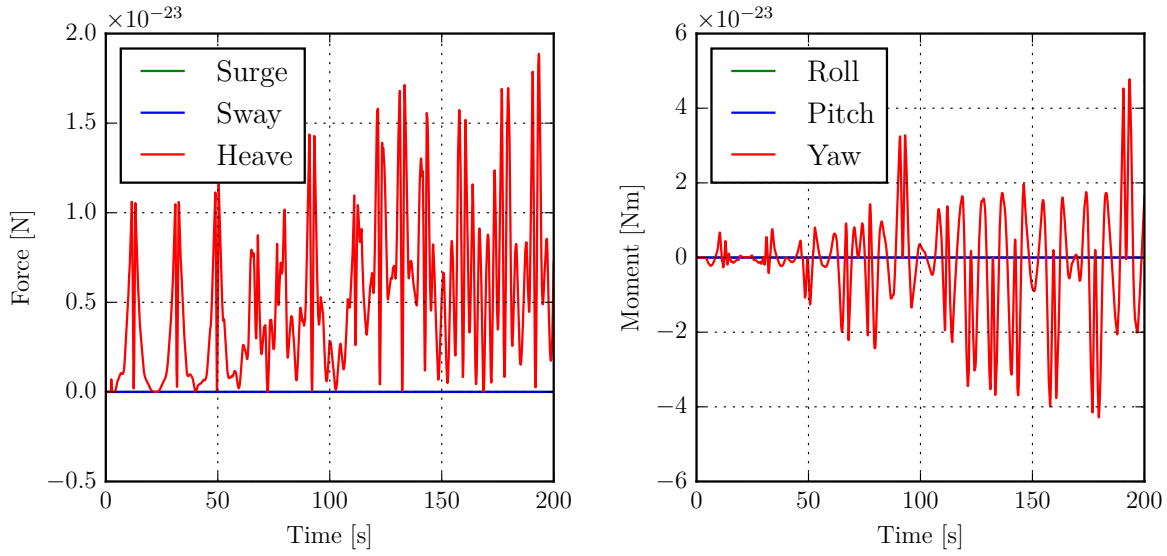

(a) FI forces on barge

(b) FI moments on barge

Figure B.21: Effect of free stream on FI calculation.

B.10.5. soifactor

Objective: Verify soifactor handle;

- **Result:** Not as expected;
- **Objects:** Single barge with coarse mesh in a semi infinite fluid (table 4.1) and a waveProbe to measure motion induced current at [0,0,-12.500] in the global coordinate system;
- **Simulation time:** 14 seconds with dt=0.01 second;
- **Situation:** the barge is simulated as single body in a semi infinite fluid with a kinematic excited oscillation in the heave direction with period 7s and amplitude 2m. At (51,0,-10) and at (54,0,-10), this is next to the barge, the fluid velocities are measured. See table B.10.5 for FI handle settings;
- **Criteria:** The soifactor is set to 1.0 which should give the barge an interaction range of 53.15 meters from the centre of geometry. The expectation is that fluid velocities are only induced at the first measurement point. The second one is out of range. Figure B.23b indicates that both measurement points feel the influence of the barge, it is concluded that the handle is not working as intended.

Handle	Input possibilities	Value
enableVisualisation	"true"/"false"	"true"
soifactor	double	0.5
perturbCurrent	"true"/"false"	"true"
direct	"true"/"false"	"true"
squat	"true"/"false"	"true"
vmin	double	0
banksuction	"true"/"false"	"true"

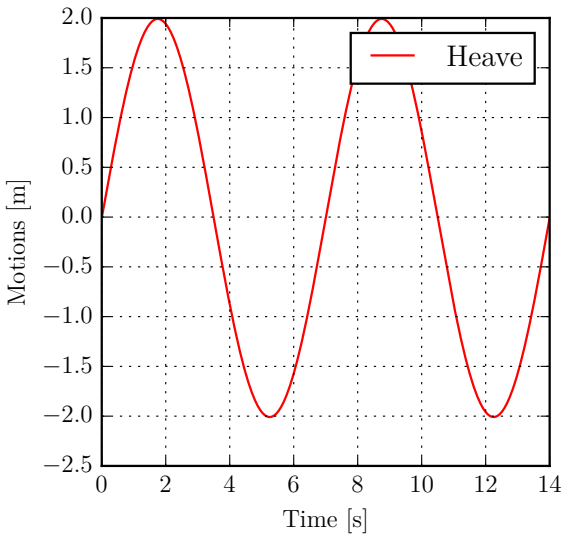

(a) Kinematic excited motion of the barge (dt=0.01s)

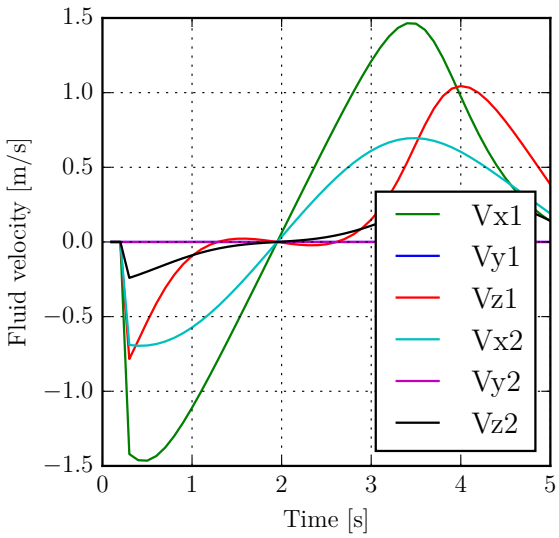

(b) Fluid velocities at 2 defined points (dt=0.01s)

Figure B.22: Verification soifactor handle

B.10.6. perturbCurrent and vmin

Objective: Verify the perturbCurrent and vmin handle

- **Result:** As expected;
- **Objects:** Single barge with coarse mesh in a semi infinite fluid (table 4.1) and a waveProbe to measure motion induced current at [0,0,-13] in the global coordinate system;
- **Simulation time:** 14 seconds with dt=0.01 second;
- **Situation:** the barge is simulated as single body in a semi infinite fluid with a kinematic excited oscillation applied to the barge in the heave direction with period 7s and amplitude 2m. Three meters underneath the hydrostatic equilibrium position of the keel of the barge, the velocities are measured. See table B.9 for FI handle settings;
- **Criteria:** the vmin handle is set to 1 m/s, meaning that when the barge has a velocity below 1 m/s the FI calculation will not be done. The perturbCurrent is set to false, no fluid velocities induced by the vessels motion should lead to simulated water motions. From figure B.23a it is clear that the simulated forces drop indeed to zero when the velocity is smaller than 1 m/s. From figure B.23b it is clear that the pertubCurrent handle is working as well. Both handles are functional.

Handle	Input possibilities	Value
enableVisualisation	"true"/"false"	"true"
soifactor	double	100.1
perturbCurrent	"true"/"false"	"false"
direct	"true"/"false"	"true"
squat	"true"/"false"	"true"
vmin	double	1.000
banksuction	"true"/"false"	"true"

Table B.9: Set simulation properties (FI handles)

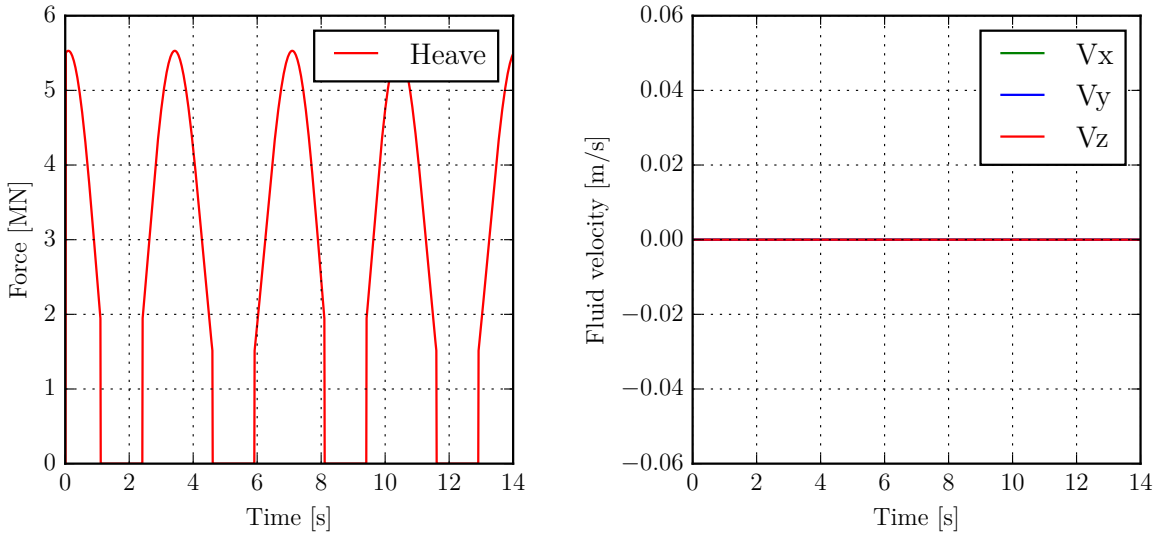

(a) FI forces on barge (dt=0.01s)

(b) Fluid velocities induced by the motions of the barge

Figure B.23: Verification perturbCurrent and vmin handle

C

User guide and limitations

In this appendix, recommendations and properties for practical use are found. The recommendations follow from the behaviour of the FI module identified during this thesis: partly from documented information and a part based on experience in working with the module. First some practical recommendations and possible explanations for unexpected behaviour is discussed, then the handles and properties of the module are explained.

C.1. Practical recommendations

The FI module enables aNySIM to find an expression for the whole fluid domain at every time step. For computational efficiency, some physics is not included in the module. Next to this neglect, some additional choices were made leading to a fast, but less widely applicable model. Some use of this module is not recommended:

- **No high speed events:** In high speed passing events, free surface effects become significant. Since these are not simulated by the FI module, recommended use restricts to the evaluation of passing events happening at a Froude number lower then 0.3 [-]. Equations 2.1 and 2.2 show how to determine the Froude number;
- **|Drift angles|** < 3 **[deg]:** When the passing ship is propagating with a large drift angle, viscous effects become significant. As a consequence of the applied potential theory, these effects are not simulated. The use of the FI module should be restricted to events with a drift angle of the passing ship between -3 and 3 degrees;
- **Simple harbour geometries:** When a ship is moored in a notch, or the event takes place in a complex harbour geometry, low frequency free surface effects might become significant. These free surface effects are not accounted for. The correctness of the simulated FI forces is not guaranteed when a passing event through a complex harbour geometry is simulated;
- **Shallow water coefficients:** The shallow water coefficients are showed to not fully account for shallow water effects. A shallow water passing event is only recommended to be simulated when the bottom is implemented as a panelled body. Note that this might be a problem because of limited working memory of the module.

The FI module is special because it allows for free motions. The free motions through the vertical plane are recommended to be disabled. Or the squat handle should be set to "false". This to prevent that motions in the vertical plane lead to simulated non-physical behaviour. If free motions through the vertical plane are restrained and the self-inflicted FI forces are simulated, remember the following behaviour might be simulated:

- **Non-physical behaviour:** the added mass force is not simulated. This force is dominant in vertical plane and the neglect leads to a non-physical behaviour in case of significant motions through the vertical plane. This is because cushion forces dominate the event when added mass is not simulated, these lead to a mean positive upward force;

- **Disabled time step adaptation of ODE solver:** because the FI calculation and the equations of motion are solved parallel to each other, the automatic time step adaptation of the ODE solvers is disabled. This is to ensure a synchronized time step in the FI calculation and the ODE solver. A small enough time step needs to be manually chosen;
- **Evade panel interfaces near the free surface:** when a panel is clipped very close to the panel interface, then a spike in FI forces toward zero is observed. Such a force spike is seemingly not accounted for by body motions. Yet it might lead in some cases to motional errors of the body.

C.2. Handles module

The mathematics and physics behind the FI module is found in Chapter 3. Here available handles implemented in the programming is discussed. The properties that can be set for this module are enumerated below, the layout is as follows: '**Handle name - Input/Output - Option - Default setting,** Functionality of the handle':

- **enableVisualisation - Input - "true/false" - [default="false"],** this handle provides the possibility to show the body in the visualisation tool as it is simulated. A convenient tool to evaluate if the input is set correctly. (Functional: figure **??** is a printscreen of the visualisation tool);
- **soifactor - Input - value - [default="1.2"],** this handle influences the reach of the sources. The reach of the sources is equal to the radius (from the centre of geometry) of the smallest sphere fitting the whole simulated geometry multiplied with the soifactor. This, for most ships, amounts to a reach of: soifactor$\times 0.5 \times L_{pp}$ from the centre of geometry. (Not functional, see verification case B.10.5);
- **perturbCurrent - Input - "true/false" - [default="false"],** this handle determines whether the generated flow field should be added to the global current field. When set as false, the fluid motions will not be simulated, the FI forces acting on simulated bodies are still present. (Functional: verification case B.10.6);
- **direct - Input - "true/false" - [default="false"],** this handle provides the possibility to approximate the hull shape by eleven polygons (panels) thus increasing the simulation speed significantly, yet introducing significant errors due to coarsening body mesh (example shape approximation is be found in figure C.1). The algorithm used for the approximation is explained in the next section;
- **squat - Input - "true/false" - [default="false"],** this handle enables the simulation of self inflicted FI forces. If chosen to be "false", then no draw down of a moving body is simulated. Cushion forces induced between a mirrored and real body are disabled as well. Inertia forces and kin. Bernoulli forces between two different bodies are still simulated. (Functional: verification cases B.4, B.7 and B.9);
- **vmin - Input - value - [default="0.5"],** the minimum velocity [m/s] of a body required for flow interaction to take effect. Note that the EOM itself is still solved that time step, just not containing FI forces on the concerned body. The presence of the body does influence other structures. (Functional: verification case B.10.6);
- **banksuction - Input - "true/false" - [default="false"],** this handle provides the possibility of neglecting interaction with static collision geometries (banks/quays) when set to false. (Functional: verification case B.10.2);
- **bdot- Input - "true/false" - [default="false"],** this handle enables the use of body accelerations from the previous time step to estimate the added mass forces. This approach to including added mass often leads to unstable simulations, recommended use: only apply when a kinematic excited geometry is simulated. (Functional: verification case B.5).

C.2.1. Algorithm direct handle

The direct approach chooses the eleven polygon shape based on corresponding displace volumes. The water line length of the approximated ship is divided in three equal parts:

- The middle part of the ship is approximated as a cube with the breadth of the water plane area. The draft is based on the total displaced volume of the middle one third of the ship;

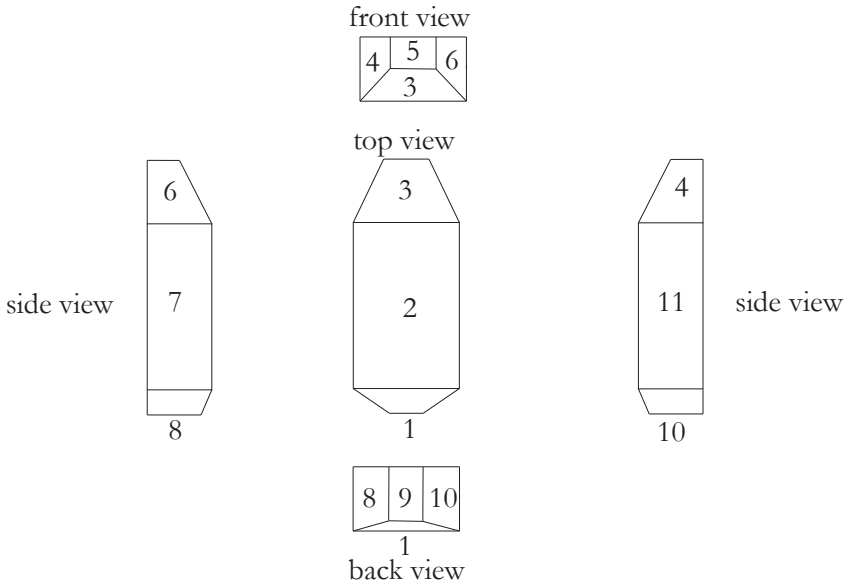

Figure C.1: Eleven polygon approximation of total ship mesh (direct="false" handle)

- The first and last part of the ship is approximated as a trapezoidal prism. The panels describing the stern and the bow are on one side connected to the middle cube. The sharpness of the approximated stern and bow are dependent on the shape of the water plane area. A round shape, e.g. for the stern will be approximated with a more blunt trapezoid shape (when observing the top view). The draft at the ends of the shape is chosen so that the displaced volume of the approximation and the inserted hull shape are equal for that one third of the ship.

Beware: In Appendix **??** the shape direct handle approximation for a simulated hull shape with 700 panels was different than for one with 300 panels. This was because of a difference in volume of the 700 and 300 panelled hull. The front bulb of the vessel was more accurately included in the hull shape with 700 panels, giving it more volume here compared to the hull with 300 panels. The difference between simulations with the two different approximations can be of serious influence on the simulated results, this is shown in Appendix **??**.

C.3. Properties of FI

The FI module, neglects certain behaviour. This is due to a combination of reasons: some is implicated by used physics, some were conscious choices to prevent interference with other aNySIM functionality.

- **Free stream:** the FlowInteraction module fully neglects the free stream. This is to prevent double current forces added to the EOM through the FI module and other modules;
- **Asymmetric fluid flow induced Yaw:** to prevent interference of FI forces on manoeuvring forces on ships in aNySIM, the yaw FI moment induced by sway and surge motions is disabled. Manoeuvring effects are already taken into account by empirically based coefficients in a manoeuvring model which is coupled as input to a ship in the simulation;
- **No added mass:** the added mass is neglected for computational efficiency, section 3.4 elaborates on this;
- **No damping:** damping is not simulated by the FI module. Both physical mechanisms to damping are neglected:
  - **No potential damping:** potential damping is not present since no pressure nor free surface waves can propagate in this simulation. This is an implication of the applied double body flow method;
  - **No viscus damping:** viscosity is neglected. This is a consequence of the applied potential theory.

- **Shallow water coefficients:** note that when the choice is made to set the handle 'depth' in the 'waves' child to a low number, empirical coefficients will be used to be multiplied with the deep water forces. In this manner shallow water effects are, in a computational efficient manner, taken into account. From Chapter 5 it is concluded that these shallow water coefficient do NOT account for the full shallow water effect.

C.4. Possible problems for dis-functionality

The FI module only allows for approximately 2000 panels in the simulation. Then the 32bit programming runs out of working memory when it is composing the influence matrix.

If a body is simulated, but seemingly not taken into account in the FI calculation, check the following: the xship::hull property hasfi (hasfi = has FlowInteraction) might not be set. The default setting of hasfi is false. If it is set to true, the body will be included in the FI calculation.

Bibliography

[1] Tim Bunnik and Serge Toxopeus. Viscous flow effects of passing ships in ports. In *ASME 2011 30th International Conference on Ocean, Offshore and Arctic Engineering*, pages 1–10, Rotterdam, The Netherlands, 2011.

[2] John Grue and Dag Biberg. Wave forces on marine structures with small speed in water of restricted depth. *Applied Ocean Research*, 15(3):121–135, 1993. ISSN 01411187. doi: 10.1016/0141-1187(93)90036-W.

[3] J. L. Hess and A. M. O. Smith. Calculation of Potential Flow About Arbitrary Bodies. Technical report, Douglas Aircraft Company, Long Beach, California, USA, 1967.

[4] J.M.J Journée and W.W Massie. *OFFSHORE HYDROMECHANICS (lecture notes)*. Delft University of Technology, Delft, Netherland, second edition, 2008.

[5] Jozeph Katz and Allen Plotkin. *LOW-SPEED AERODYNAMICS*. McGraw-Hill, Inc., San Diego, second edition, 2001. ISBN 0-07-050446-6.

[6] F T Korsmeyer, C.-H Lee, and J N Newman. Computation of Ship Interaction Forces in Restricted Waters. *Journal of Ship Research*, 37(4):298–306, 1993. ISSN 0022-4502.

[7] W.H. Pauw and K.W. Lam. RESEARCH ON PASSING EFFECTS ON MOORED SHIPS: ROPES JIP, WP3 model tests performed by MARIN. Technical Report Report No. 23920-5BT, MARIN, Wageningen, 2013.

[8] W.H. Pauw and K.W. Lam. Research on Passing Effects on Moored Ships: ROPES JIP WP5 correlation, comparison of modeltests, ROPES and aNySIM simulations. Technical Report Report No. 23920-5BT, MARIN, Wageningen, Nederland, 2013.

[9] J A Pinkster and H J M Pinkster. A fast, user-friendly, 3-D potential flow program for the prediction of passing vessel forces. In *PIANC World Congress*, page 12, San Francisco, USA, 2014.

[10] J a Pinkster and M N Ruijter. The Influence of Passing Ships on Ships moored in Restricted Waters. In *Offshore Technology Conference*, pages 1–10, Houston, Texas, U.S.A, 2004. ISBN 9781615679713.

[11] J.A. Pinkster. The Influence of a Free Surface on Passing Ship Effects. *International Shipbuilding Progress*, 51(4):313–338, 2004.

[12] Paul Tschirky, J. A. Pinkster, Sarah Rollings, Eric Smith, and Andrew Cornett. Modeling Moored Ship Response to a Passing Ship. In *Ports 2010*, volume 41098, pages 669–678, 2010. ISBN 978-0-7844-1098-1. doi: 10.1061/41098(368)69. URL `http://ascelibrary.org/doi/10.1061/41098{%}28368{%}2969`.

[13] H.J.J. van den Boom, M. Pluijm, and W.H. Pauw. ROPES; Joint Industry Project on effect of passing ships on moored vessels. In *PIANC World Congress*, volume c, page 19, San Franscisco, USA, 2014.

[14] E. Wictor. Ropes full scale measurements - Oude Maas Measurement Campaign. Technical report, MARIN, Wageningen, 2013.

[15] E. Wictor. Ropes full scale measurements: Canal, Caland Campaign, Measurement Report 23920-7-TM. Technical report, MARIN, Wageningen, Nederland, 2013.